LEVEL II

Report ONR 252-008-1

FEED LENS PORTION OF 3-D DOME ANTENNA STUDY

DR. DAVID T. THOMAS
S. DOUGLAS BIXLER

RAYTHEON COMPANY
ELECTROMAGNETIC SYSTEMS DIVISION
6380 HOLLISTER AVENUE
GOLETA, CALIFORNIA 93017

388
923

CONTRACT N00014-77-C-0760
ONR TASK 252-008-1

OCTOBER 1979

FINAL TECHNICAL REPORT FOR PERIOD OCT 77 - APR 79

Approved for public release; distribution unlimited.

PREPARED FOR THE

OFFICE OF NAVAL RESEARCH • 800 N. QUINCY ST. • ARLINGTON • VA • 22217

NOTICES

Change of Address

Organizations receiving reports on the initial distribution list should confirm correct address. This list is located at the end of the report. Any change of address or distribution should be conveyed to the Office of Naval Research, Arlington, VA 22217, Attn: Code 221.

Disposition

When this report is no longer needed, it may be transmitted to other authorized organizations. Do not return it to the originator or the monitoring office.

Disclaimer

The findings in this report are not to be construed as an official Department of Defense or Military Department position unless so designated by other official documents.

Reproduction

UNCLASSIFIED
SECURITY CLASSIFICATION OF THIS PAGE (When Data Entered)

REPORT DOCUMENTATION PAGE

READ INSTRUCTIONS BEFORE COMPLETING FORM

1. REPORT NUMBER: ONR 252-008-1	2. GOVT ACCESSION NO.
3. RECIPIENT'S CATALOG NUMBER	
4. TITLE (and Subtitle): Feed Lens Portion of 3-D Dome Antenna Study	5. TYPE OF REPORT & PERIOD COVERED: Final Technical Report, 1 Oct 77 - 3 Apr 79
6. PERFORMING ORG. REPORT NUMBER: -	
7. AUTHOR(s): David T. Thomas, S. Douglas Bixler	8. CONTRACT OR GRANT NUMBER(s): N00014-77-C-0760
9. PERFORMING ORGANIZATION NAME AND ADDRESS: Raytheon Company, Electromagnetic Systems Division, 6380 Hollister Avenue, Goleta, California 93017	10. PROGRAM ELEMENT, PROJECT, TASK AREA & WORK UNIT NUMBERS: ONR TASK 252-008-1
11. CONTROLLING OFFICE NAME AND ADDRESS: Department of the Navy, Office of Naval Research, Arlington, Virginia 22217	12. REPORT DATE: 10 Oct 79 13. NUMBER OF PAGES: 102
14. MONITORING AGENCY NAME & ADDRESS (if different from Controlling Office): -	15. SECURITY CLASS. (of this report): UNCLASSIFIED 15a. DECLASSIFICATION/DOWNGRADING SCHEDULE

16. DISTRIBUTION STATEMENT (of this Report)

Approved for public release; distribution unlimited.

17. DISTRIBUTION STATEMENT (of the abstract entered in Block 20, if different from Report)

18. SUPPLEMENTARY NOTES

19. KEY WORDS (Continue on reverse side if necessary and identify by block number)

Antenna, Lens-Fed Array, Dome Antenna, Hemisphere Scan Antenna, Broadband Antenna

20. ABSTRACT (Continue on reverse side if necessary and identify by block number)

A 3-D Dome/Rotman Lens Antenna system is described which offers the capability for (1) greater than hemisphere scan coverage from a single feed array, (2) greater than octave bandwidth, and (3) multiple simultaneous beams. The history and selected results of related programs are included.

Results of the analysis performed show peak phase errors of 15 degrees for scanning in the major axis planes. This error level would produce about 28 dB peak sidelobe levels for low sidelobe distributions. Complete descriptions of the analysis, computer programs and results are included.

DD FORM 1 JAN 73 1473 EDITION OF 1 NOV 65 IS OBSOLETE

UNCLASSIFIED
SECURITY CLASSIFICATION OF THIS PAGE (When Data Entered)

TABLE OF CONTENTS

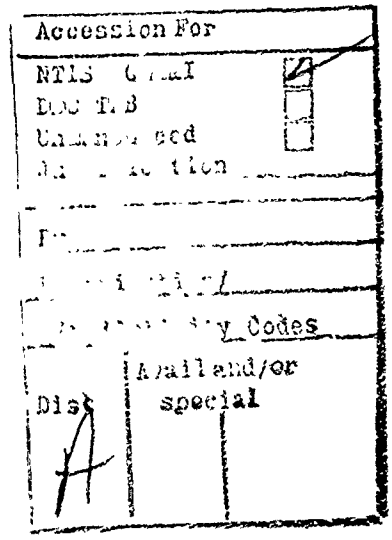

LIST OF ILLUSTRATIONS

SECTION I
SUMMARY

The purpose of this contract was to investigate the feed lens portion of a 3-D dome antenna system.

The 3-D dome/Rotman lens antenna system offers a capability new to antenna technology. The dome antenna extends the scan capability of a single feed array. Incorporation of the Rotman lens for the feed lens system offers the following capabilities for the combined system:

1) greater than hemisphere scan coverage from a single feed array,
2) greater than octave bandwidth, and
3) multiple simultaneous beams from a single feed array.

Figure 1 is an artist's concept of the 3-D dome/Rotman lens antenna system.

A summary of the history of related programs appears in Section II. The analyses and results of this study appear in Sections III and IV, and descriptions of computer programs used are included in the Appendix.

The recommended feed lens and array design presented in Section IV achieved very favorable results. Peak phase error for major axis scanning is less than 15 degrees, with RMS errors less than 6 degrees. Figure 2 illustrates the phase error at the feed array surface for a scan angle of 90 degrees (horizon). This error level would result is about 28 dB peak side-lobe levels for low side-lobe amplitude distributions. Figure 3 estimates the achievable peak side-lobe level for all scan angles throughout the hemisphere.

Gain variation with elevation scan angle is shown in figure 4. Gain is estimated from the projected aperture size of the feed array after passing through the dome. The shape of projected array aperture is given in Section IV. Scan-tailored gain variation to achieve desired antenna system performance is possible via different dome designs.

While the results achieved in this study are very good, further investigaand tradeoff studies of feed lens design should be undertaken. Major effort was expended in creating the computer programs for design of 3-D dome/Rotman lens antenna systems. The results represent studies of a limited sampling of cases. Further case studies would improve the final results at little cost, since the computer programs now exist. In addition, new configurations of dome and/or feed array should be investigated to address various 3-D dome/Rotman lens antenna system applications.

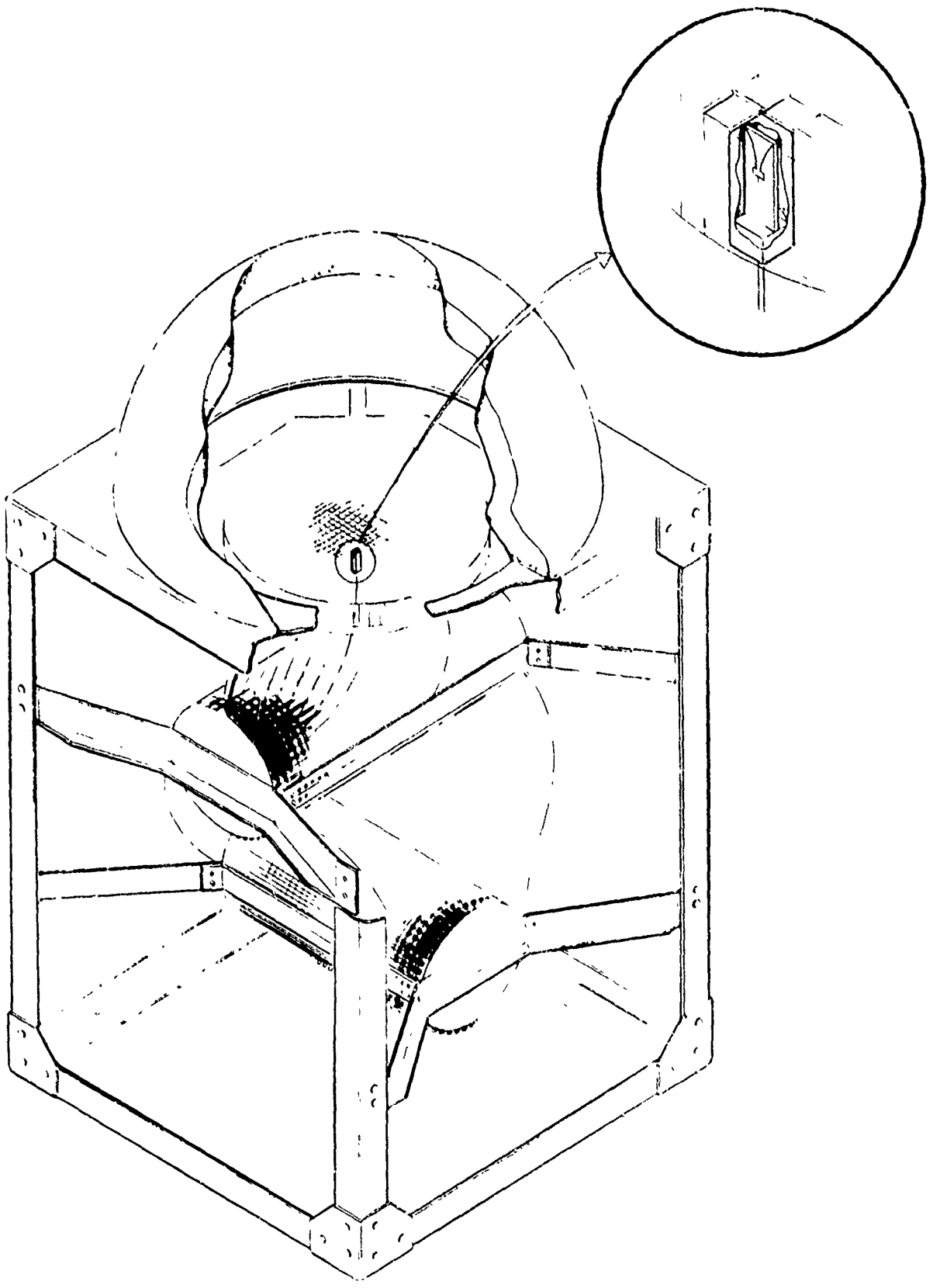

Figure 1. 3-D Dome/Rotman Lens Antenna

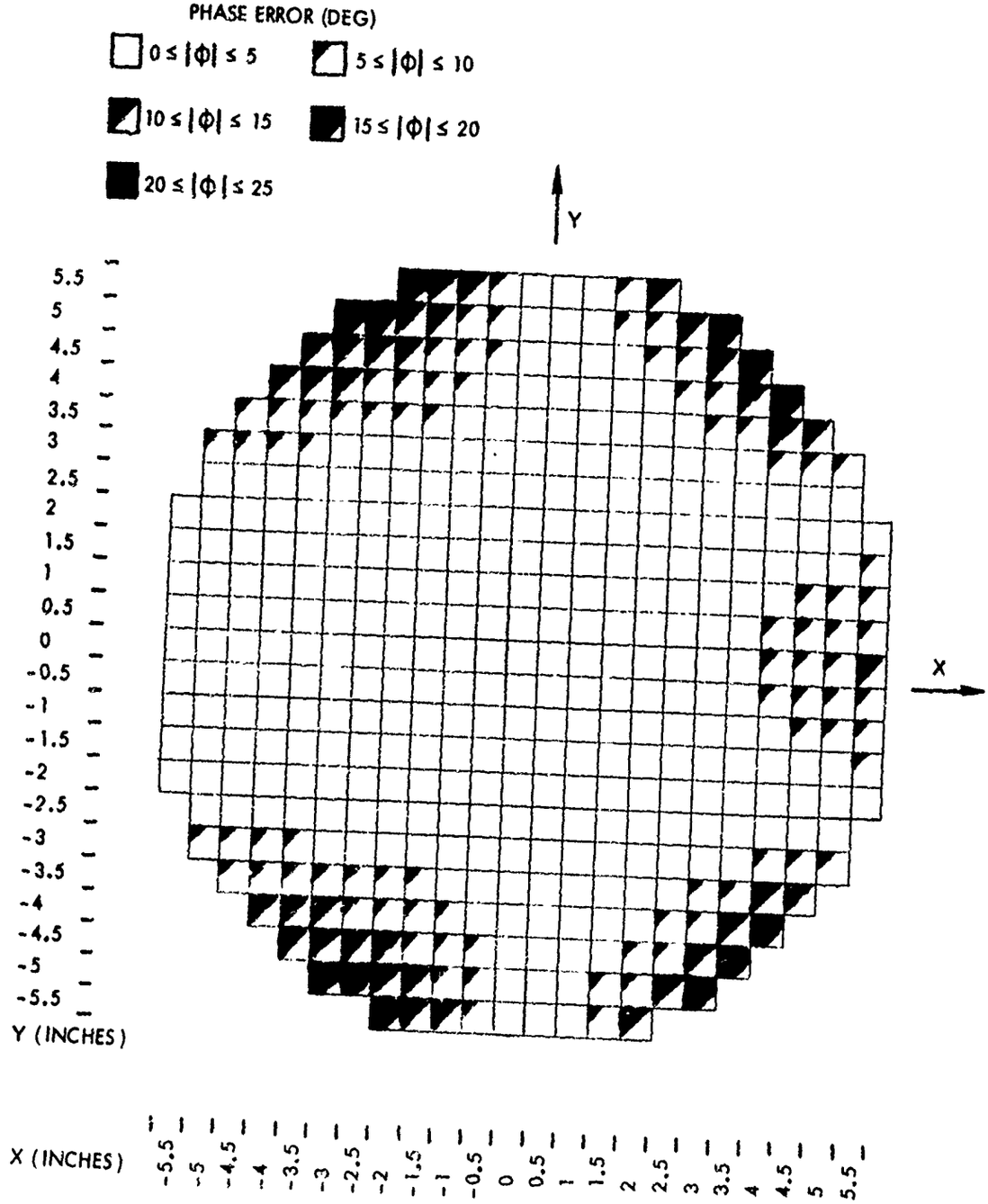

Figure 2. Phase Error for 90-degree Scan Angle

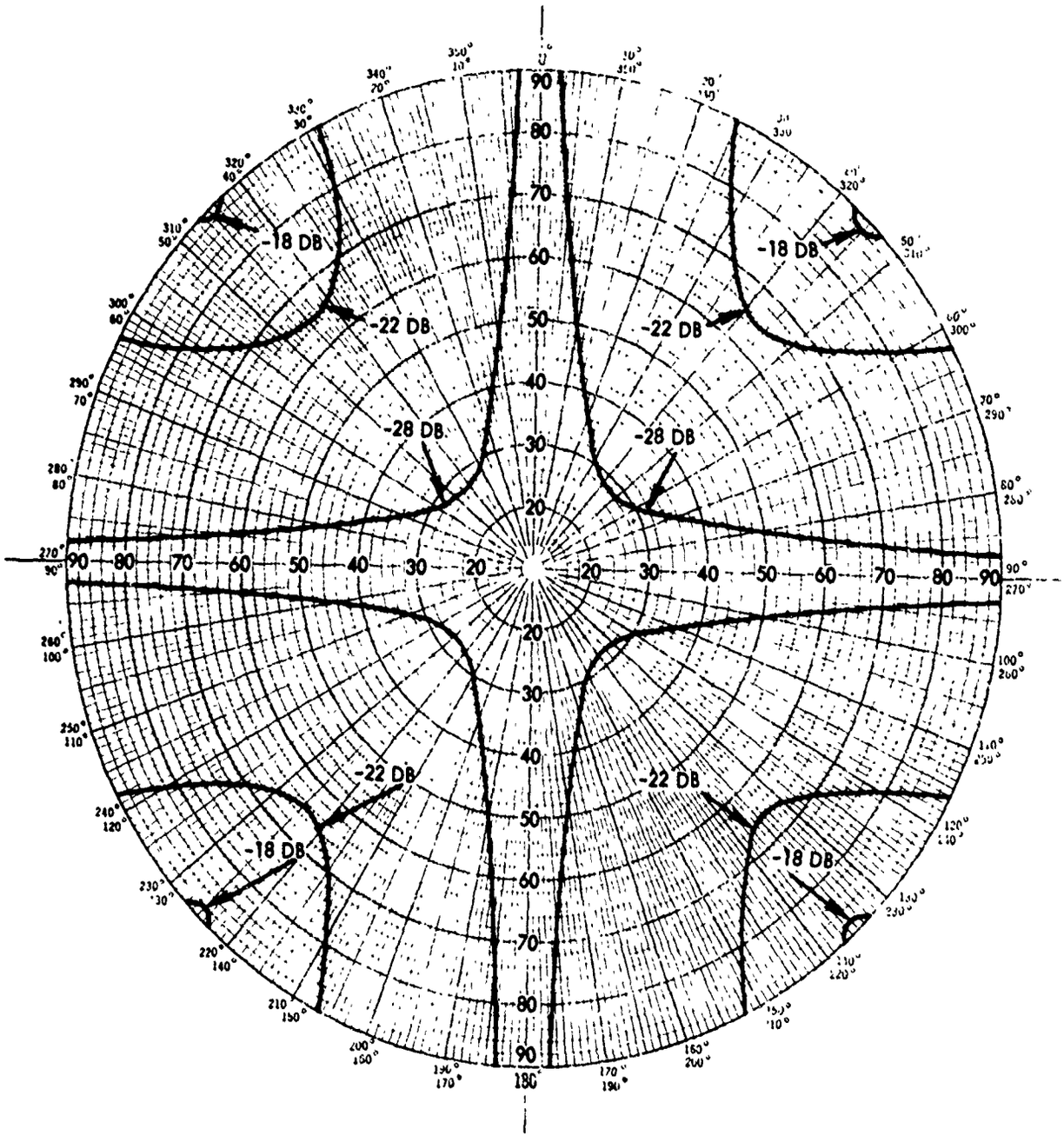

Figure 3. Top View of Achievable Side-Lobe Level over Hemisphere

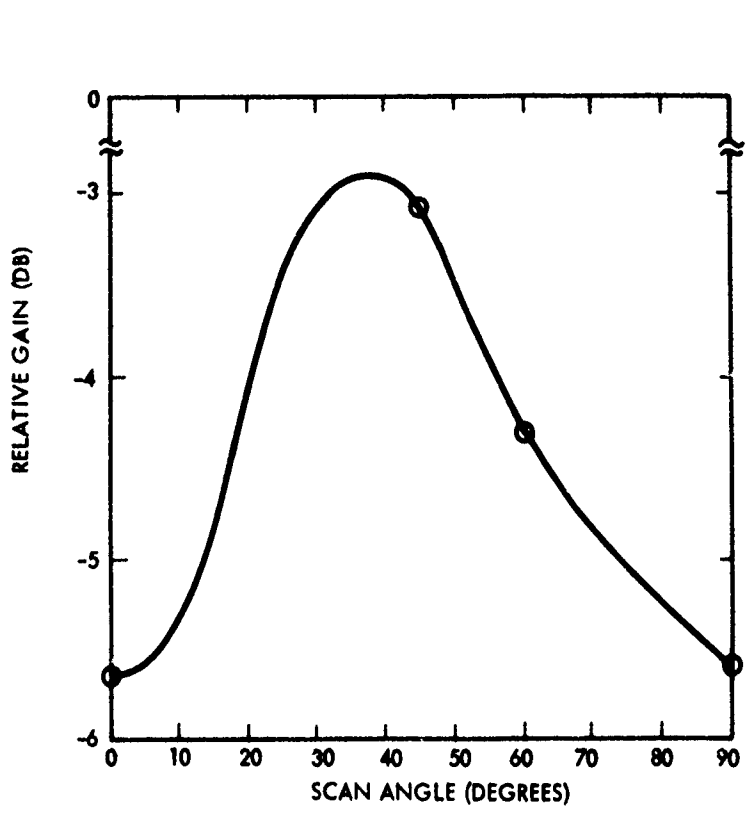

Figure 4. Relative Gain as a Function of Scan Angle

SECTION II
PROGRAM HISTORY

In 1975, the first of a series of programs was initiated to investigate a new antenna system concept which combines the 3-D dome antenna technology with Rotman lens-fed array technology.

The dome antenna[1] incorporates a new concept in electronic-scan antenna design which affords cost-effective applicability to a wide range of current and future systems. The dome antenna uses a passive conformal lens to extend the scan range of a conventional planar array to hemispheric (or greater) coverage. This represents a new capability heretofore unknown in antenna technology. The result is a substantially less complex antenna with fewer electronic control devices and lower in cost than alternate configurations.

Conceived and initially studied under Sperry's internal research and development activity, the continuing development of the dome antenna technique has been receiving support from a number of Government agencies, including the U.S. Army Ballistic Missile Defense Advanced Technology Center (BMDATC), U.S. Army Missile Command (MICOM), U.S. Air Force Rome Air Development Center (RADC), and Office of Naval Research (ONR).

The Rotman lens-fed array technology[2,3] is capable of generating multiple scanned beams from a single array aperture, and doing so over extreme bandwidths (3 to 1 or more). This technology has had extensive development at Raytheon ESD over the past twelve years. Over $10 million in Raytheon internal development funds and over $100 million in Government contract funds have been expended on research, development, and production of systems employing lens-fed multibeam arrays. Section 2.3 describes the operation of the Rotman lens.

The first joint program, Octave Bandwidth Wide Angle Antenna Study (ONR Contract #N00014-76-C-0652) studied a 2-dimensional dome slice and designed the required feed lens. Results of that study indicated that large phase errors and poor lens shape would result from feeding a dome antenna with its flat feed array.

Subsequent to this first contract, new investigations were carried out on Raytheon internal research funds. A new concept was discovered which offers substantial improvements in performance. This effort was continued on Raytheon internal funds to design, fabricate, and test a two-dimensional breadboard model. (A patent application on this invention was filed in November 1978.) The results of this effort are summarized in section 2.1.

The current program, Feed Lens Portion of 3-D Dome Antenna Study (ONR Contract #N00014-77-C-0760) is a 15-month study program to design and predict performance of the feed lens portion of a 3-D dome antenna. The ultimate goals are the development of wideband, multibeam 3-D dome antenna systems.

Several tasks are identified for the current program:

1) studies and analyses to develop a frequency-independent 2-D feed lens,
2) upon receipt of dome data from Sperry, design a 3-D lens feed to drive the system,

---

1. Stangel, J.J. and Valention, P.A. "Phased Array Fed Lens" U.S. Patent No. 3755815.
2. D.H. Archer, "Lens Fed Multibeam Arrays", Electronic Progress (Raytheon Co.), Vol. XVI, No. 4, pp. 24-32, Winter 1974.
3. Rotman, W. and Turner, R.F., "Wide Angle Lens for Line Source Applications", IEEE Trans., Vol. AP-11, pp. 623-632 (1963).

3) analyze the performance (amplitude and phase distributions) of the most promising 3-D lens designs, and provide that information to ONR and Sperry.

4) assess the overall system performance, and

5) prepare the final report.

The first task was deferred pending completion of Raytheon-funded work, results of which are presented in section 2.1. Results of remaining tasks are presented in later sections of this report.

The 3-D dome/Rotman lens antenna will use a two-stack feed lens similar to that developed on the MUSTRAC program described in section 2.4.

2.1 WIDE-ANGLE, ARRAY-FED LENS (2-D DOME SLICE)

2.1.1 DESIGN STUDIES

The wide-angle, array-fed lens (WAAFL) is a marriage of the dome antenna[3] and Rotman lens-fed multibeam arrays[4]. It offers the capability for:

- greater than hemisphere scan coverage from a single feed array,
- greater than octave bandwidth, and
- multiple simultaneous beams.

This paper describes WAAFL design studies which led to a novel curved feed array with substantial improvements in performance over conventional planar feed arrays. The curved feed array results in feed lens designs (using Rotman lens technology) which are superior to previous designs employing planar feed arrays.

A wide-angle, array-fed lens is designed to provide scan amplification, i.e., wide-angle scanning (hemisphere or greater) from a single array face. A ray path diagram (to scale) of a WAAFL with Rotman feed lens attached is shown in figure 5. The design shown is for a scan amplification factor K of 1.5.

The advantages realized by the curved feed array are:

- reduced amplitude distortion,
- improved feed lens design which is 30 percent smaller and of a more efficient shape (less mismatch or spillover), and
- significantly lower path-length errors.

The ability to scan extremely wide angles is not accomplished without loss, however. A reduction in effective aperture occurs which translates directly to reduced gain (with respect to full feed array gain). Boresight aperture loss of 2.5 to 4.0 dB should be anticipated (one plane only) for wide-angle, array-fed lens antennas.

The uniform amplitude distribution can be seen in the ray path diagram of figure 5. Figure 6 shows the actual low distortion for two curved feed arrays. In contrast, the flat feed array distortion is asymmetrical and varies about 7 dB over the aperture, a fact which contributes significantly to sidelobe levels.

The greatly reduced path length errors for a curved feed array are shown in figure 7. The order-of-magnitude improvement in path length error makes the difference between an infeasible feed lens and an attractive design and performance.

---

4. L. Schwartzmann and J. Stangel, "The Dome Antenna," Microwave Journal, Oct. 1975, pp. 31-34.

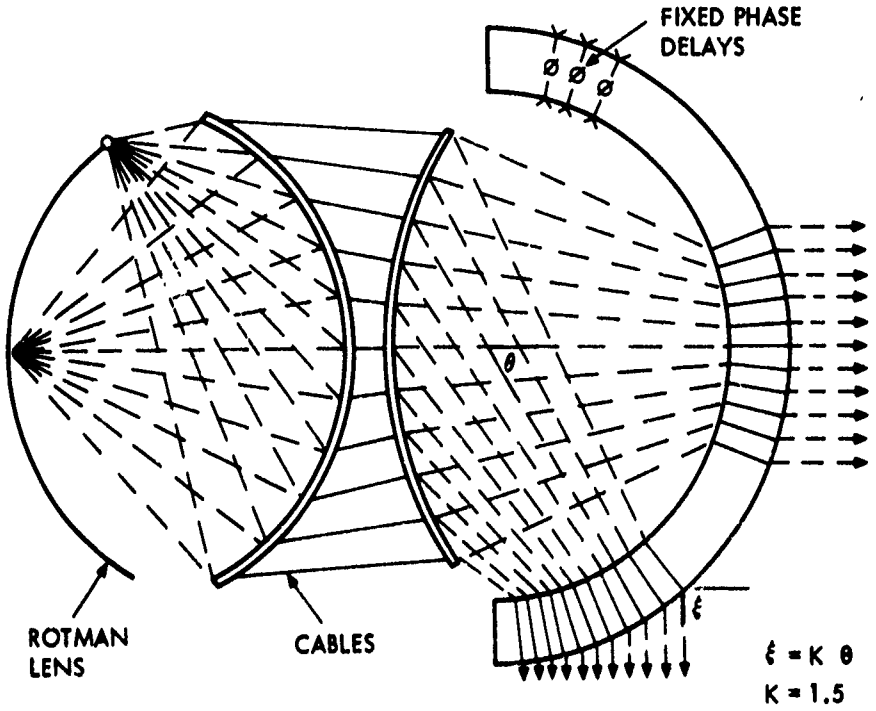

Figure 5. Wide-Angle, Array-Fed Lens (WAAFL)

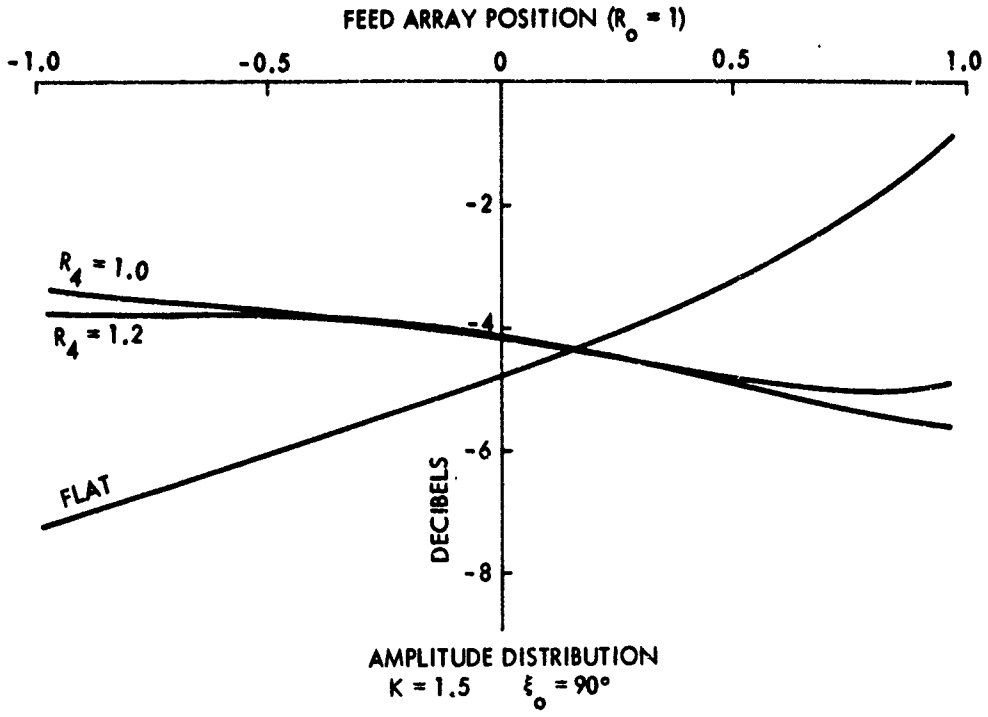

Figure 6. Amplitude Distortion in Array-Fed Lens

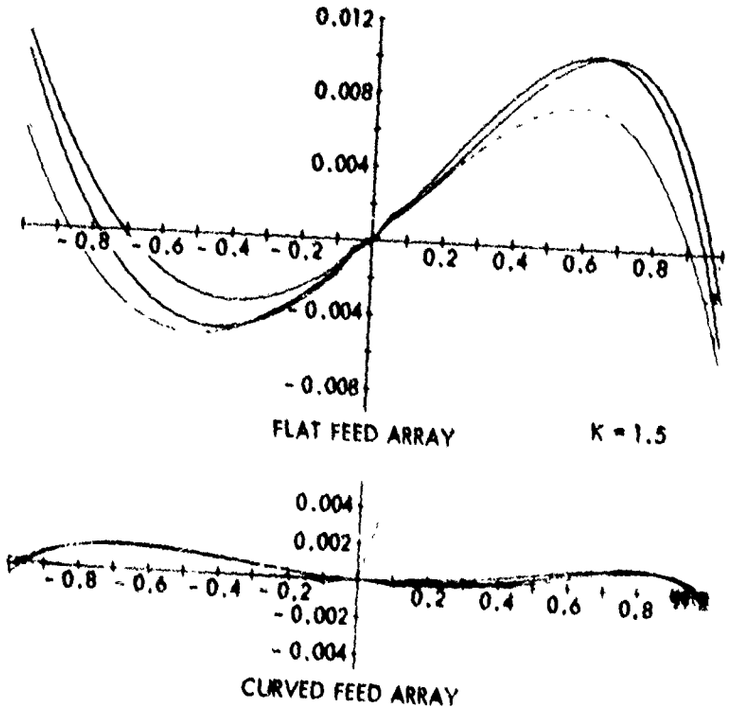

Figure 7. Feed Lens Path-Length Error

Three sets of computed low-sidelobe radiation patterns are shown in figure 8. A Taylor-like aperture taper for 38 dB side-lobe level was imposed on the feed array. The effects of amplitude distortion and (for 60-degree scan) the lens phase error are evident in the side-lobe levels. However, the curved feed array clearly fares better at all three scan angles (0, 60 and 90 degrees). Significant beam broadening and shoulders are present when the flat feed array distortion is included.

Results of other cases (e.g., scan amplification of K = 1.8 and 2.0) and representative lens designs have also been computed.

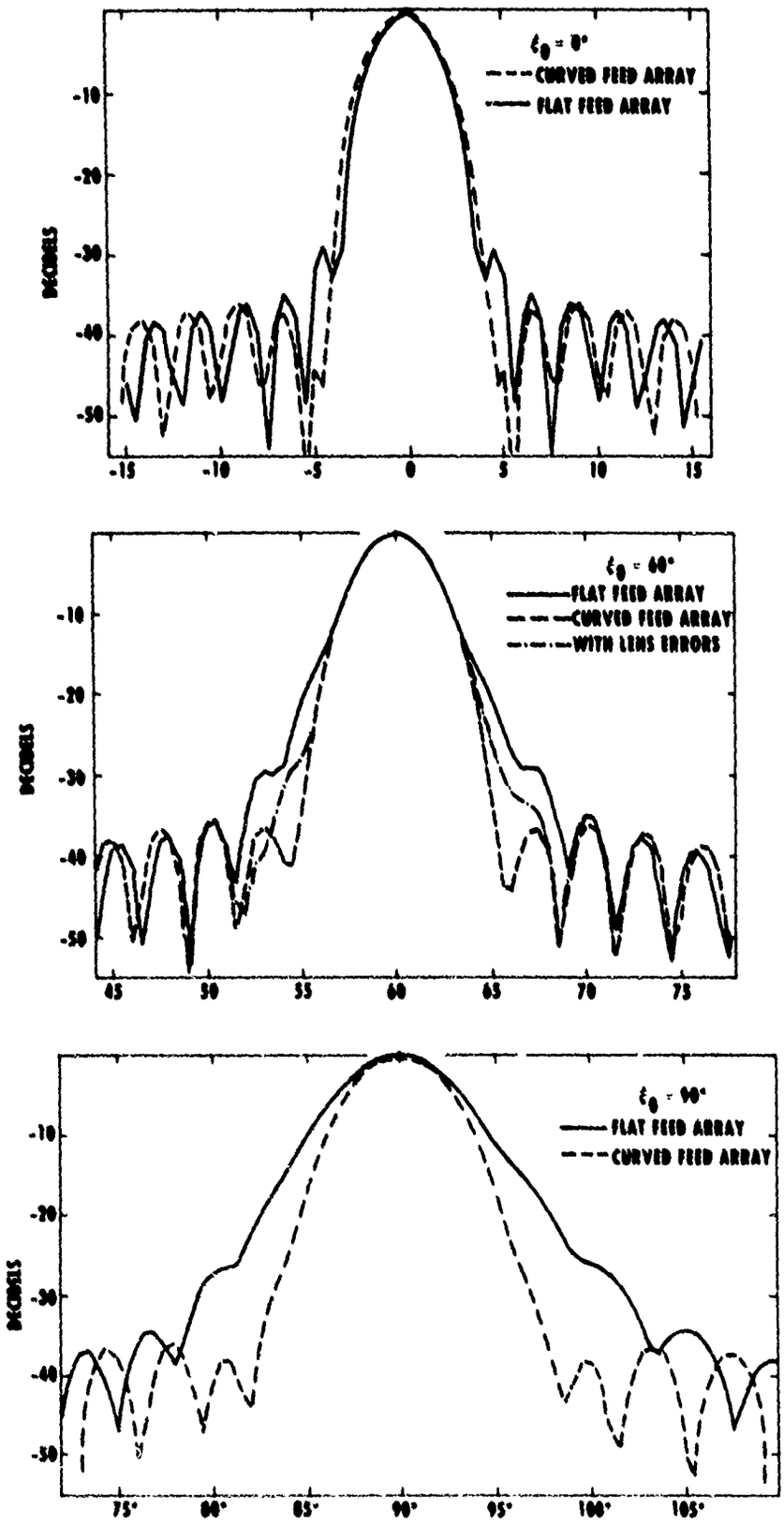

Figure 8. Computed Low-Sidelobe Patterns

2.1.2 HARDWARE DEMONSTRATION

A two-dimensional wide-angle, array-fed lens has been built and tested which demonstrates:

1) 180-degree scan coverage,
2) 7 to 18 GHz frequency bandwidth, and
3) multiple beams.

The design concept for this demonstration WAAFL was selected from the results of earlier design studies. Design parameters are summarized in table 1. A photograph of the completed hardware appears in figure 9.

The demonstration hardware consists of three items: (1) a semicircular array of double-ridge elements; (2) a printed stripline, array-fed lens which provides the scan amplification; and (3) a printed stripline Rotman lens for scanning the beams. In the resultant system, each beamport produces a scanned beam in space. One advantage of the array-fed lens is the absence of frequency-dependent beam squint.

Table 1. WAAFL Design Data

Scan Coverage	180 Degrees
Bandwidth	7 to 18 GHz
Beamwidth (Nominal)	
6 Degrees	(15 GHz)
11 Degrees	(8 GHz)
Semicircular Array	
69 Elements (180 Degrees)	
9.08 in. Radius (Phase Center)	
Array-Fed Lens	
7.26 in. Semicircular Arc Radius	
35-Element Feed Array	
12.1 in. Feed Array Width	
Scan Amplification, K = 1.5	
Rotman Feed Lens	
35 Array Ports, 29 Beamports	
$G = 1.10$, $\alpha = 40$, $\eta = 0.65$	

11498

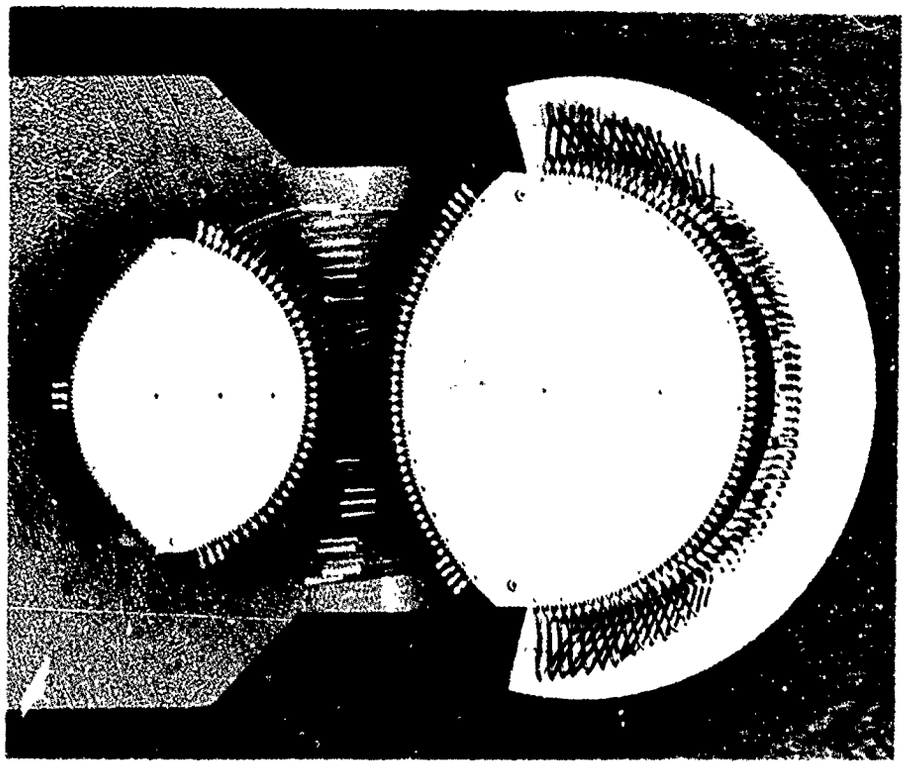

Figure 9. WAAFL Demonstration Hardware

Test results confirm the performance capability of the wide-angle, array-fed lens. Scan capability of 180 degrees was measured over frequencies from 7 to 18 GHz. Figures 10 through 13 show measured radiation patterns at 8, 12, 15, and 18 GHz, respectively. (Figure 10 shows the full-beam rosette of 29 beams for 8 GHz. The remaining figures show only selected beams covering the 180-degree scan sector.

In all cases, beam patterns are well formed with good side lobes, and confirm the expected performance, including low-scan rolloff.

The excellent results of the hardware demonstration confirm the feasibility of two-dimensional, wide-angle array-fed lenses with Rotman lens feed.

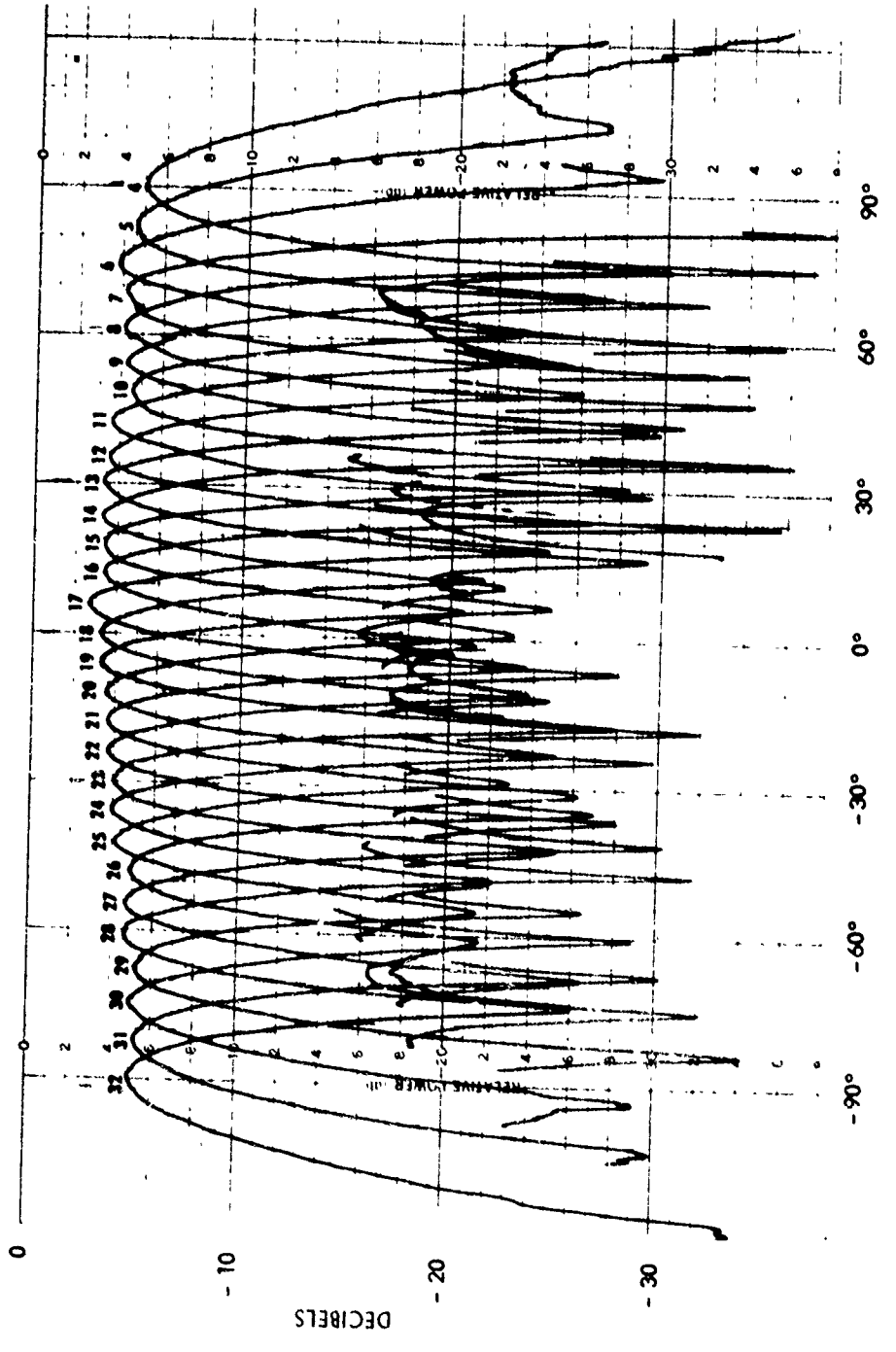

Figure 10. WAAFL Measured Radiation Patterns (9 GHz)

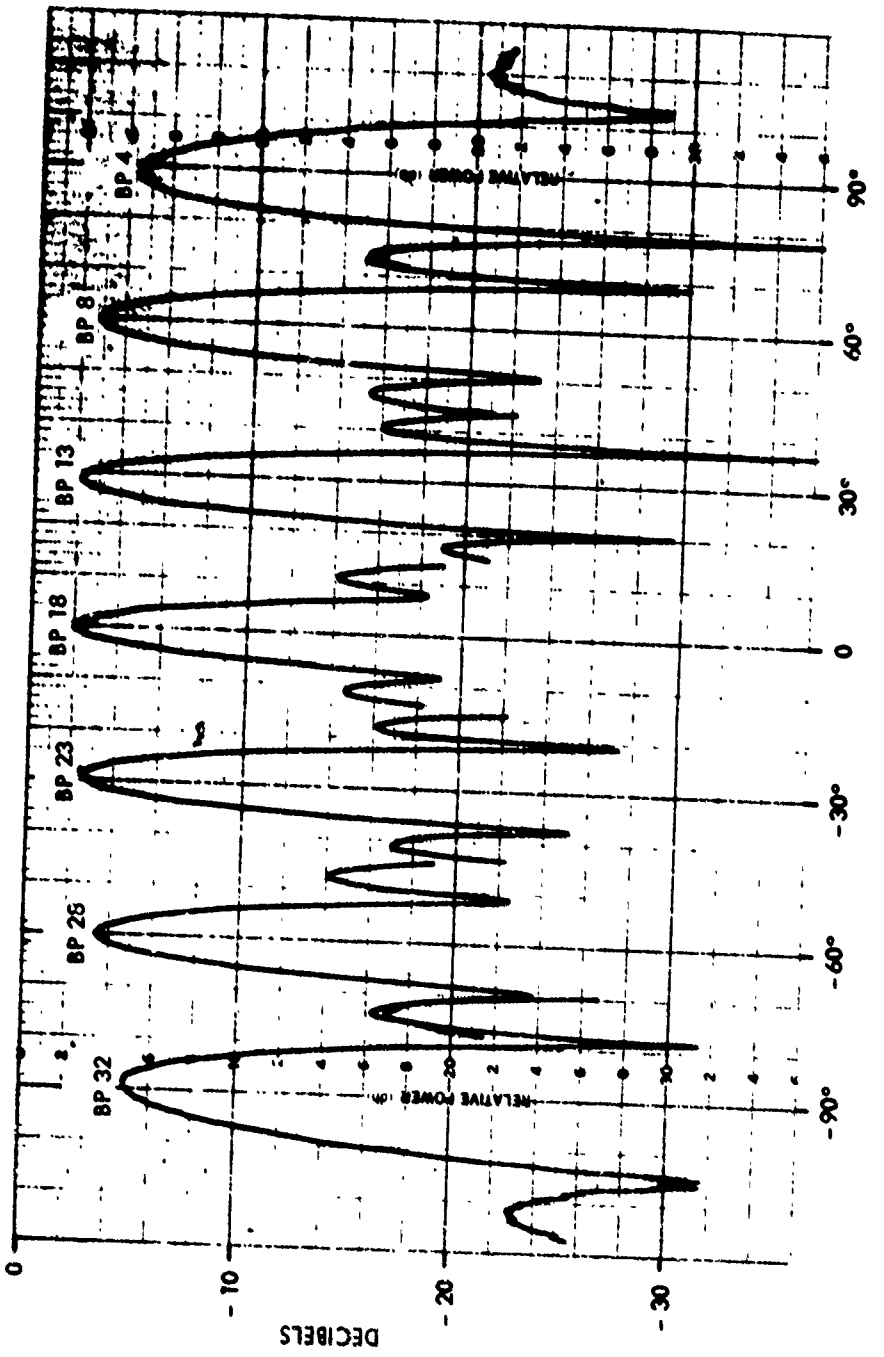

Figure 11. WAAFL Measured Radiation Patterns (12 GHz)

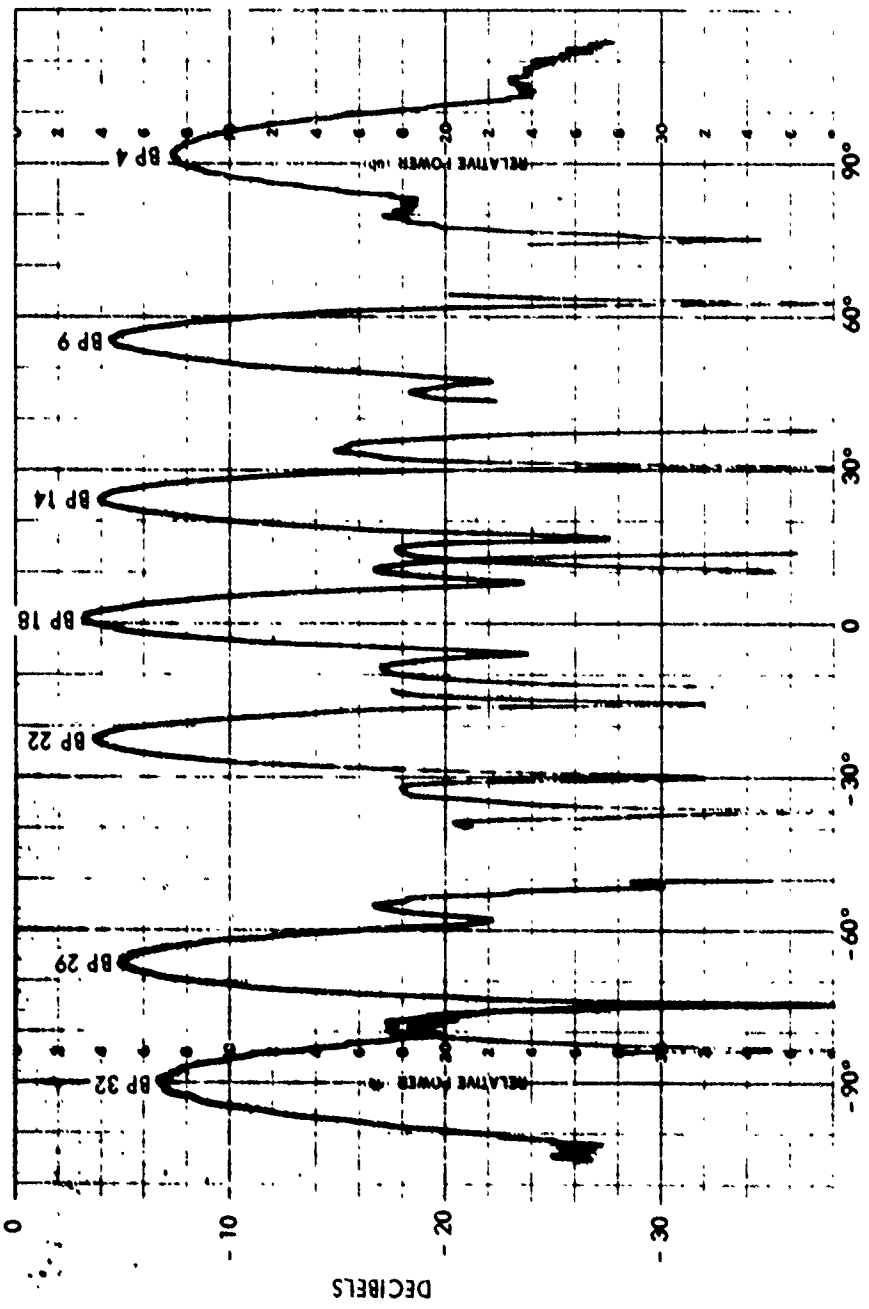

Figure 12. WAAFL Measured Radiation Patterns (15 GHz)

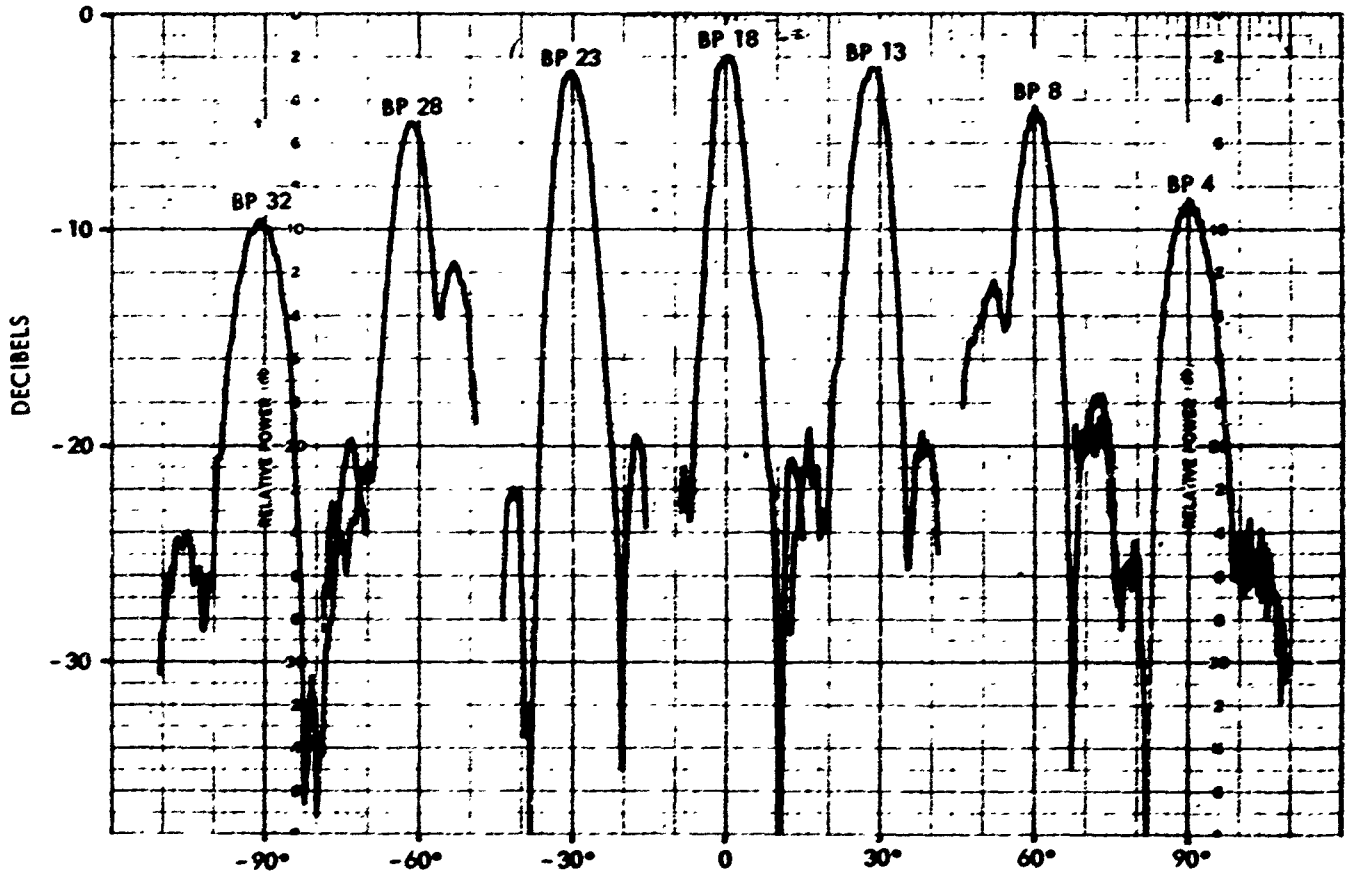

Figure 13. WAAFL Measured Radiation Patterns (18 GHz)

2.2 LENS-FED MULTIBEAM ARRAYS (ROTMAN LENS)

One type of phased array which is capable of generating multiple simultaneous beams from a single array aperture is the lens-fed array[2]. Several types of lens array feeds exist, but the one of concern here is the bootlace lens first described by Rotman and Turner[3] and illustrated in figure 14. This type is characterized by a parallel-plate region and RF cables of specified length connecting the array to the parallel-plate region. The geometry of the lens and cable lengths is so designed that all ray paths from a plane wavefront (beam 1) to beam ports no. 1, 4 and 7 are of identical length, giving a total of three perfect-focus beam ports. Departure from perfect focus at intermediate beam ports (nos. 2, 3, 5, and 6 in figure 14) can usually be made negligible.

The lens-fed array is a quasi-optical device which depends on differing RF path lengths for its focusing properties, rather than on phase shifters (which are constant with frequency). As a result, scanned beam positions in space tend to be independent of frequency (no beam squint). Thus, lens-fed arrays can have very wide bandwidth, typically an octave or more.

Lens-fed arrays also have the capability for multiple simultaneous beams, with each beam enjoying the full aperture gain. Each beamport in figure 14 is essentially an independent antenna with a beam pointing in a fixed direction in space. Any beam coupling which occurs is normally significant only for adjacent beamports, and can be made small. This multibeam capability renders the lens-fed array equivalent to several conventional antennas.

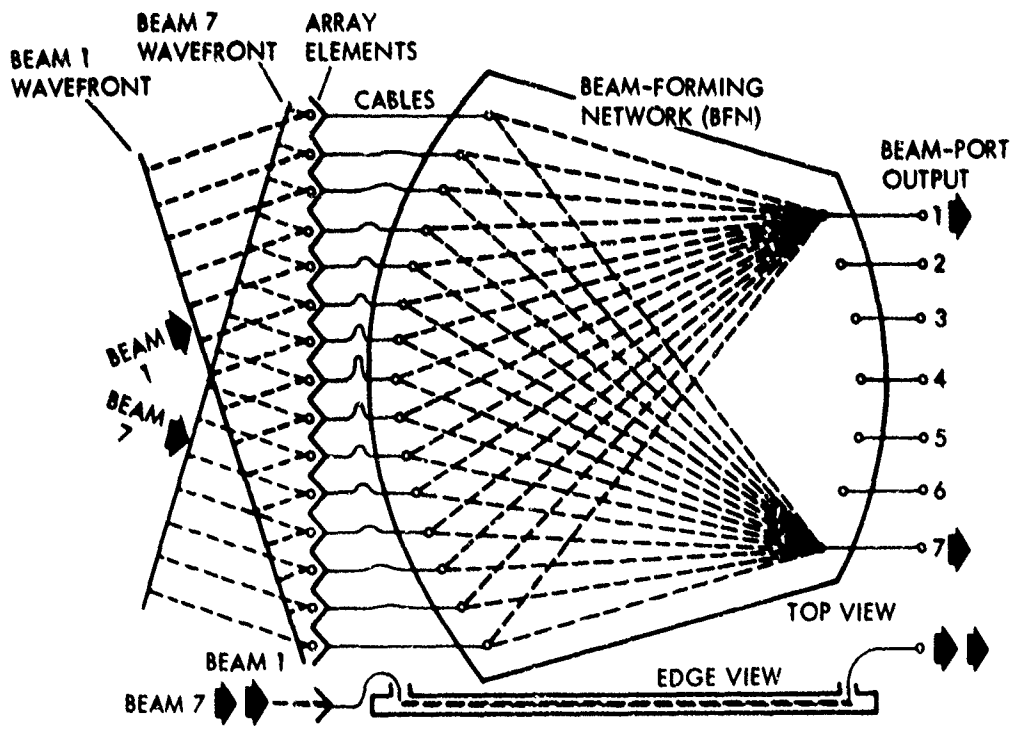

Figure 14. Rotman Lens Beam-Forming Network

While it is convenient to explain the operation of a Rotman lens in terms of a parallel-plate region fed with coaxial probes in front of a reflecting ground plane, this construction has been largely superseded at Raytheon ESD by printed-circuit techniques. Lenses are constructed as either stripline or microstrip devices, and employ substrate materials with dielectric constant ϵ ranging from 2.5 (teflon-fiberglass) to 230 (cadmium titanate) or higher, depending on the specific electrical and mechanical design constraints of each system application. The linear dimensions of an RF lens are reduced by a factor equal to $\sqrt{\epsilon}$. Here the probe and backwall transition from coaxial cable is replaced by a printed-circuit "horn" which provides the transition into the low impedance of the parallel-plate region. The ceramic substrates yield excellent electrical and mechanical performance under environmental stresses, and the designs are highly reproducible due to the etched-circuit techniques employed. Figure 15 shows an example of a printed lens.

The design of lens-fed arrays is highly mechanized in a set of computer programs which determine the RF circuit coordinates of the photo negative used in the etching process, and also plot the far-field beam patterns of the lens-fed array.

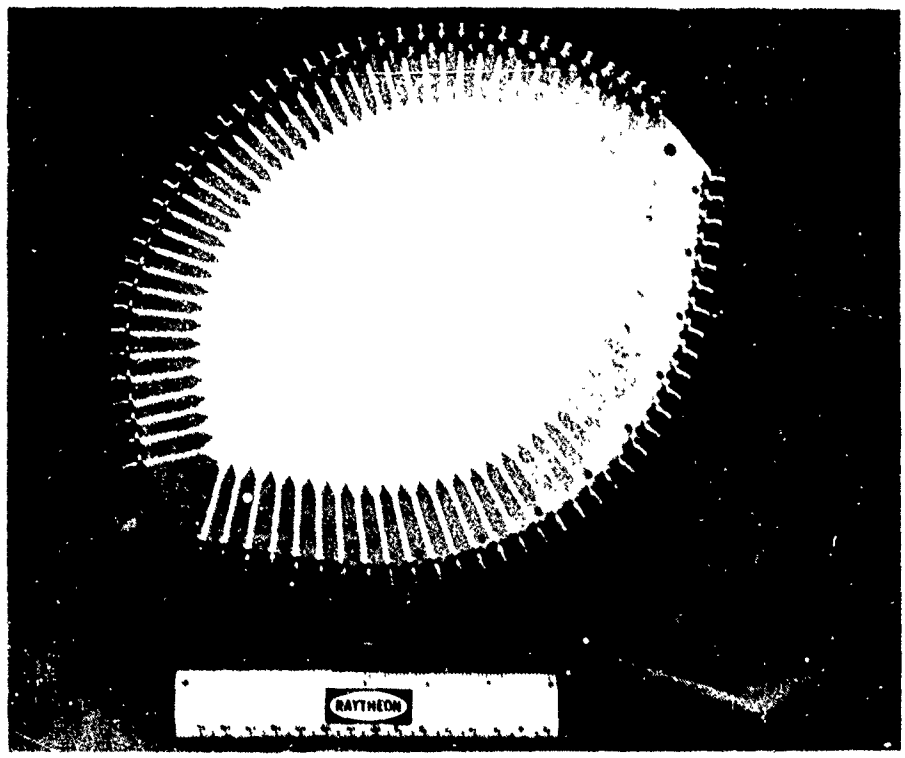

11478

Figure 15. Printed Stripline Lens

2.3 TWO-DIMENSIONAL MULTIBEAM ARRAYS

A two-dimensional multibeam array can be constructed of multiple linear arrays (rows and columns of elements on a surface) and a two-axis-scan beam-forming network composed of multiple two-dimensional Rotman lenses. The basic arrangement is illustrated schematically in figure 16. The columns of radiating elements are each fed by a vertical lens. Each column would then, by itself, form a cluster of conical fan beams stacked in the vertical plane. The corresponding beam ports on each of the vertical lenses are led through RF cables of appropriate lengths to a stack of similar horizontal lenses. The lenses of the second stack provide beam forming (focusing) for all elements in the array face in the horizontal plane. Each beam port of the second stack then corresponds to a pencil beam in space. The azimuth and elevation beamwidths of the beams are determined by the array face dimensions and the operating frequency, and the pointing direction of each beam is established by the geometry of the array and multiple lens beam-forming network, independent of RF frequency.

2.3.1 MULTIPLE TRACKING STEERABLE TELEMETRY TRACKER (MUSTRAC)

The two-dimensional cluster of beams generated by the two stack feed lens described above is illustrated in figure 17. The shaded beams represent the four-beam clusters which enable two-axis monopulse tracking and data reception of (in this case) four simultaneous, independent communications transmitters within the solid angle of array coverage.

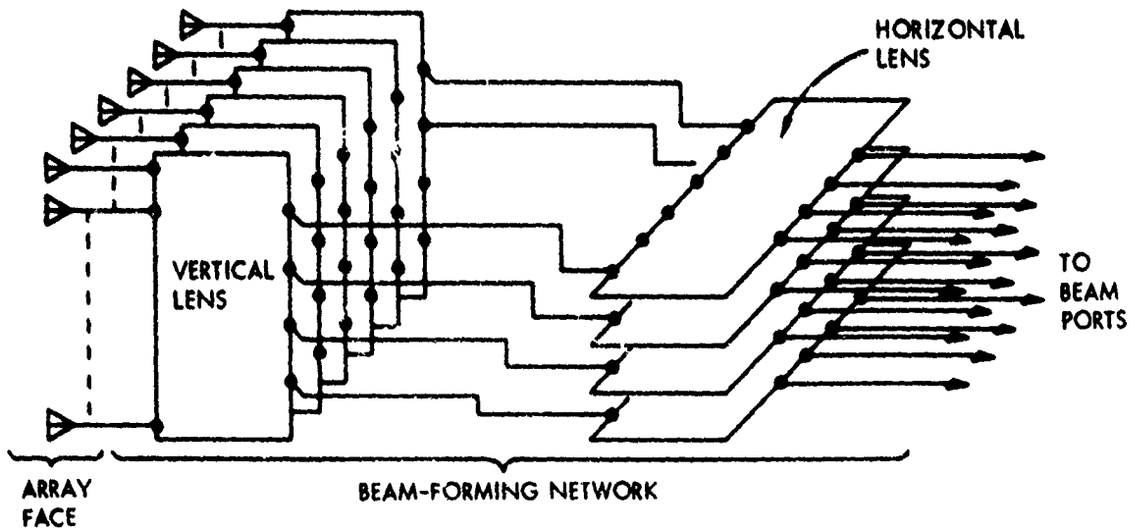

Figure 16. Two-Stack Lens Beam Formation

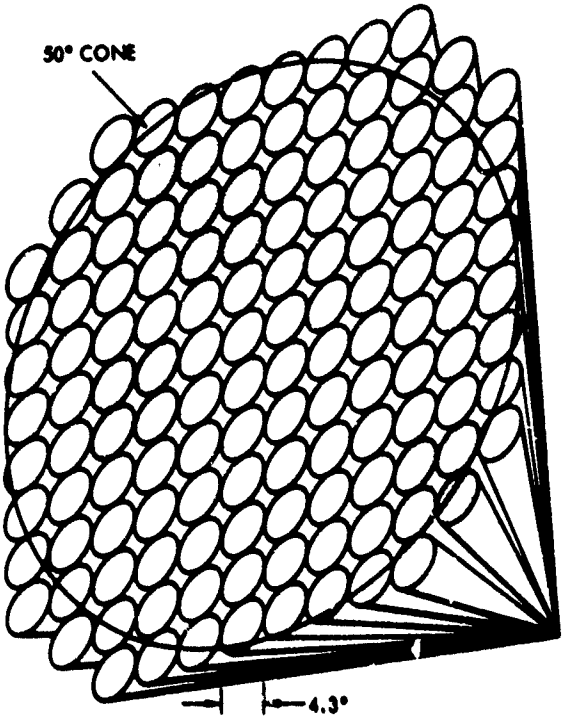

Figure 17. Two-Dimensional Beam Cluster

A two-dimensional multibeam array antenna of this type is shown in figure 18. This array is employed in a multiple-simultaneous-target steerable telemetry tracking system (MUSTRAC) which has satisfactorily completed Air Force evaluation and been in service for several years in the Eastern Test Range.

The 376 circularly polarized array radiating elements are fed by a beam forming network to provide a cluster of 132 pencil beams (4-degree beamwidth) filling a 50-degree cone. The beam forming network is shown in the rear view of the array in figure 19. Measured radiation patterns for one row of beams are presented in figure 20. Appropriate beams from this cluster are selected by means of a PIN diode switching network to form four simultaneous monopulse tracking beams that independently track separate telemetry sources over the 50-degree field of view. A four-beam cluster pattern is shown in figure 21. Note especially the low side-lobe level resulting from a combination of taper and geometry.

Figure 18. MUSTRAC Antenna (Front View)

3758

Figure 19 MUSTRAC Antenna (Rear View, Two-Stack Lenses)

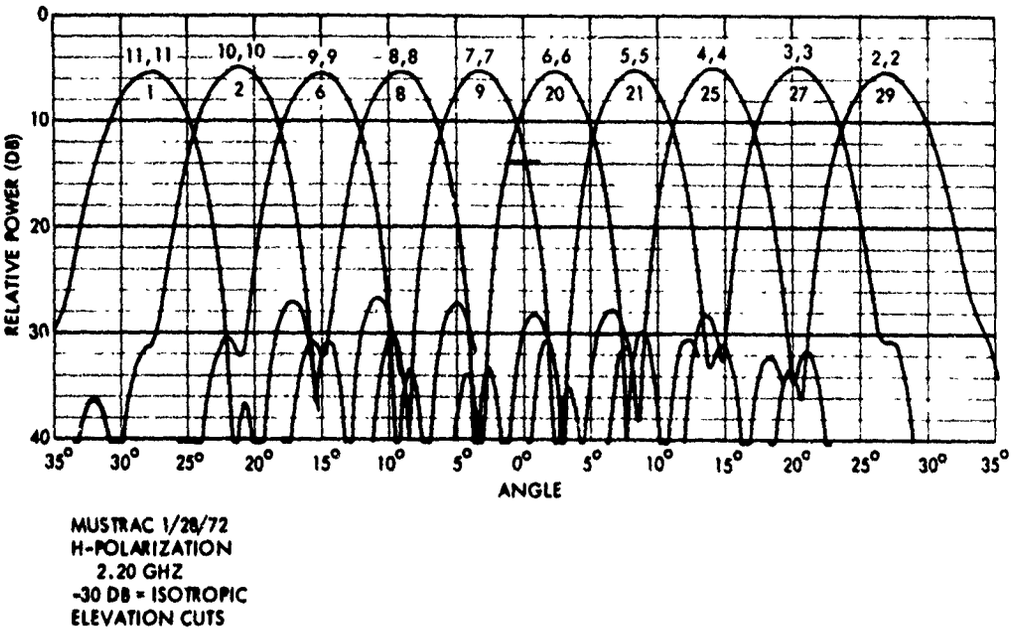

Figure 20. MUSTRAC Measured Patterns

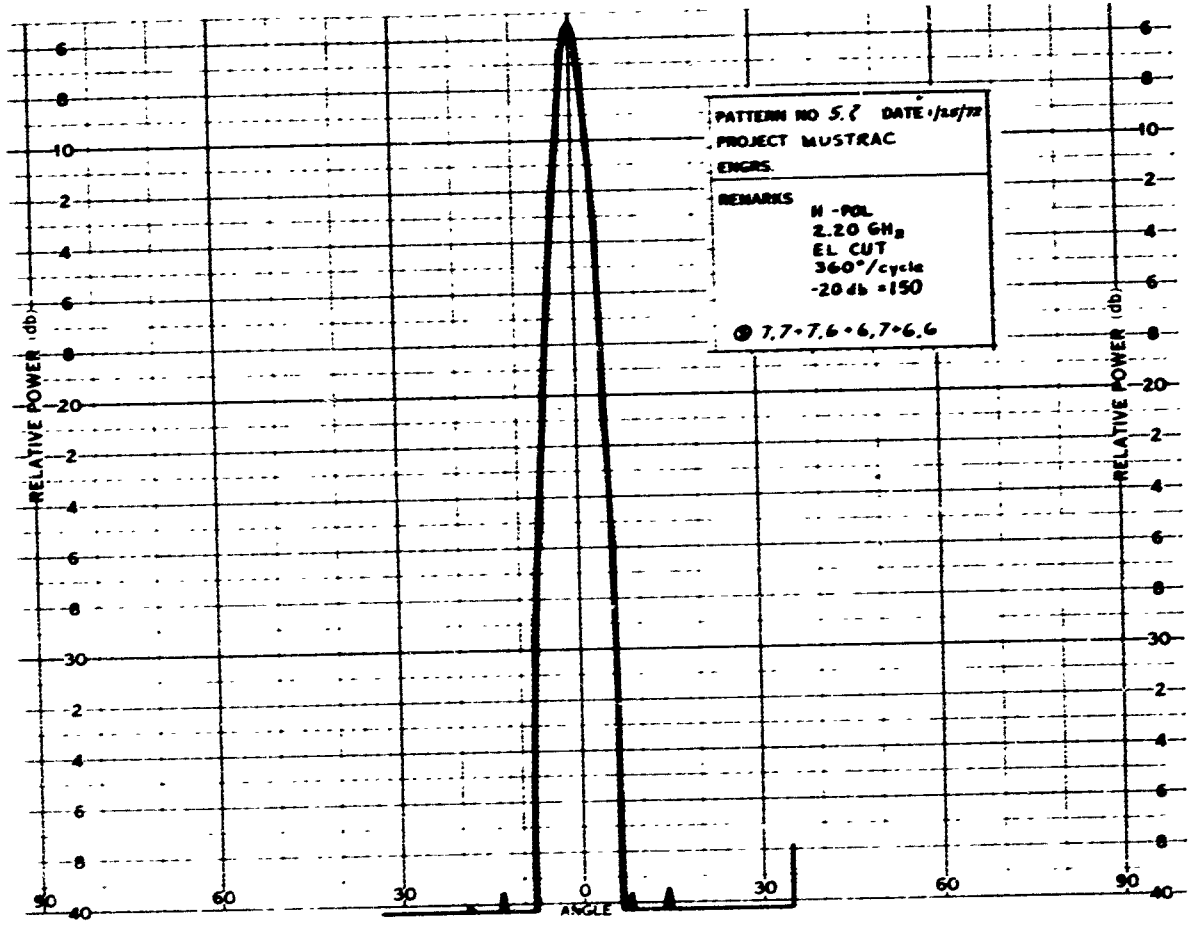

Figure 21. MUSTRAC Measured Four-Beam Cluster

SECTION III
ANALYSIS

This section gives a complete description of the dome and stack of lenses, including their governing equations, mathematical computer models and sources of error. Once identified and defined, the sources of error are the primary objects of consideration in a parametric tradeoff discussion.

3.1 FEED ARRAY ANALYSIS

The dome is a lens-like device with fixed phase delays which vary with angle, θ (figure 22). The physical basis of the analysis uses geometric optics ray path analysis to determine the amplitude and phase distributions, including refractive effects of the dome itself.

Consider a plane wave incident on a hemispherical dome or array-fed lens from a direction, $\hat{N}_2$, where $\hat{N}_2$ is the unit vector defining the incident plane wave propagation direction (figure 22). Then:

$$\hat{N}_2 = -\hat{X} \sin \xi_o - \hat{Z} \cos \xi_o \qquad (1)$$

Due to axial symmetry, we need not consider other incident wave directions. The dome has outer radius, R_2, inner radius, R_1, and scan amplification, K. The centrai angle, $\theta_o = \xi_o/K$, is the ray which will pass through the center of the hemispherical dome.

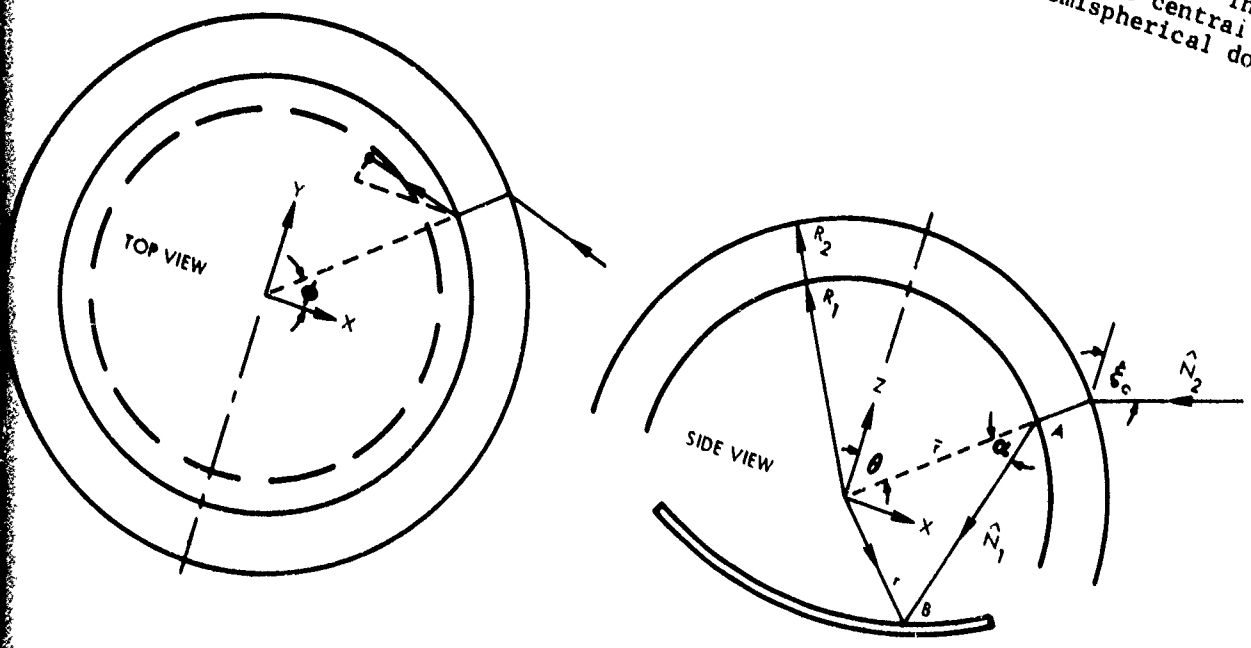

Figure 22. Dome Geometry

The incoming planewave which strikes the outer dome surface (radius, R_2) will be refracted by the dome so that a new ray path direction, $\hat{N}_1$, will be defined for rays leaving the inner dome surface (radius, R_1). The rays leaving the inner dome surface no longer form a plane wave but are functions of position, $\bar{r}_1$, using position vector notation with $\bar{r}_1$ being the vector from the origin to any point on the inner dome surface. In spherical coordinates, $\bar{r}_1=(R_1, \theta, \phi)$. This being said, the first goal of the dome analysis is to define the new ray path direction, $\hat{N}_1$.

The dome is axially symmetric and has phase delay, P , which is a function only of θ, defined by;

$$\frac{dP}{d\theta} = R_2 \sin (K\theta - \theta) \tag{2}$$

If K is constant with respect to θ, equation (2) can be integrated to yield:

$$P(\theta) = \frac{R_2}{K-1} \left[1 - \cos (K\theta - \theta)\right] \tag{3}$$

Equation (2) relates the phase delay incurred passing through the dome, as a function of θ. A boundary condition of the dome is that the path length variation at the dome surfaces must equal the phase variation caused by the dome, $P(\theta)$. To solve the dome boundary value problem for $\hat{N}_1$, the interior dome ray path direction requires spherical coordinates. As a first step, $\hat{N}_2$ is expressed in spherical coordinates. From (1);

$$\hat{N}_2 = -\hat{x} \sin \xi_o - \hat{z} \cos \xi_o$$

Rectangular to spherical transformation;

$$\hat{x} = \hat{R} \sin\theta \cos\phi + \hat{\theta}\cos\theta \cos\phi - \hat{\phi}\sin\phi$$

$$\hat{y} = \hat{R} \sin\theta \sin\phi + \hat{\theta}\cos\theta \sin\phi + \hat{\phi}\cos\phi$$

$$\hat{z} = \hat{R} \cos\theta - \hat{\theta}\sin\theta$$

Then;

$$\hat{N}_2 = \hat{R} \left[\sin\theta \cos\phi \sin\xi_o + \cos\theta \cos\xi_o\right] - \hat{\theta}\left[\cos\theta \cos\phi \sin\xi_o - \sin\theta \cos\xi_o\right]$$

$$+\left[\hat{\phi} \sin\phi \sin\xi_o\right] \tag{4}$$

Since $\hat{N}_1$ does not vary in the ϕ direction,

$$N_1 \cdot \phi \text{ component} = \hat{N}_1 \cdot \hat{\phi}.$$

but: $R_1\hat{N}_1 = R_2\hat{N}_2$ in the $\hat{\phi}$ direction

so: $R_1\hat{N}_1 \cdot \hat{\phi} = R_2\hat{N}_2 \cdot \hat{\phi}$

or: $N_{1_\phi} = \frac{R_2}{R_1} \hat{N}_2 \cdot \hat{\phi} = \frac{R_2}{R_1} \sin\phi \sin\xi_o$

Thus, $\boxed{N_{1_\phi} = \frac{R_2}{R_1} \hat{N}_2 \cdot \hat{\phi} = \frac{R_2}{R_1} \sin\phi \sin\xi_o}$ (5)

The ratio R_2/R_1 expresses the fact that the dome transmits the incoming wave along radial transmission lines from the outer surface, R_2, to the inner surface, R_1.

In the θ direction, both dome phase delay and incident plane-wave phase variation are present:

$$R_1\hat{N}_1\cdot\hat{\phi} = R_2\hat{N}_2\cdot\hat{\theta} + dP/d\theta = R_1 N_{1_\theta}$$

or:
$$N_1 = \frac{R_2}{R_1}\hat{N}_2\hat{\theta} + \frac{1}{R_1}\cdot\frac{dP}{d\theta} \tag{6}$$

Then, from (2) and (4):

$$N_{1_\theta} = \frac{R_2}{R_1}\left[-\cos\theta\cos\phi\sin\xi_o + \sin\theta\cos\xi_o + \sin(K\theta - \theta)\right] \tag{7}$$

or:

$$N_{1_\theta} = \frac{R_2}{R_1}\left[\sin(K\theta-\theta) - \sin\xi_o\cos\theta + \cos\xi_o\sin\theta + \sin\xi_o\cos\theta - \sin\xi_o\cos\phi\cos\theta\right]$$

$$= \frac{R_2}{R_1}\left[\sin(K\theta - \theta) - \sin(\xi_o-\theta) + \sin\xi_o(1-\cos\phi)\cos\theta\right]$$

Then:
$$\boxed{N_{1_\theta} = \sin\alpha + \frac{R_2}{R_1}\left[\sin\xi_o(1 - \cos\phi)\cos\theta\right]} \tag{8}$$

where:
$$\boxed{\sin\alpha = \frac{R_2}{R_1}\left[\sin(K\theta - \theta) - \sin(\xi_o-\theta)\right]} \tag{9}$$

To complete the $\hat{N}_1$ derivation, N_{1_R} must be found. But:

$$\boxed{N_{1_R} = \hat{N}_1\cdot\hat{R} = -\sqrt{1-N_{1_\phi}{}^2 - N_{1_\theta}{}^2}} \tag{10}$$

In rectangular coordinates:

$$N_{1_x} = N_{1_R}\sin\theta\cos\phi + N_{1_\theta}\cos\theta\cos\phi - N_{1_\phi}\sin\phi$$

$$N_{1_y} = N_{1_R}\sin\theta\sin\phi + N_{1_\theta}\cos\theta\sin\phi + N_{1_\phi}\cos\phi$$

$$N_{1_z} = N_{1_R}\cos\theta - N_{1_\theta}\sin\theta$$

It must be remembered that $\hat{N}_1$ is merely a unit vector from the point of contact on the inner dome surface (A in figure 22) to the spot of intercept with the array feed surface (B in figure 22). The next task is to determine the path length L from A to B in figure 22. Put simply, in vector notation (figure 22):

$$\bar{r} = \bar{r}_1 + L\hat{N}_1.$$

where $\bar{r}$ is the vector to the array surface intercept point from the origin. The feed array arc is defined by:

- the distance from the origin of its center of curvature ($R_4\hat{Z}$), and
- its radius of curvature or distance from the point $R_4\hat{Z}$.

$$\left|\bar{r} - R_4\hat{Z}\right|^2 = R_5^2 \tag{12}$$

from (8) :

$$\left|\bar{r}_1 + L\hat{N}_1 - R_4\hat{Z}\right|^2 = R_5^2$$

Expanding:

$$\left|\bar{r}_1^2 + 2\bar{r}_1 L\,\hat{N}_1 - 2\bar{R}_1 r_4\hat{Z} + L^2\hat{N}_1^2 - 2LR_4\hat{N}_1\hat{Z} + R_4^2\hat{Z}^2\right| = R_5^2$$

$$r_1^2 + L^2 + R_4^2 - 2R_4\bar{r}_1 \cdot \hat{Z} - 2LR_4\hat{N}_1 \cdot \hat{Z} + 2L\bar{r}_1 \cdot \hat{N}_1 = R_5^2.$$

then: $$L^2 = R_5^2 - r_1^2 - R_4^2 + 2R_4 r_1 \cos\theta - 2L\left[R_4\,(\hat{N}_1 \cdot \hat{Z}) - (\bar{r}_1 \cdot \hat{N}_1)\right].$$

but: $$R_4\,(N_1 \cdot Z) - (N_1 \cdot r_1) = N_1\,(R_4 Z - r_1).$$

then: $$L^2 = R_5^2 - r_1^2 - R_4^2 + 2\,R_4\,r_1\cos\theta + 2L\,\hat{N}_1 \cdot (\bar{r}_1 - r_4\hat{Z}).$$

Put into the form $aL^2 + bL + c = 0^o$:

$$L^2 + \left[2\hat{N}_1 \cdot (\bar{r}_1 - R_4\hat{Z})\right] L - \left[R_5^2 - r_1^2 - R_4^2 + 2R_4 r_1\cos\theta\right] = 0$$

then: $$L = \frac{b + \sqrt{b^2 - 4ac}}{2a};$$

where: $$a = 1,\ b = 2\hat{N}_1 \cdot (r_1 - R_4\hat{Z}),\ C = R_5^2 - R_1^2 - R_4^2 + 2R_4 r_1\cos\theta$$

then: $$L = -N_1 \cdot (r_1 - R_4 Z) + \sqrt{\left[N_1 \cdot (r_1 - R_4 Z)\right]^2 - (R_5^2 - r_1^2 - R_4^2 + 2r_1 R_4\cos\theta)} \tag{13}$$

The intercept point is at (X, Y, Z), where;

$$X = R_1\sin\theta\cos\phi + LN_{1x} \tag{14}$$

$$Y = R_1\sin\theta\sin\phi + LN_{1y} \tag{15}$$

$$Z = R_1\cos\theta + LN_{1z} = R_4 - \sqrt{R_5^2 - x^2 - y^2} \tag{16}$$

This concludes the direct solution, or "receive" case, of the 3-D dome geometry.

Equations (13) through (16) can be programmed for computer directly, as shown in Appendix B.

3.1.1 INDIRECT "TRANSMIT" SOLUTION

The feed lens concept selected for the dome will consist of two stacks of Rotman lenses, a concept first used on MUSTRAC. This approach is similar to row/column steering in phased arrays in that it provides separate stacks of lenses for X-plane and Y-plane beam formation.

Use of the concept requires the ability to specify X, Y (Z is determined by feed array surface equation), and then project the ray path "transmitted" from that point through the dome in the exit plane-wave direction.

In reality, this requires that, for any X, Y, we must be able to determine θ, ϕ of the ray which will intersect the feed array at X, Y. This will require solution of two simultaneous non-linear equations.

3.1.1.1 Derivation of Nonlinear Equations

The appropriate equations for starting are (14), (15) and (16). They can be combined to show:

$$L^2 = (X - R1 \sin\theta \cos\phi)^2 + (Y - R1 \sin\theta \sin\phi)^2 + (Z - R1 \cos\theta)^2, \quad (17)$$

since, of course, $N1 \cdot X^2 + N1 \cdot Y^2 + N1 \cdot Z^2 = 1$ (unit vector).

Combining (14), (15), (16) and equation (5) gives:

$$-X \sin\theta + Y \cos\phi = L \quad N1\phi = L \frac{R2}{R1} \sin\xi_o \sin\phi .$$

Solving for ϕ gives,

$$\phi = \tan^{-1} \left[\frac{Y}{X + L \frac{R2}{R1} \sin\xi_o} \right] . \quad (18)$$

This is a nonlinear equation for ϕ. A similar nonlinear equation for θ can be derived using a different combination:

$$(X \cos\phi + Y \sin\phi) \cos\theta - Z \sin\theta = L \, N1\theta = L \left[\sin\alpha + \frac{R2}{R1} \sin\xi_o (1-\cos\phi) \cos\theta \right].$$

Solving for θ gives:

$$= \tan^{-1} \left(\frac{1}{Z} \left[X \cos\phi + Y \sin\phi - L \frac{\sin\alpha}{\cos\theta} - L \frac{R2}{R1} \sin\xi_o (1 - \cos\phi) \right] \right). \quad (19)$$

When equations (18) and (19) are simultaneously solved, we have the correct solution for θ, ϕ

3.1.1.2 Solution of Nonlinear Equations

Simultaneous solution of two nonlinear equations requires a substantial computer program. The speed and accuracy will be greatly improved if a good initial guess is obtained. A good estimate of θ, ϕ can be obtained from a linear approximation of equations (18) and (19), or equivalent.

Let $\theta_o = \xi_o/K$ be the scan angle, and let $\theta = \theta_o + \Delta\theta$ and $\phi = \Delta\phi$, where $\Delta\theta$, $\Delta\phi$ are assumed to be small so that only linear or first-order terms need be considered.

Substitution and first order approximation gives:

$$\sin\theta \sim \sin\theta_o + \Delta\theta \cos\theta_o , \tag{20}$$

$$\cos\theta \sim \cos\theta_o - \Delta\theta \sin\theta_o ,$$

$$\sin(K\theta - \theta) \sim \sin(K\theta_o - \theta_o) + (K-1)\Delta\theta \cos(K\theta_o - \theta_o),$$

$$\sin(K\theta_o - \theta) \sim \sin(K\theta_o - \theta_o) - \Delta\theta \cos(K\theta_o - \theta_o),$$

and: $$\sin\alpha \sim \frac{R2}{R1} K\Delta\theta \cos(K\theta_o - \theta_o).$$

The length, L_o for $\theta = \theta_o$ and $\phi = \phi_o$ is:

$$L_o = R1 - X \sin\theta_o - Z \cos\theta_o, \tag{21}$$

and for other angles:

$$L \sim L_o - \frac{R1}{L_o}\left[\Delta\theta(X\cos\theta_o - Z\sin\theta_o) + Y\Delta\phi\sin\theta_o\right]. \tag{22}$$

From observation, it seems that θ will be relatively independent of ϕ, so $\Delta\theta$ is approximated first. From equation (19), eliminating higher order terms of $\Delta\theta$ and $\Delta\phi$, we have:

$$(X + Y\Delta\phi)(\cos\theta_o - \Delta\theta\sin\theta_o) - Z(\sin\theta_o + \Delta\theta\cos\theta_o)$$

$$= \left\{L_o - \frac{R1}{L_o}\left[\Delta\theta(X\cos\theta_o - Z\sin\theta_o) + Y\Delta\phi\sin\theta_o\right]\right\}$$

$$\cdot K\frac{R2}{R1}\Delta\theta\cos(K\theta_o - \theta_o)$$

$$X\cos\theta_o - Z\sin\theta_o + Y\Delta\phi\cos\theta_o = \Delta\theta\left[L_o \cdot K\frac{R2}{R1}\cos(K\theta_o - \theta_o)\right.$$

$$\left. + X\sin\theta_o + Z\cos\theta_o\right].$$

If we let $\Delta\phi = 0$, we have (substituting for L_o)

$$\Delta\theta \sim \frac{X \cos\theta_o - Z \sin\theta_o}{X \sin\theta_o + Z \cos\theta_o + K \frac{R2}{R1} \cos(K\theta_o - \theta_o)\left[R1 - X \sin\theta_o - Z \cos\theta_o\right]} \tag{23}$$

This angle $\Delta\theta$ ($\theta = \theta_o + \Delta\theta$) will be used as the initial guess for θ. Similarly, from equation (18), we obtain for $\Delta\phi$,

$$-X\,\Delta\phi + Y = \left[L_o - \frac{R1}{L_o}\,\Delta\theta\,(X \cos\theta_o - Z \sin\theta_o)\right] \frac{R2}{R1} \sin\xi_o\,\Delta\phi$$

$$\Delta\phi \sim \frac{Y}{X + \left[L_o - \frac{R1}{L_o}\,\Delta\theta(X \cos\theta_o - Z \sin\theta_o)\right] \frac{R2}{R1} \sin\xi_o} \tag{24}$$

Both $\Delta\theta$, $\Delta\phi$ are in radians. For a simpler expression, $\Delta\theta = 0$ can be used in equation (24).

This gives a good initial guess of the values of θ, ϕ needed for any specified X, Y. After the initial guess, a least-squares minimization or Gaussian minimization approach can be used to reiterate $\Delta\theta, \Delta\phi$ until a solution is found. Since the initial guess is good, least squares should converge rapidly.

Finally the equations used for calculating total phase path length in the receiver case remain valid in the transmitter case. By subtracting the phase path length corresponding to the point (X, Y, Z) = (0, 0, 0) given by the formula,

$$R_1 - R_4 \cos\theta_o + \sqrt{\left[R_1 - R_4 \cos\theta_o\right]^2 + 2R_1 R_4 \cos\theta_o} + \frac{R_2}{R - T}\left[1 - \cos(\xi_o - \theta_o)\right]$$

from each of the phase path lengths, we arrive at the phase delay at each point (X, Y, Z) of the feed array.

For lens design, it is also necessary to calculate the amplitude weight function

$$W(X, Y, \xi_o) = \lim_{r \to o} \sqrt{\frac{S'(X, Y, \xi_o)}{S(X, Y, \xi_o)}}$$

where $S(X, Y, \xi_o)$ is the area of the disc of radius r centered at (X, Y) in the xy plane and $S'(X, Y, \xi_o)$ is the area of the image of that disc in the uv plane.

3.2 LENS SYSTEM

Several three-dimensional lens feed formats were considered for the 3-D dome/Rotman lens antenna system. The three-dimensional bootlace lens and the "MUSTRAC" style format of stacking single lenses were considered to be most promising. The complete analysis of the 3-D bootlace lens system is included in Appendix A. This lens is compact and efficient, but the phase error resulting at the scan angles required by the dome antenna system specifications renders this approach unattractive for hemispherical coverage.

The MUSTRAC approach of stacking lenses as discussed in Section II, was determined to be the best method of feeding the dome for minimum phase error with hemispherical coverage and octave bandwidth.

Figure 23 illustrates the lens configuration with the dome feed array. Included are cable connections between selected lens sets, expressly for the purpose of illustrating orientation. As an example to illustrate the correspondence between excitation of a particular beamport and pointing of a beam in a particular direction, figure 23 shows an example in which an outer beamport of the third lens from one end is excited. Note that only the array ports of that third lens of the lower stack are excited to produce a phase ramp across that row of ports. This row of array ports is connected to the third beamport from the edge of all lenses on the upper stack of lenses. Each lens on the upper stack, then, produces a "ramped" phase distribution on its array port surface, to excite the entire upper stack array port surface. Note that the phase ramp contributed by the single lens on the lower stack is imposed on the array port distributions of the upper stack, orthogonal to the phase ramps produced by the lenses of the upper stack. Thus, the normal to the phase distribution surface is pointed somewhat toward the diagonal of the upper stack. The phase distribution is transmitted through cabling directly to the dome array feed surface. Once at the array feed surface, the phase front behaves, as described in the dome analysis section, to point a beam outside the dome in the direction indicated in figure 23. Before all considerations are discussed as to optimum lens stack configuration for least phase error and best efficiency and minimum distortion, a discussion of the unique method of design for dome antenna application is in order.

3.3 ROTMAN LENS DESIGN

Behind each row of elements in both orthogonal directions is a Rotman feed lens. The Rotman lens used in the dome/Rotman lens antenna system differs from the typical Rotman lens in two important ways:

1) The array fed by each lens is concave;
2) The wavefront required by the array is curved, as determined by the dome geometry.

Thus, the classic design equations for a Rotman lens used to excite a linear array of elements to propagate a plane wave is not appropriate. A set of Rotman lenses specially designed to suit the dome geometry must be considered.

The Rotman lens geometry is shown in figure 24. The feed array must have a defined length or distance parameter, S. Three focal points are chosen, at 0^{o} and $\pm\alpha$. The center of the arrayport arc is the origin. The ratio of focal distance, F, to maximum array dimension, S_{max}, relates the lens size to array size ratio, η_{max}:

$$\eta_{max} = \frac{S_{max}}{F} \tag{25}$$

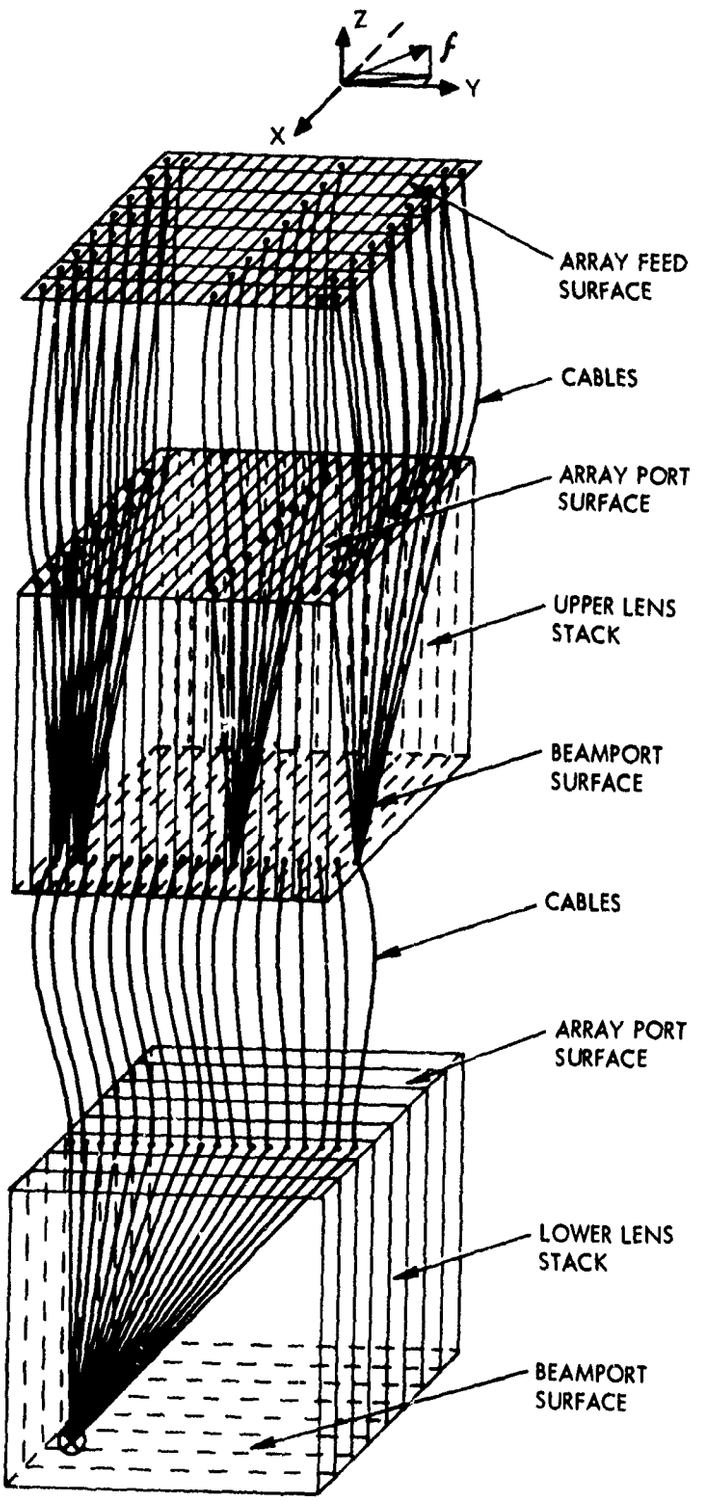

Figure 23. 3-D Dome Lens Stack

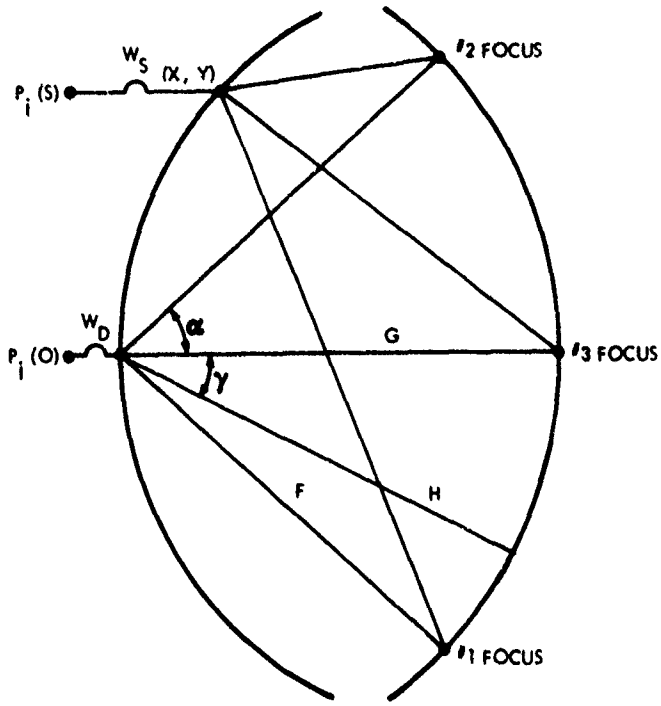

Figure 24. Geometry of Rotman Lens for Arbitrary Phase Fronts

Three arbitrary phase fronts generated by the WAAFL are defined as $P_1(S)$, $P_2(S)$ and $P_3(S)$ for the three focal points (F,α), $(F,-\alpha)$ and $(G,0)$, respectively. It is assumed that $P_1(0) = P_2(0) = P_3(0) = 0$. In the case of the array-fed lens, focal points are selected for maximum scan angles, $\pm\xi_1$ and zenith angle $\xi = 0$. The arbitrary phase fronts are then the path length differentials from the external wavefronts to the feed array. The three path-length equations for the Rotman lens are:

$$F+W_o = (F\cos\alpha - X)^2 + (F\sin\alpha + Y)^2 + W(S) + P_1(S) \tag{26}$$

$$F+W_o = (F\cos\alpha - X)^2 + (F\sin\alpha - Y)^2 + W(S) + P_2(S) \tag{27}$$

$$G+W_o = (G-X)^2 + Y^2 + W(S) + P_3(S) \tag{28}$$

Since uniform changes of path length cannot change the performance, let W_o equal zero in the analysis. From (26) and (27):

$$Y = \frac{P_1(S) - P_2(S)}{4F\sin\alpha}\left[P_1(S) - P_2(S) - 2F) + 2W\right] = Y_o + Y_1 W. \tag{29}$$

From (3-8), (3-9), and (3-10):

$$X = \left[1/2\ (G-F\cos\alpha)\right]\left[\frac{P_1(S)^2}{2} + \frac{P_2(S)^2}{2} - P_3(S)^2 + 2GP_3(S) - FP_1(S) - FP_2(S) + 2W(G-F+P_1 + P_2 - 2P_3)\right] = X_o + X_1 W. \tag{30}$$

Substitution of (29) and (30) into

$$G^2 + X^2 + Y^2 - 2GX = (G-W)^2 + P_3^2 - 2P_3 (G-W)$$

yields a quadratic in W:

$$AW^2 + 2BW + C = D,$$

where: $A = 1-X_1^2 - Y_1^2,$

$B = P_3(S) - G - X_1 G-Y_oY_1 - X_oX_1,$ and

$C = P_3(S)^2 - 2GP_3(S) + 2GX_o - X_o^2 - Y_o^2.$

The solution is

$$W = \frac{-B \pm \sqrt{B^2 - AC}}{A}. \qquad (31)$$

This completes the lens design. The amount of path length error at beamports not at the three focal points depends on P (S,ξ) of the dome and L (S,γ,H) of the lens,

where L (S,γ,H) is the path length provided by the lens:

$$L\ (S,\gamma,H) = (H\ \cos\gamma - X)^2 + (H\ \sin\gamma + Y)^2 + W - H \qquad (32)$$

where: γ = beamport arc angle,

H = beamport distance at angle.

The total path error is

$$P(S;\xi) + L(S,\gamma,H) = E(S;\xi).$$

3.4 LENS STACK DESIGN CONSIDERATIONS

As an early joint task in this analysis phase of the dome contract, Sperry was to provide Raytheon with phase and amplitude distribution data over the surface of a flat-feed array for various scan angles (ξ). Then, Raytheon was to provide the lens system design which would provide the required distributions to the array feed surface corresponding to the appropriate scan angle. In order to maintain concurrence with the basic dome parameters chosen by Sperry for the generation of their array feed distribution data, the following dome parameters were chosen;

R_0 = 6 inches,

R_1 = 9 inches,

R_2 = 11.25 inches, and

K = 1.5.

These parameters produce array feed distribution data on a flat surface which closely agrees with the data provided by Sperry. As discussed in Section I, the feed array surface chosen for the dome was spherical rather than flat, in order to minimize phase error and amplitude distortion.

In order to provide the most nearly constant beamwidth possible as a function of azimuth angle (ϕ), the array feed is to be circular, rather than the square, corresponding to the array ports of the upper stack. To accomplish this, the outer array ports of the outer lenses were loaded to form an approximate circle of 6-inch radius. Since the most severe phase errors occur at the extreme array ports (figure 25), the loading of these ports eliminates the largest contributors of phase error in the array feed.

Because the end beamports of the end lenses correspond to scan angles greater than 90 degrees, these beamports on the lower stack are also loaded. As a check, the planar phase slope resulting from any unloaded (or useful) beamport excitation should not exceed the planar phase slope produced by excitation of an end beamport on the central lens. Thus, as a result of loading the beamports corresponding to scans greater than 90 degrees, a circular set of beamports is available for excitation. To approach best symmetry with respect to zenith, both stacks of lenses contained identical lenses corresponding to each lens position in a stack. It would be possible to adjust the lens designs of one stack to achieve symmetry if symmetry were disturbed, due to some, yet to be defined, source of error. The method of adjustment would be as follows:

- Design the upper stack of lenses using the phase data at the feed array surface.
- Design and lower stack of lenses using the phase data available at the beamports of the upper stack.

3.4.1 SOURCES OF PHASE ERROR

The lens stack concept chosen thus far has associated with the following sources of phase error:

- Conduit error -- associated with path length variations arising from different lens designs for each lens in the upper lens stack.
- Lens implementation error -- The lenses are designed for correct phase focus at only three scan angles; phase errors exist at all other angles.
- Single lens design error -- When using the phase distribution correct for only one row of elements on the feed array to suffice for all rows, the difference between desired and required phase distributions from row to row is the error addressed here.

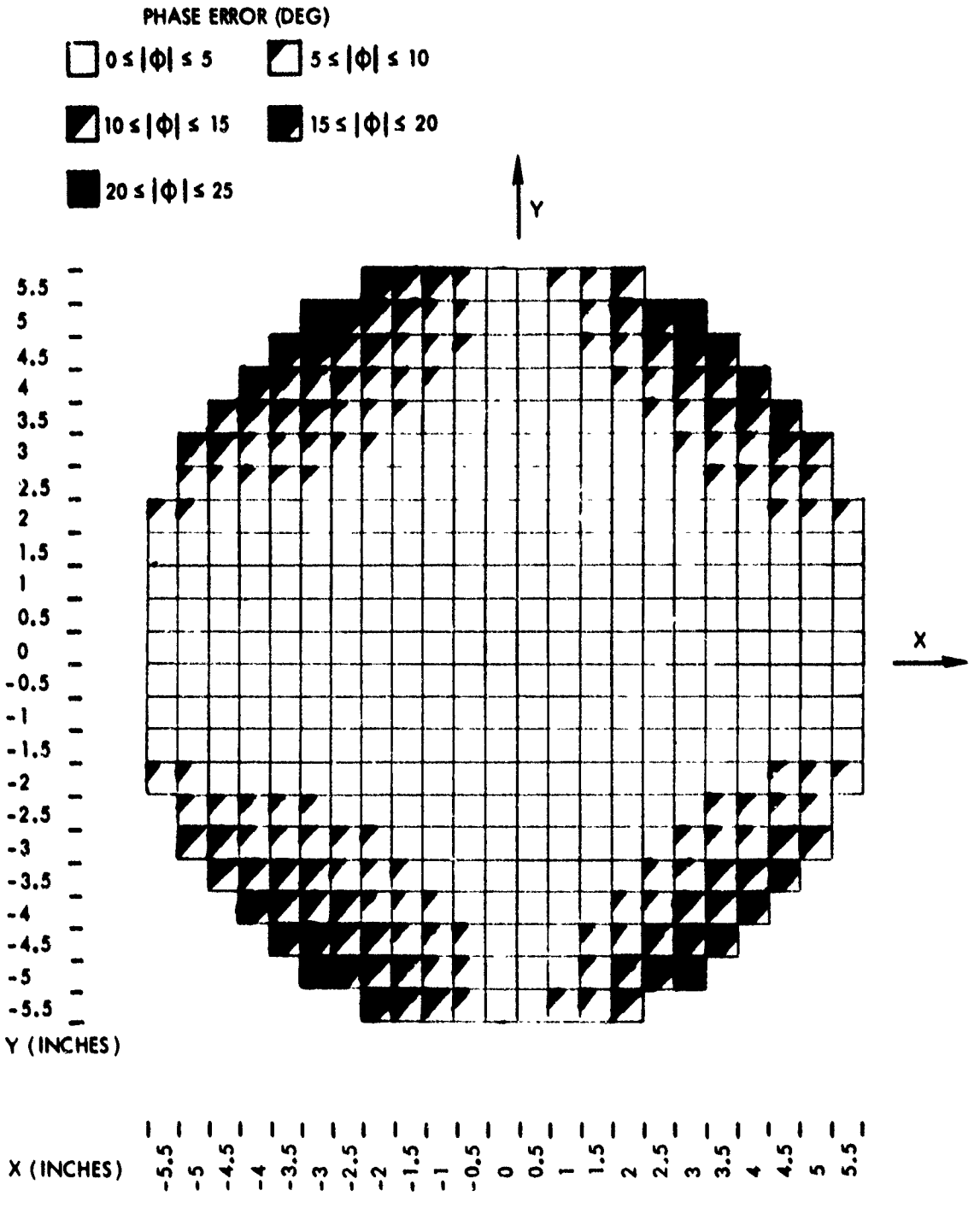

Figure 25. Phase Error Distribution on Array Feed Surface

- Co-phase error -- multiple phase distribution requirements on a single minor axis row of elements to fit varying scan angles along a major axis.

- Minor axis lens error -- Difference in phase distribution required by the dome along a minor axis corresponding to a particular scan angle (ξ), and the phase distribution provided by the lens feeding that minor axis row, corresponding to the slant of the scan plane used.

These errors are discussed in detail below.

3.4.1.1 Conduit Variation in the Case of Unique Lens Designs

It was assumed that the phase distribution contributed by a lens of the lower stack would be held intact at the feed array surface, in spite of the upper stack being between them. This assumption was based on the fact that all lenses in the upper stack are identical, and excitation from a lens of the lower stack would excite the same corresponding beamport number of all the lenses of the upper stack. Thus, the lenses of the upper stack would merely add an equal phase length (or conduit) to the phase distributions of the lower stack (figure 26). If each lens in both stacks is of a unique design, then the path length contributions of the upper lenses vary from their respective beamports to the end of their respective cables. This reshapes the curvature of the phase distribution of the lenses of the lower stack. Furthermore, this phase error source is direction-sensitive, since the lower stack cannot correspondingly interface with the upper stack.

This source of phase error is present only with the unique lens design approach, and must be compared with the phase error experienced using a single lens design for the stack. The worst case of this error should occur at extreme scan angles.

3.4.1.2 Lens Implementation of Dome Distribution Requirements

The phase distribution at the dome feed array for three scan angles is used to design the lenses of the lens stack. The lenses are, consequently, in focus at only three scan angles. The peak-to-peak phase variation across the array ports of the lens at scan angles farthest from angles of perfect focus is the lens implementation error. This type of error occurs regardless of the dome design or decisions concerning lens stack possibilities. The peak-to-peak variation in phase is minimal for dome feed array designs of shallow curvature and lowered slightly below the position contacting the dome (figure 27).

3.4.1.3 Row-to-Row Phase Error When Single Lens Design is Used for Entire Lens Stack

To simplify fabrication of the lens stack, investigation was undertaken of the phase error resulting from use of the lens design of one (well chosen) array row for the lenses to feed all rows. On the surface, it appeared that the maximum error at the worst set of conditions would be approximately 20 degrees, but the single lens stack approach increases the effect of co-phase error and makes variation of other options a much more sensitive maneuver. This source of error is minimized for lens designs for rows chosen well away from a central row, where phase differences are shared between the central row and the outer row.

3.4.1.4 Co-phase Error; Multiple Phase Distribution Requirements on a Single Minor Axis Row of Elements to Fit Varying Scan Angles Along a Major Axis (Figure 28)

There exists no lens in the stack to provide the phase distribution in rows of the minor axis when scanning in a major axis. The phase distribution from a lens in the minor axis is, of course, fixed and is determined only by the slant of the scan plane of the major axis. Thus, this type of error is worse for scan angles requiring phase curvatures more different from each other, such as zero and 90 degrees The error should be worse at the outer edges of the feed array.

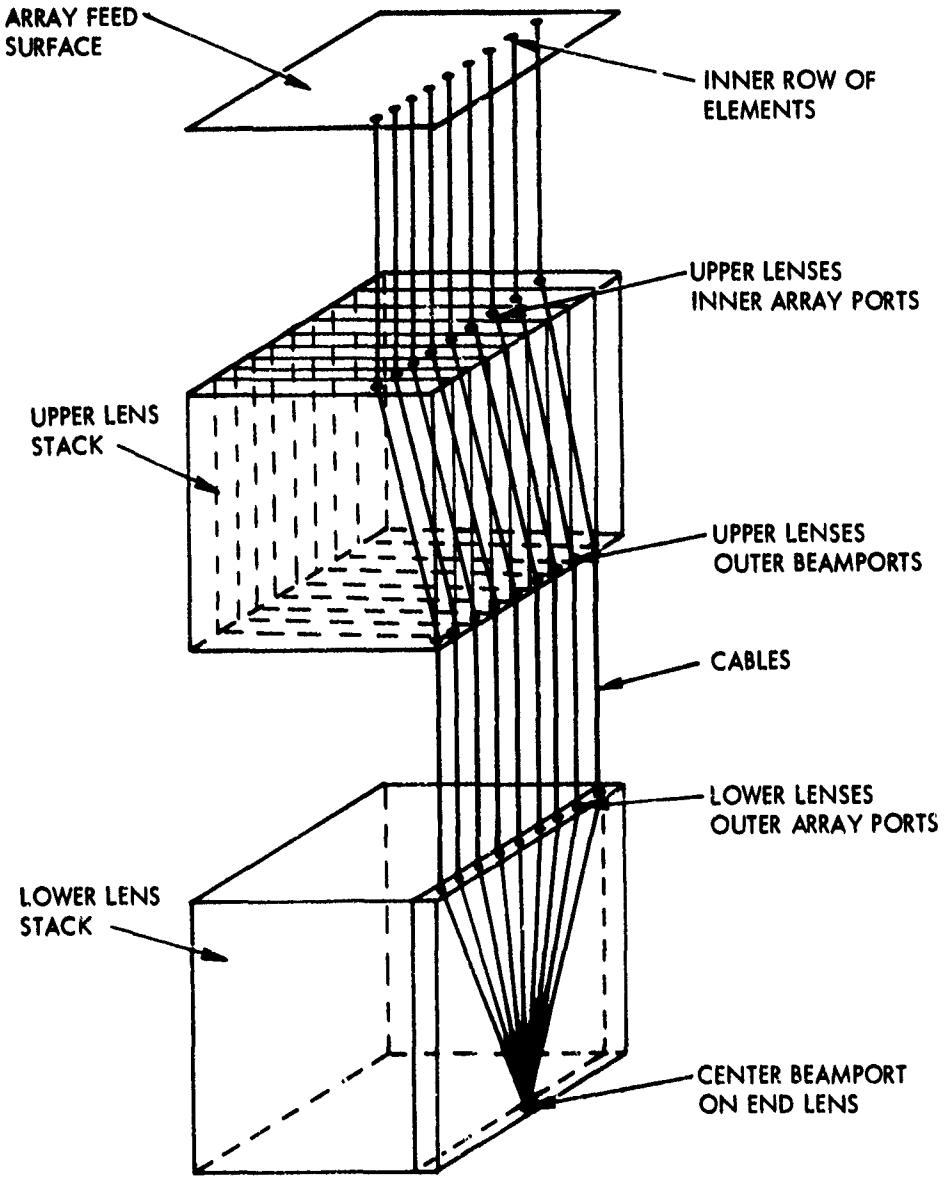

Figure 26. Lens Stack Implementation with Conduit Variation

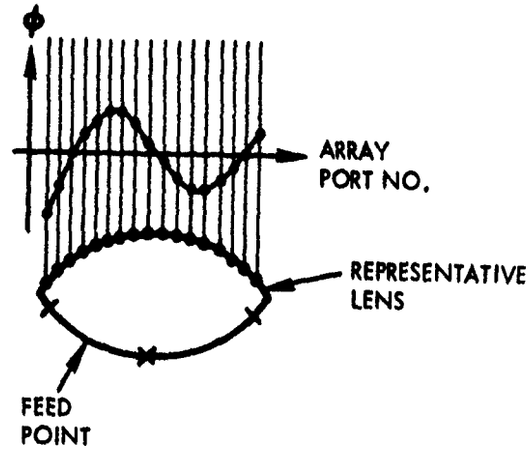

Figure 27. Phase Error of Lens Implementation

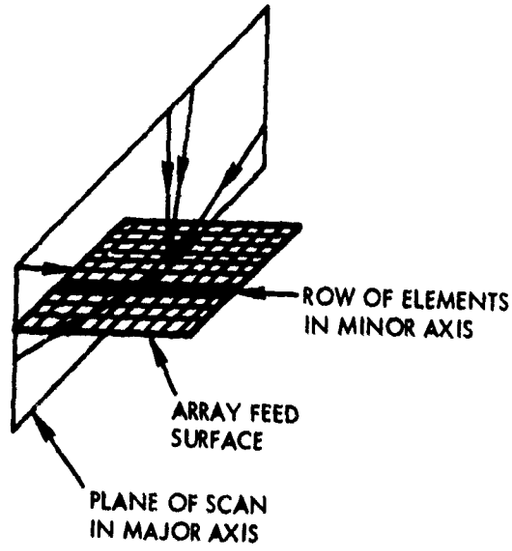

Figure 28. Diagram of Co-Phase Error Distribution

3.4.1.5 Minor Axis Lens Error (Figure 29)

At any particular scan angle (α), the dome design requires a particular phase distribution in a-l rows of elements parallel to the plane of scan (x) and a different phase distribution in all rows of elements perpendicular to the plane of scan (y). There exist lenses to provide phase distributions in rows parallel to the plane of scan, but none for the perpendicular rows. The only phase distribution provided to the rows perpendicular to the plane of scan is that provided by lenses intended to scan in a plane perpendicular to the vertical scan plane of interest. Consequently, the phase distribution provided by this perpendicular set of lenses is determined only by the incline (β) of the scan plane, and is independent of the particular scan angle (α) in that plane. Minor lens error, in this context, is identified as the phase difference between that required by the dome on a minor axis (y) for any scan angle (α) and that provided by the lens in that minor axis row (y) for the scan angle corresponding to the slant of the scan plane (β).

The worst case of this error occurs for $\alpha = 90^{\circ}$ and $\beta = -90^{\circ}$. This source of error is inherent in the stacked lens approach.

The minimization of the phase errors resulting from the error sources described previously is the subject of the next section.

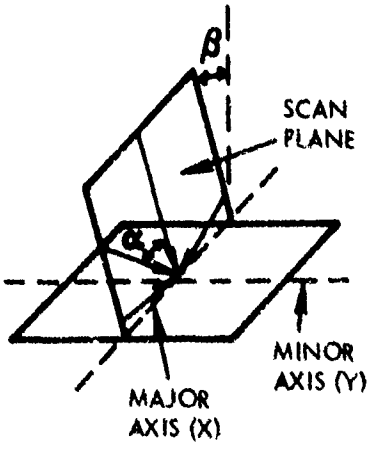

Figure 29 Minor Axis Lens Error

3.5 COMPUTED PERFORMANCE RESULTS

To illustrate the basis for the design tradeoff decisions made, each subsection is titled as a type of phase error to be considered.

3.5.1 CO-PHASE ERROR

This error is discussed in section 3.4.1.4. To reduce co-phase error, the maximum variation in internal scan angle could be reduced. If the external scan angle requirement is fixed at ± 90 degrees, K could be increased to 2 or 3 (from 1.5) and the internal scan requirement cut to 45, or even 30, degrees.

Another technique for co-phase error reduction is lowering of the array feed, while optimizing its curvature for any amount of drop. Lowering the feed has the effect of reducing the internal scan angle, thus reducing co-phase error. As an added benefit, lowering the feed array also changes the shape requirement on the Rotman lenses feeding the array. The lenses approach a much more optimum shape for minimum phase error. Figures 30 and 31 illustrate the lens shapes as a function of array feed drop. Note that the "undropped" feed configuration lens has a much more deeply curved array port and beam port arc than the "dropped" feed lens. This results in greater phase variations across the array port arc, and a greater lens contributed peak to peak phase error. Included in figures 30 and 31 are plots of phase variation versus array port position. Note that the "dropped" array feed configuration produced 69.1 percent of the peak-to-peak phase variation that the "undropped" configuration does. Figure 32 is a contour plot of phase error over the feed array surface, illustrating the cylindrical shape of conduit error at $\xi = 90$ degrees. Figures 33 and 34 illustrate the variation of phase error with respect to array feed drop for $\xi = 90$ degrees and $\phi = 0$ degree (co-phase), and $\phi = 90$ degrees (conduit), respectively. From figures 33 and 34, a drop of 3.3 inches was determined optimum. Figure 35 illustrates co-phase error as a function of minor axis distance from $y = 0$, for a drop of 3.3.

3.5.2 LENS IMPLEMENTATION ERROR

As shown in figures 30 and 31, the phase error contributed by the lens to the total system phase error can be reduced significantly by dropping the feed array with respect to the dome and correspondingly adjusting the feed array curvature. The lens required to properly feed the dome with dropped feed array has much flatter array port and beamport contours than the undropped configuration. Thus, its phase deviations should be greatly reduced.

As discussed earlier, the lens phase error may be further optimized by adjusting all beamports, both radially and laterally.

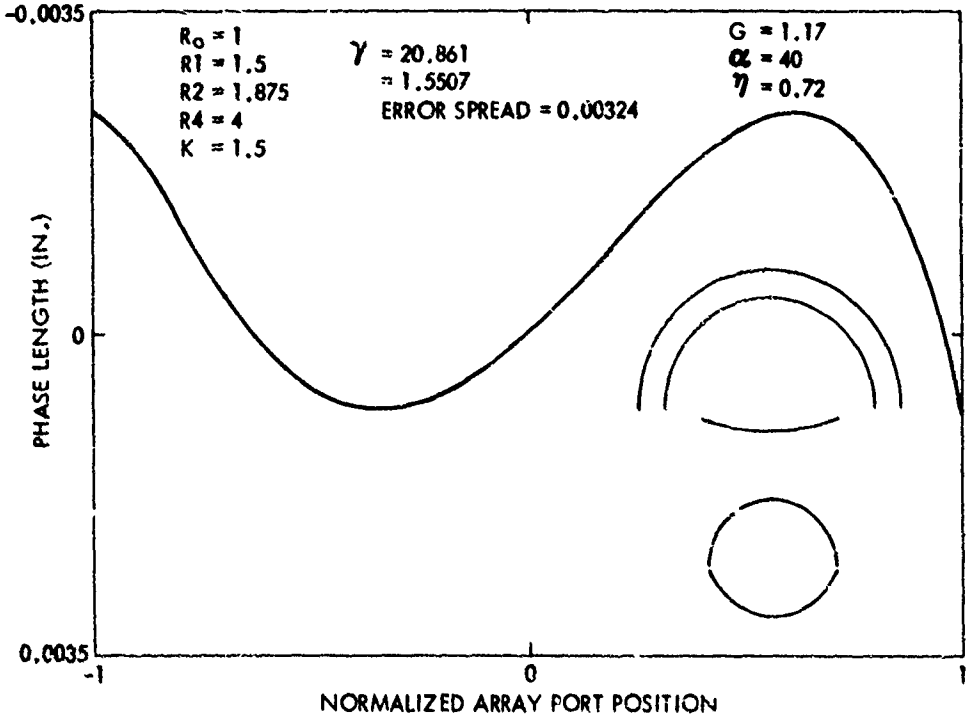

Figure 30. Phase Distribution with "Undropped" Array Feed

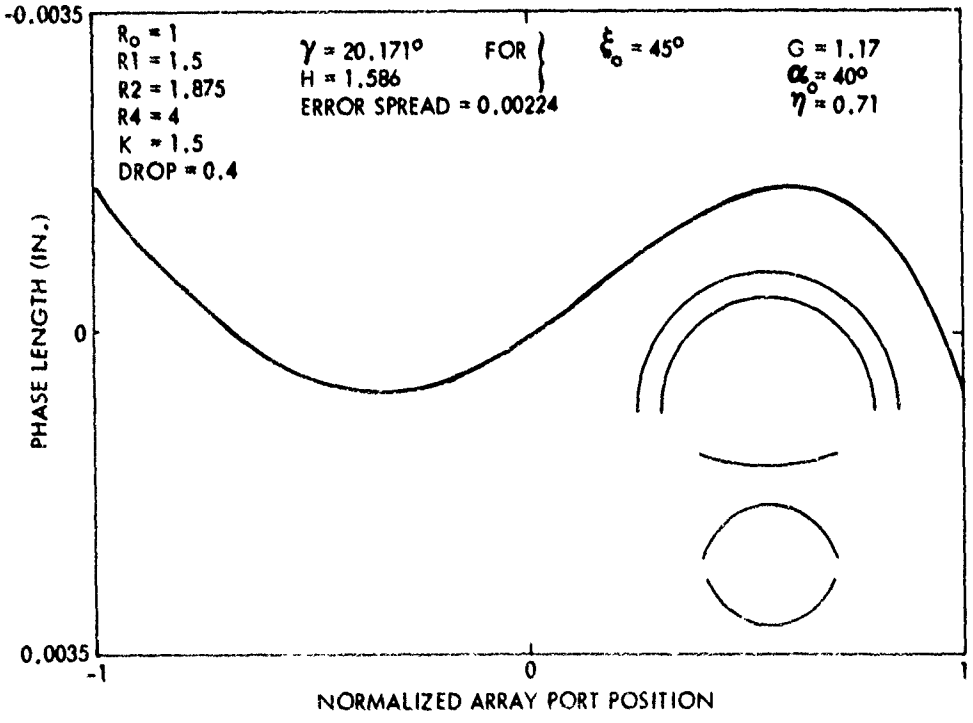

Figure 31. Phase Distribution with "Dropped" Array Feed

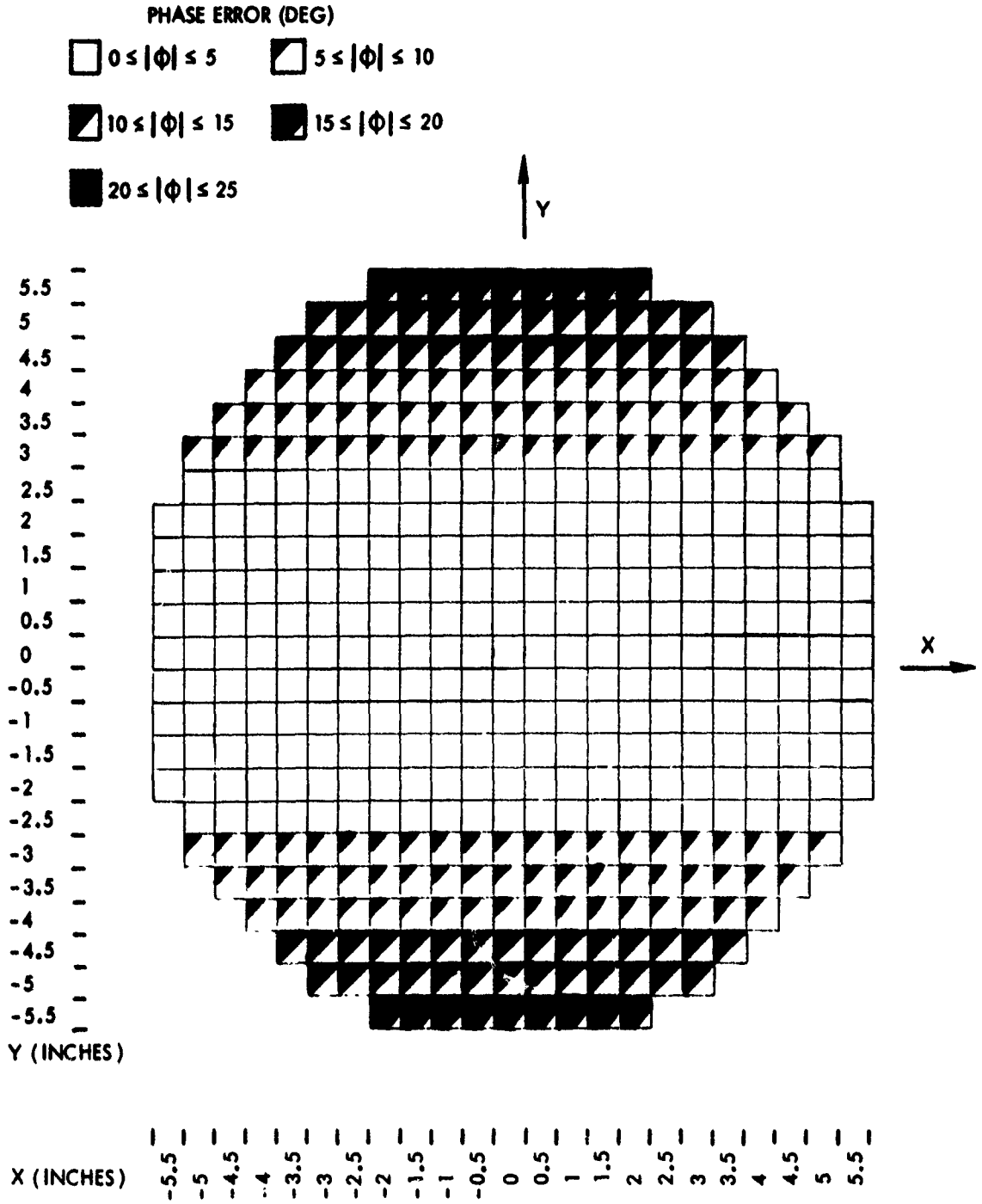

Figure 32. Phase Error for Unique Lens

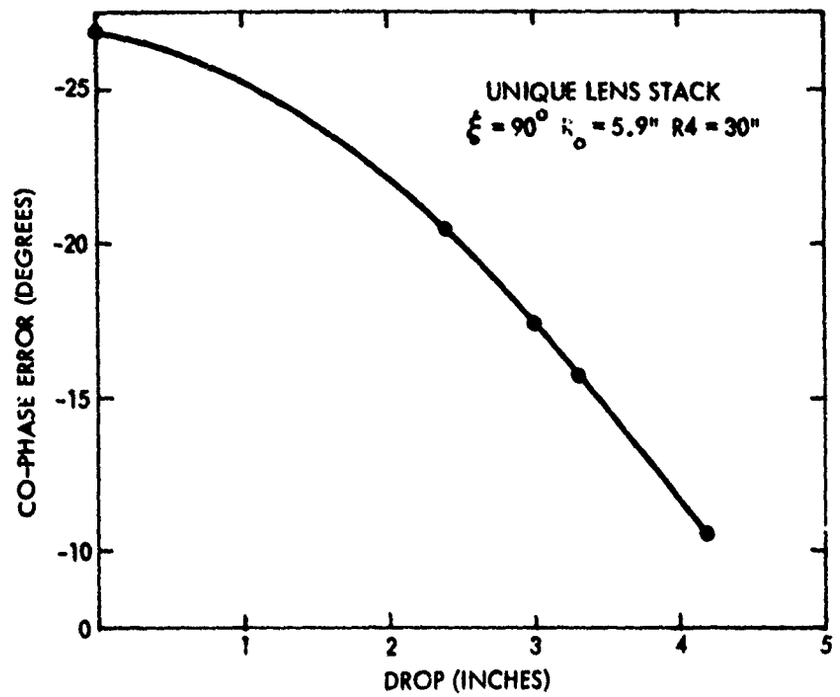

Figure 33. Maximum Co-Phase Error vs Feed Array Drop

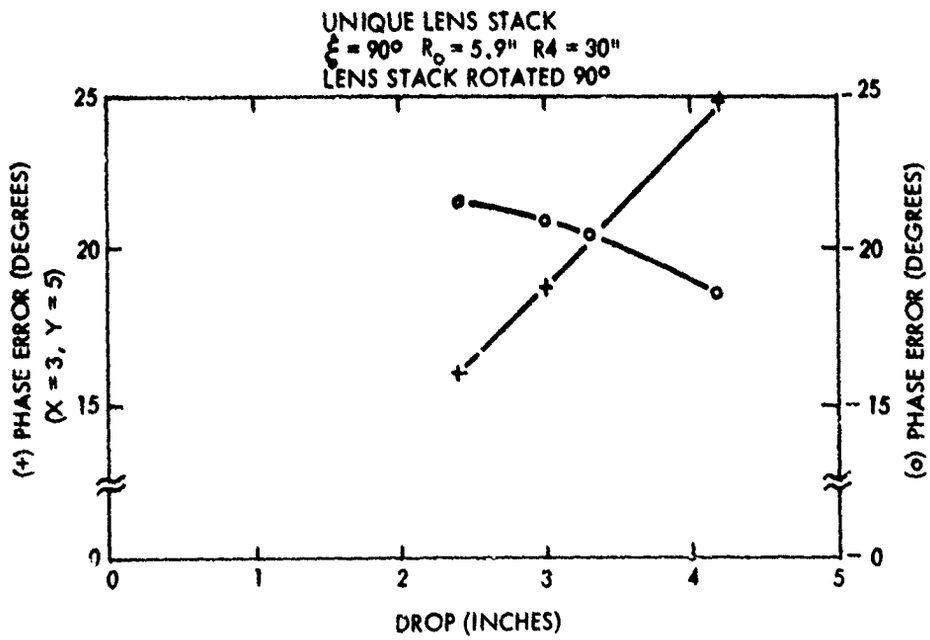

Figure 34. Phase Error vs Feed Array Drop

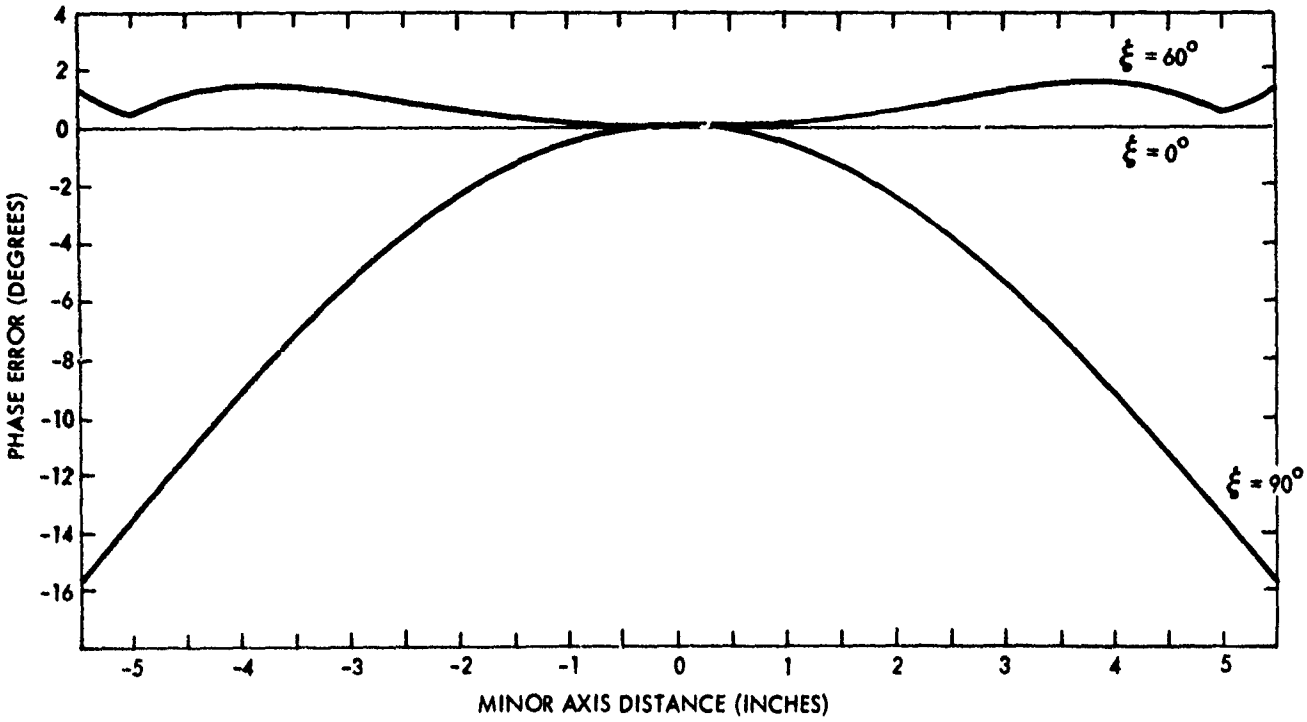

Figure 35. Co-Phase Error of Unique Lens Stack

3.5.3 MINOR AXIS LENS PHASE ERROR

As explained in section 3.4.1.5 and figure 29, the phase distribution supplied by a lens connected to elements along a row perpendicular to the intersection of the plane of scan is determined only by the slant of the scan plane (β), and not by the scan angle (α) in that plane, whereas the dome requirement of phase along the perpendicular row of elements is a function only of (α). Thus, the worst possible phase differences would occur for extreme slant plane angle (β) of one polarity and extreme scan angle (α) of the other polarity, as is the case for $\xi = 90$ degrees at an azimuth angle (ϕ) of 45 degrees. Figure 36 is a phase error contour plot illustrating the condition of worst phase error contributed by this source for the lens stack approach in which all lenses are designed identical to the perfect lens design for the row of feed array elements two inches from the center (identical stack). Figure 37 is the phase error contour at the same scan angle for a lens stack using all correct lenses (unique stack). Note that the amount of error in excess of 25 degrees is approximately the same for the two cases. Furthermore, the rms value of phase error over the entire surface for both lens stack configurations is slightly above 21 degrees. The level of rms phase error mentioned for this scan angle is at the most extreme phase error condition, and accounts for less than five percent of the hemispherical coverage.

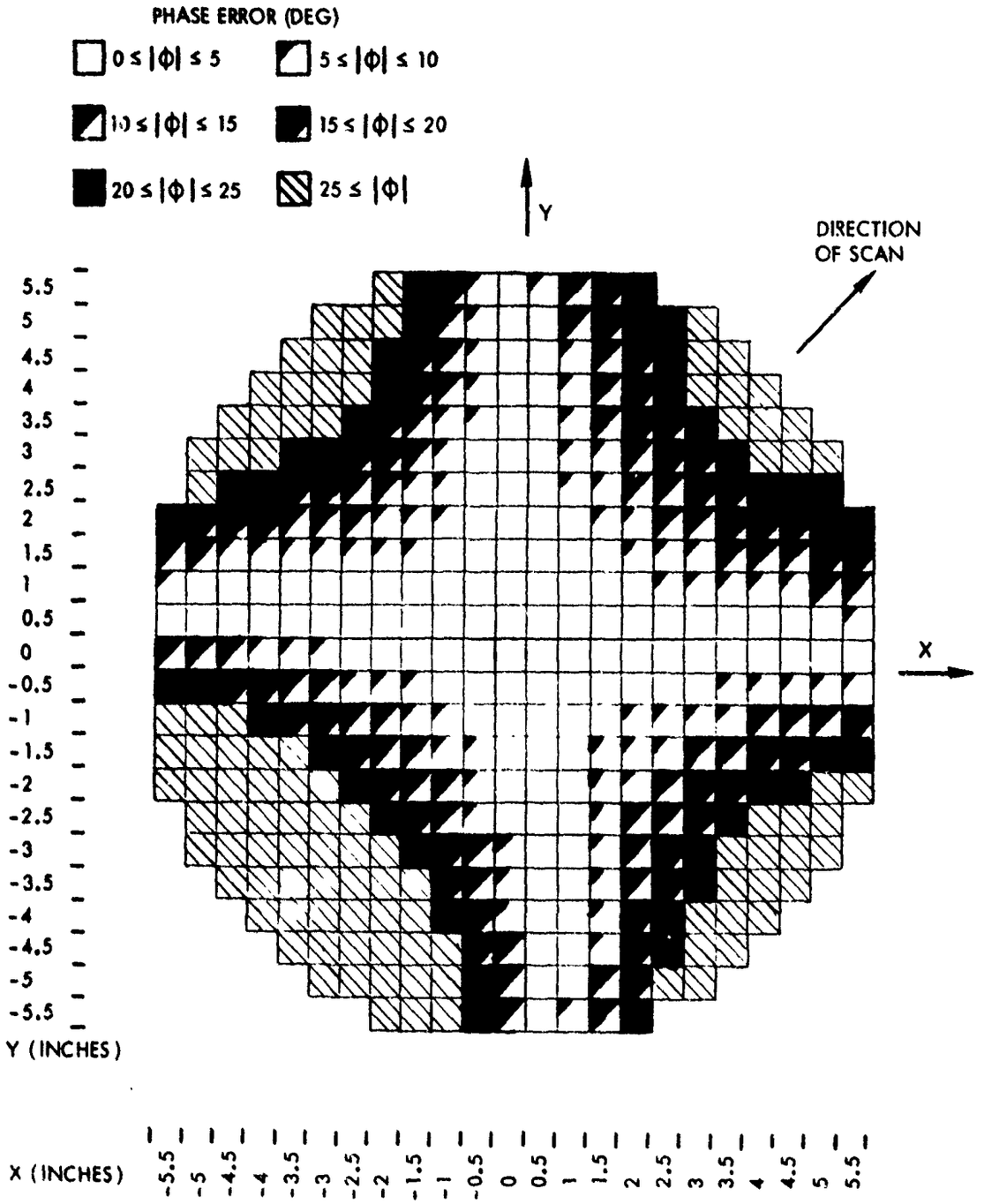

Figure 36. Phase Error for Identical Lens Stack (ξ = 90 degrees, ϕ = 45 degrees)

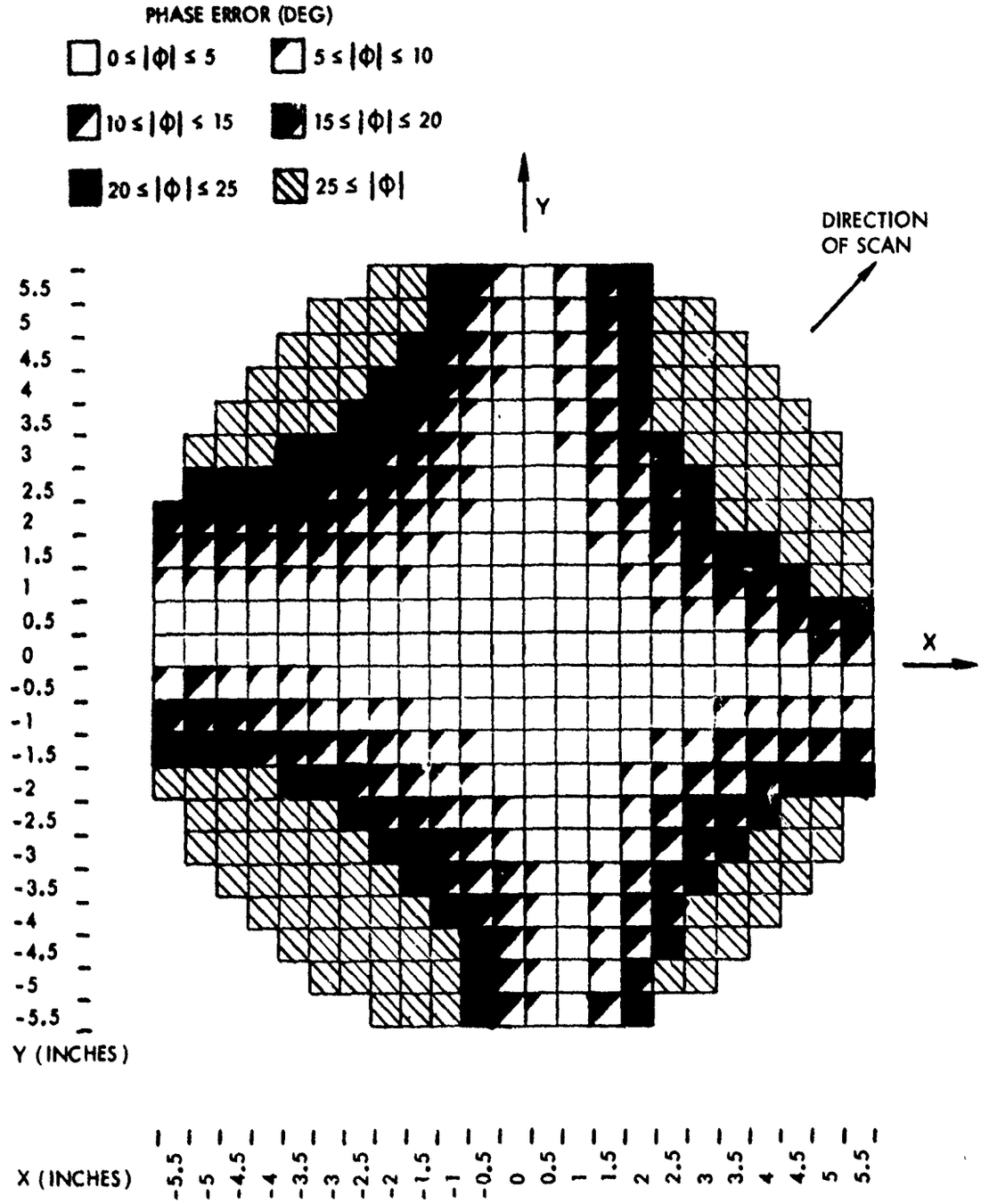

Figure 37. Phase Error for Unique Lens Stack (ξ = 90 degrees, ϕ = 45 degrees)

Figure 38 is a plot of achievable side-lobe level versus rms phase error using Taylor amplitude feed distribution. In figure 38, it is seen that the 21 degree rms error restricts the achievable side-lobe level to approximately 18 decibels. At 65 degrees scan along a diagonal, the rms phase error for both lens stack configurations is slightly over 13 degrees, which corresponds to approximately a 22 dB side-lobe level.

It appears that the two lens stack configurations exhibit approximately the same performance along the diagonals, and the identical lens stack is actually superior at extreme scan angles along the major axes The unique lens stack approach has lower rms phase error than the identical stack only around zenith. Even then, the identical lens stack exhibits only 5.5 degrees of rms phase error, which corresponds to approximately a 28 decibel side-lobe level. This achievable side-lobe level, for the identical lens stack, is true not only around zenith, but at $\xi = 90$ degrees over much of azimuth scan. Actually, the 25 dB side-lobe level is valid over approximately 92 percent of the coverage (figure 39). These figures were based on an identical lens stack configuration, without optimized beamport positions or lens parameters. Possibly another three degrees of rms phase error reduction could be achieved with optimization of these variables. That would result in 20 dB side lobes achievable over the entire hemisphere, with 30 dB side lobes over 85 percent of the coverage.

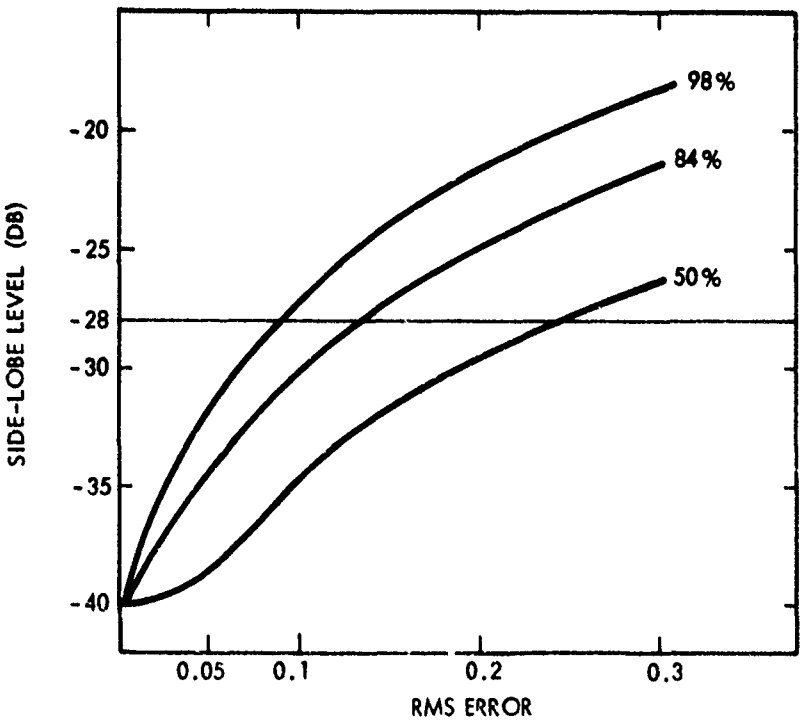

Figure 38. Sensitivity to Errors, 40-dB Taylor Distribution

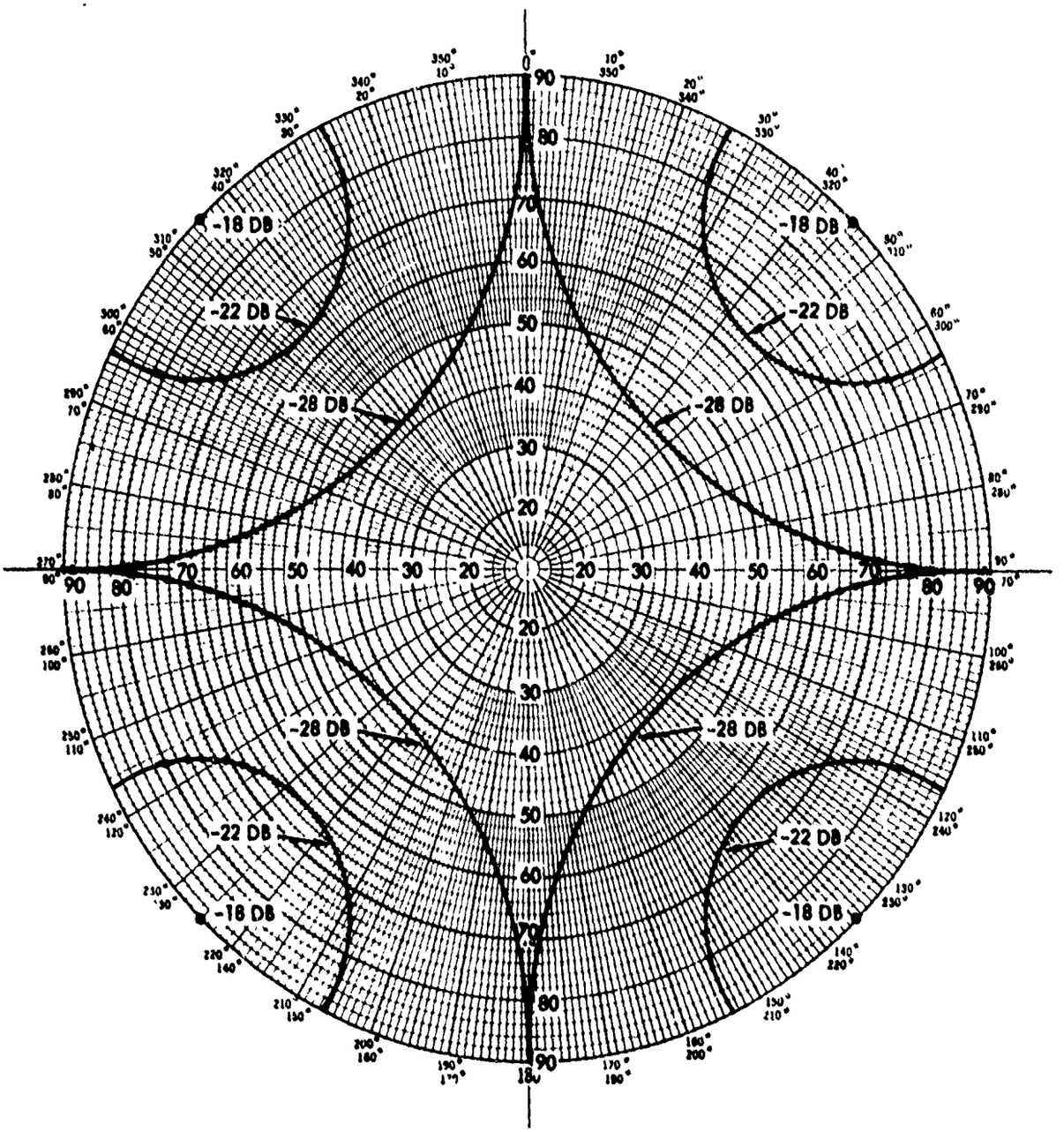

Figure 39 Top View of Dome Side Lobe Level Achievable

3.5.4 CONDUIT PHASE ERROR/IDENTICAL LENS PHASE ERROR

As alluded to in the last section, the resulting overall system rms phase errors for the total coverage favor the identical lens stack approach, which implies that, overall, the conduit phase error was more costly than the row-to-row difference in phase when implementing the identical lens stack approach. The last determination made, then, was which row of elements to choose for identical lens stack design. Figures 40 through 42 are contour plots of phase error at $\xi = 90$ degrees and $\phi = 90$ degrees for lenses identical to rows at zero inch, 2 inches, and 3 inches, respectively, from the center row. Note that, in the zero-inch case, eight elements had phase error over 20 degrees close to the outer corners, which is farthest from the pattern lens. In the 3-inch case, five elements had phase error in excess of 20 degrees along the major axis (x), which is farther from y = 3 inches. Finally, the case in which the pattern row is at y = 2 inches allows no phase error in excess of 20 degrees. The two-inch dimension balances the phase variation between the outer edge and the central row. Thus, the lens stack configuration chosen is identical lenses, patterned after those lenses feeding elements in rows two inches from the main axes.

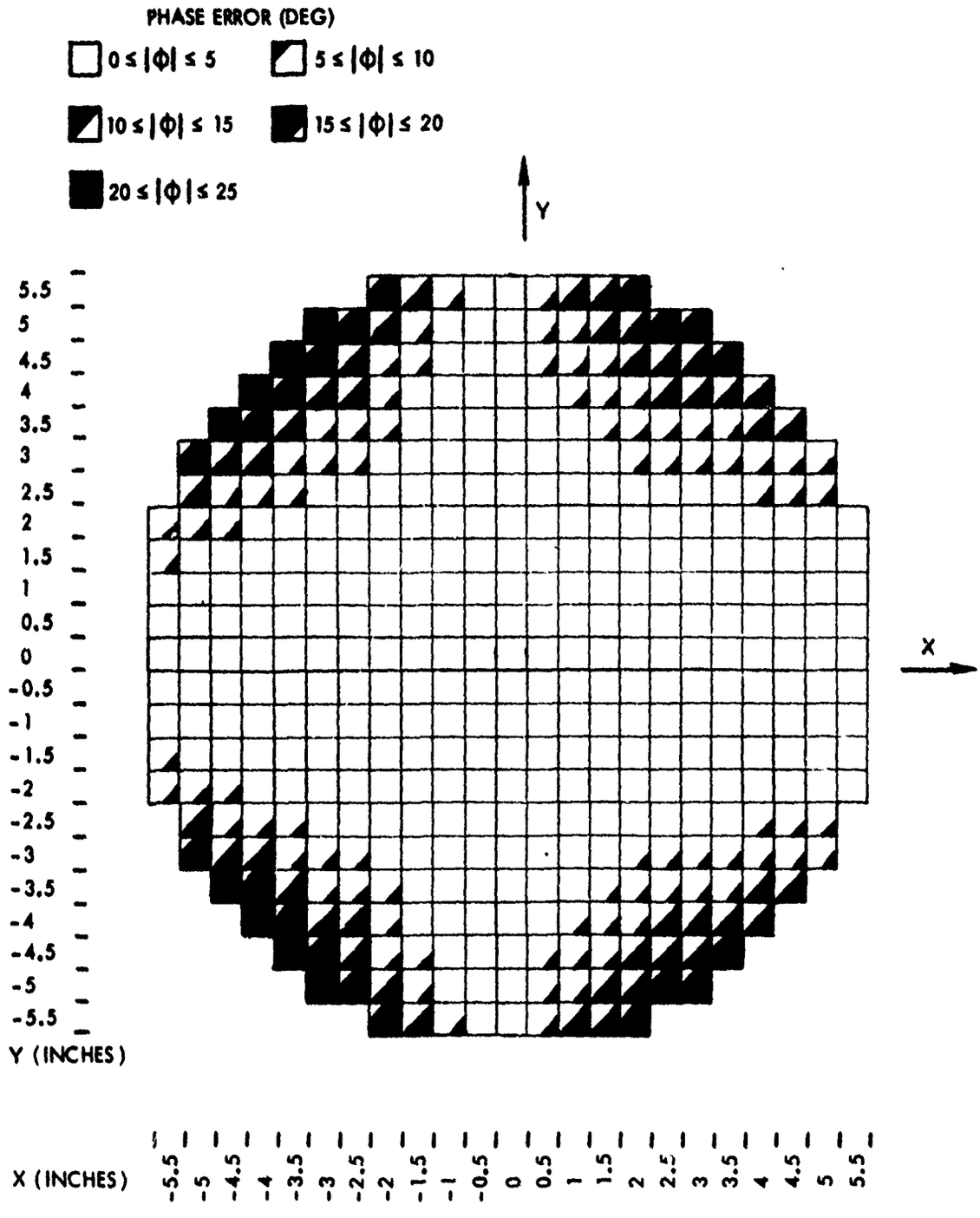

Figure 40. Phase Error for Identical Lens Stack with 3.3-inch Drop (ξ = 90 degrees, cut distance = 0 inch)

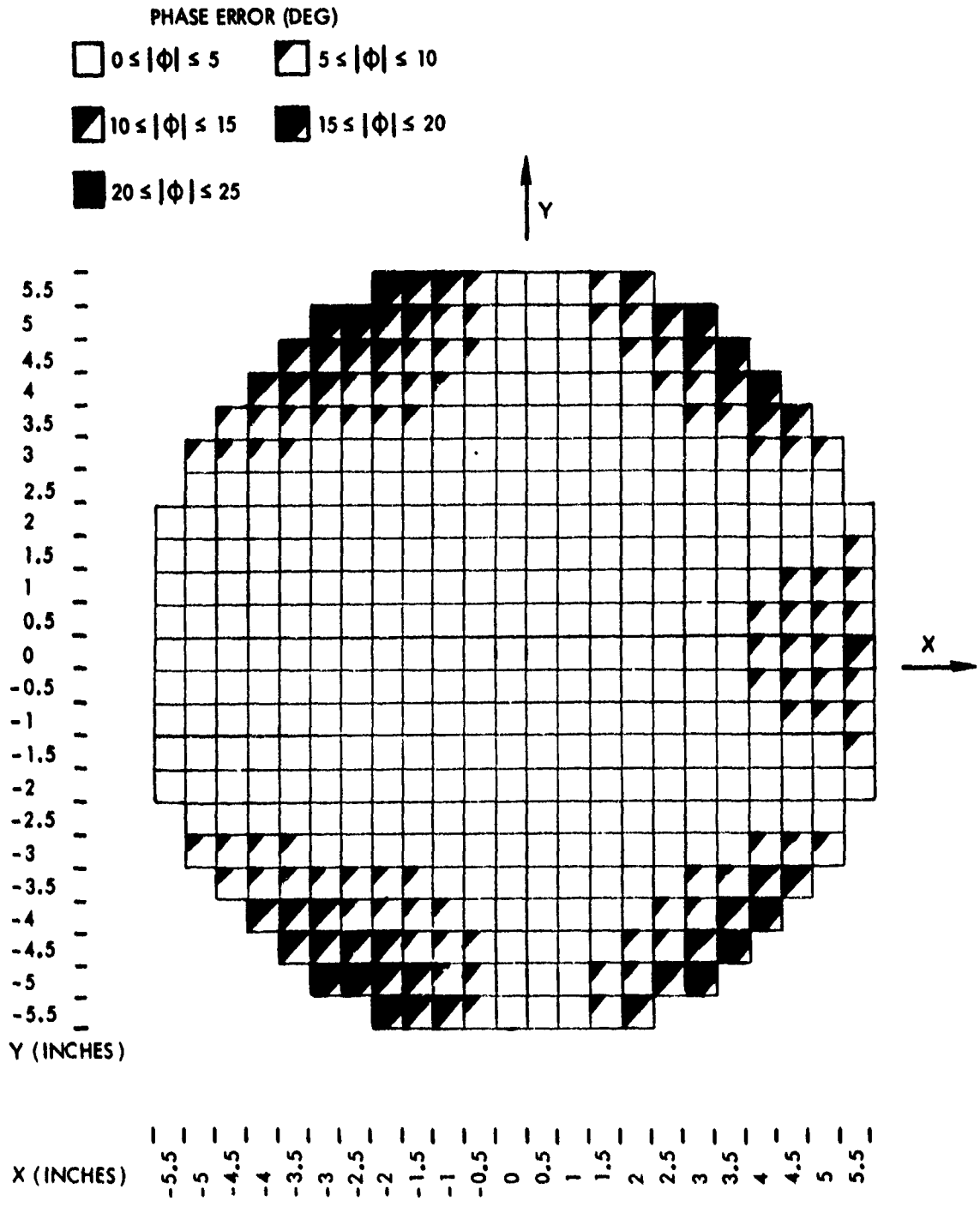

Figure 41. Phase Error for Identical Lens Stack with 3.3-inch Drop (ξ = 90 degrees, cut distance = 2 inches)

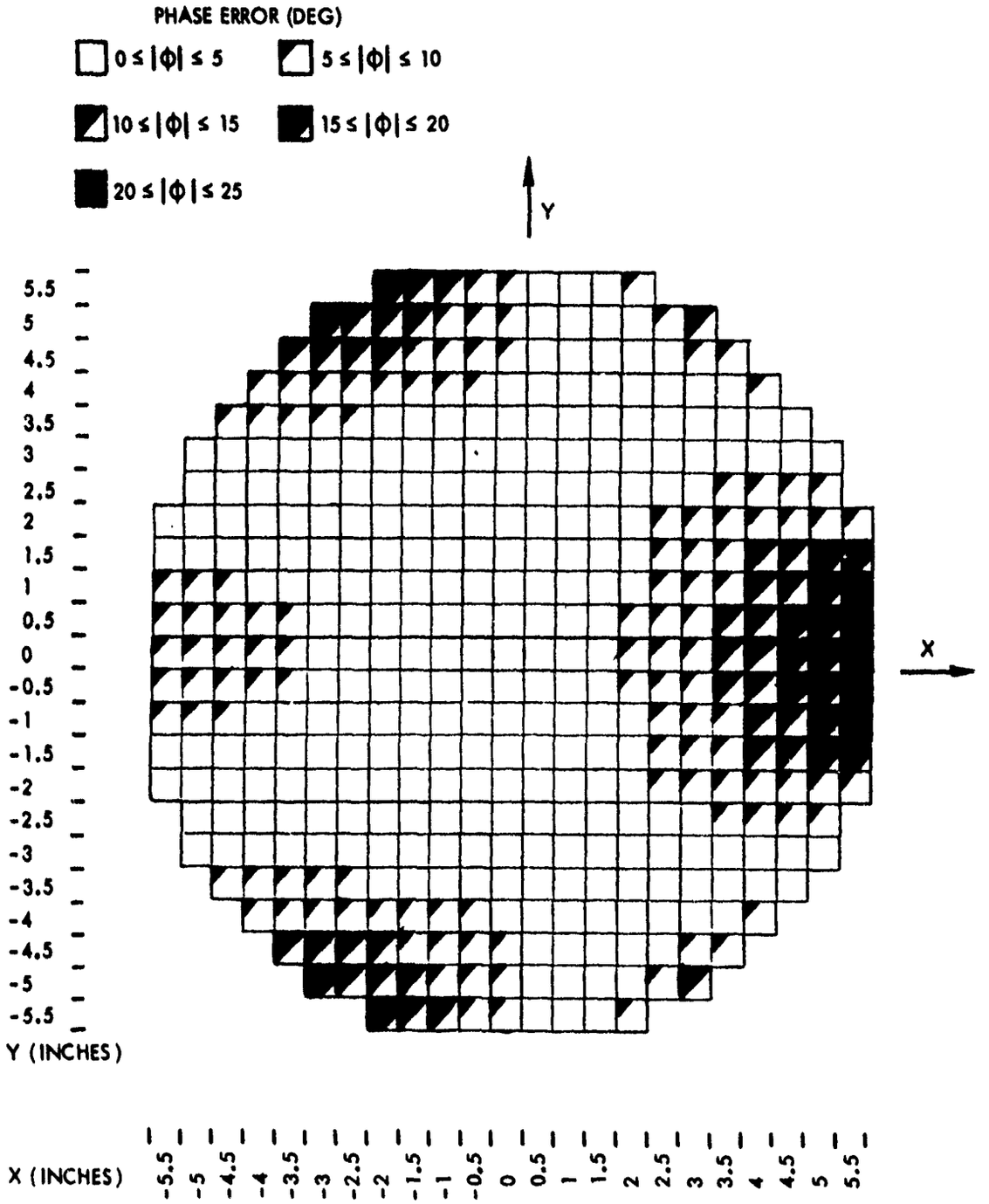

Figure 42. Phase Error for Identical Lens Stack with 3.3-inch Drop (ξ = 90 degrees, cut distance = 3 inches)

SECTION IV
RECOMMENDED DESIGN

4.1 DESIGN PARAMETERS

The dome parameters determined to be optimum in this investigation are listed in table 2.

Table 2. Dome Parameters

K	1.5
R_0	6 inches
R_1	9 inches
R_2	11.25 inches
R_4	30 inches
Drop of Array Feed	3.3 inches

The lens parameters for the identical lens stack design are listed in table 3.

Table 3. Lens Parameters

G	1.15 inches (normalized)
α	39.5 degrees
η	0.77
Design Phase Data	From row 2 inches from axis

4.2 PERFORMANCE SUMMARY

4.2.1 PHASE CONSIDERATIONS

From the design listed in tables 2 and 3, the calculated rms phase error, including the corresponding achievable side-lobe level, as a function of scan angle (ξ, ϕ) is listed in table 4. Derived from this table is figure 43, a rough contour plot of the achievable side-lobe level over the hemispherical coverage.

Table 4. Phase Error vs Scan Angle

Identical Lens Stack
Cut Distance = 2 in.
Drop = 3.3 in.

(Degrees)	(Degrees)	RMS Phase Error (Degrees)	Side-lobe Level (dB)
0	0	0.67	-37.5
	15	1.27	-36.0
	30	2.37	-33.0
	45	3.62	-31.0
	60	4.77	-28.2
	75	5.40	-28.1
	90	5.56	-28.0
90	0	0.67	-37.5
	15	1.27	-36.0
	30	2.37	-33.0
	45	3.62	-31.0
	60	4.77	-28.2
	75	5.40	-28.1
	90	5.56	-28.0
45	64.9	13.54	-22.0
	88.33	21.39	-18.0
	0	0.67	-37.5
			-28

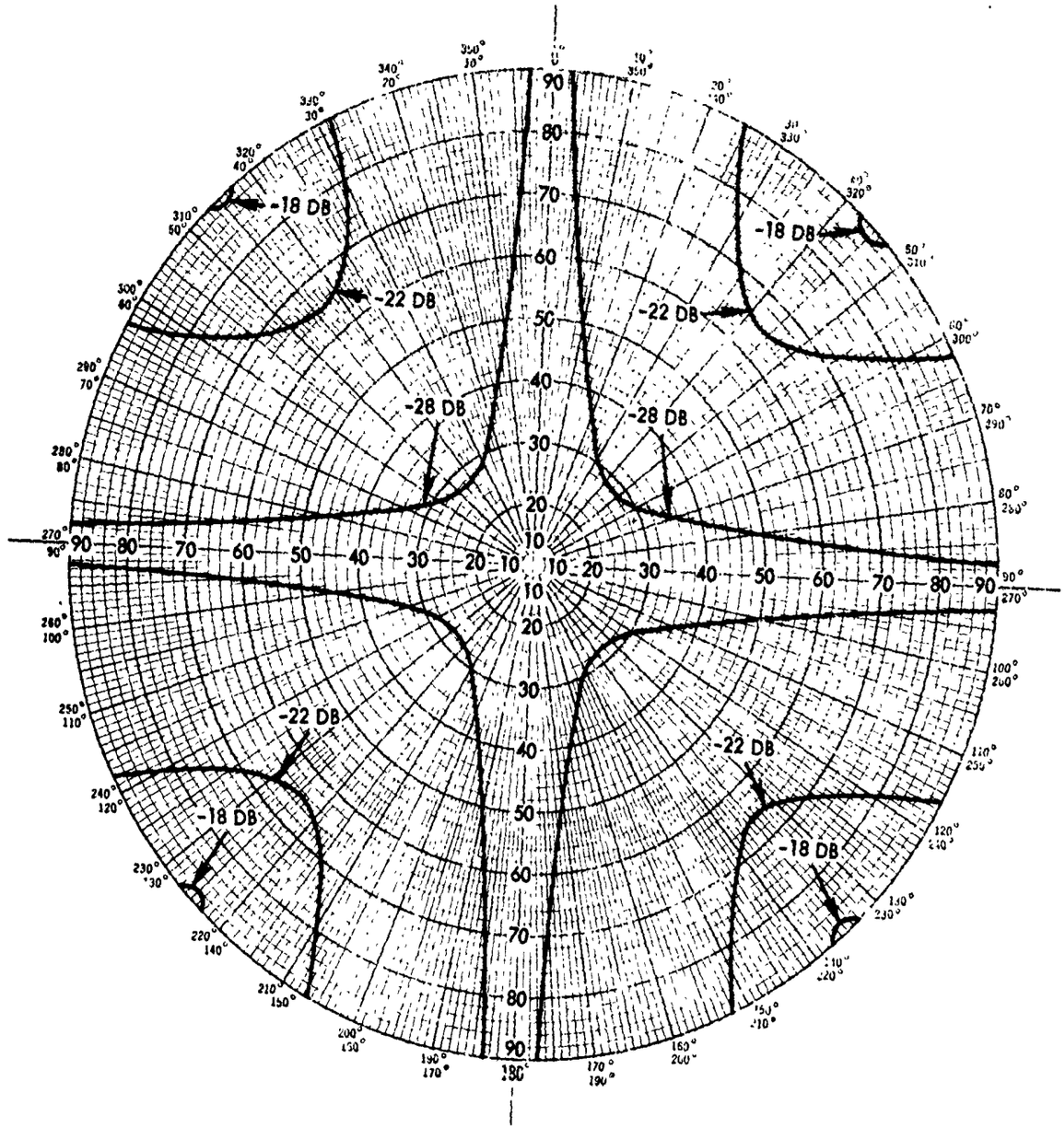

Figure 43. Top View of Achievable Side-lobe Level over Hemisphere

4.2.2 GAIN/SPOT SIZE

From the governing equations of the dome described in Section III, aperture size is calculated. Using the normalized feed array radius (R_0) of 1 inch, the internal scan angles of elements on the feed array perimeter were calculated as a function of scan angle (ξ). Using the geometry of figure 44, the spot size external to the dome is calculated. In the figure, for $\xi = 0$, the radius of the external spot is 52.3 percent of the feed array radius. Figure 45 shows the calculated size and shape of the projection of the feed array disk to the outer dome surface. Recognizing the scan angle amplification of the dome at angles other than zenith, the outer surface spot size must be reduced by approximately cos ($\xi - \theta$) to calculate relative gain. For instance, while the spot at $\xi = 0$ degree is full size, the radius at the spot for $\xi = 90$ degrees is reduced to 86.6 percent of its dome surface value. Figure 46 is a plot of the resulting relative gain versus scan angle. At 12 GHz, using $R_0 =$ 6 inches and the approximate relationship $G = 4\pi A/\lambda^2$; the 0 dB gain corresponds to 31.67 dB.

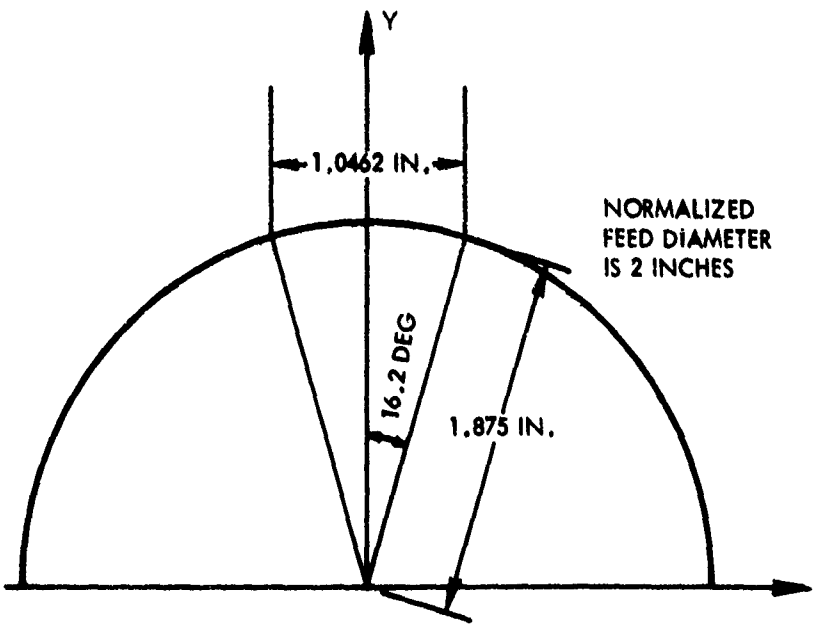

Figure 44. Dome Spot Size Geometry

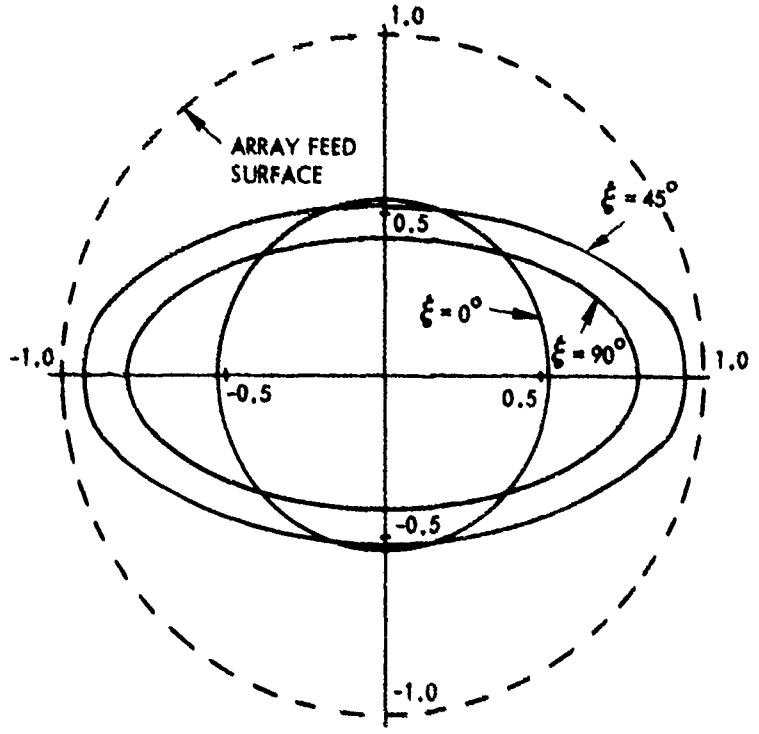

Figure 45 External Surface Dome Spot Size vs Scan Angle from Zenith

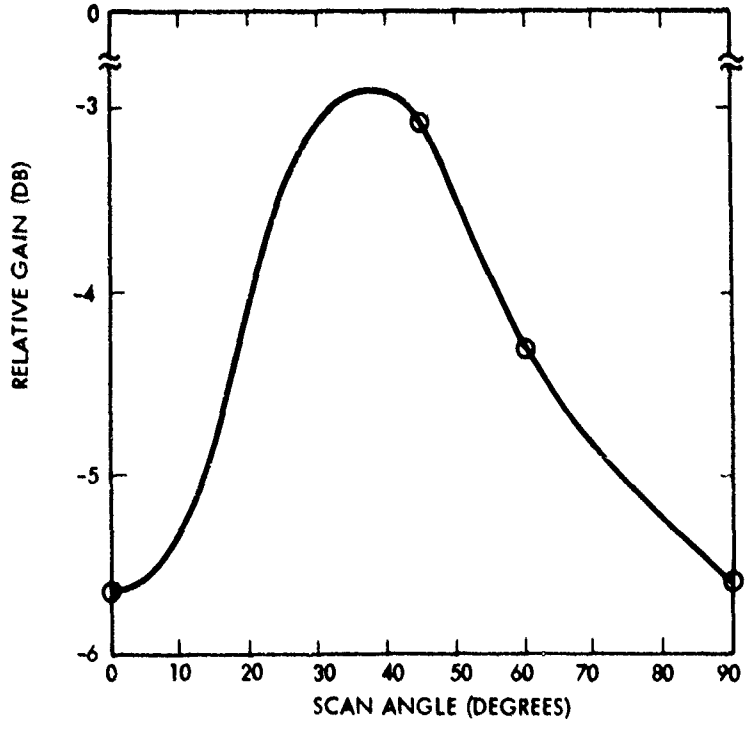

Figure 46. Relative Gain vs Scan Angle

APPENDIX A

3-DIMENSIONAL BOOTLACE LENSES

A-1. SUMMARY

The use of three-dimensional bootlace lenses for the feed array of the 3-D dome antenna has several advantages - simplicity, weight, low loss.

An investigation of three-dimensional bootlace lenses reveals several possible configurations which are described in this memo, together with some preliminary results. One configuration, a four-foci, three-dimensional bootlace lens, is believed to be a new invention of some potential value.

Unfortunately, the preliminary results indicate that the path-length errors of all three-dimensional bootlace lenses will exceed allowable limits for the sizes and wide scan angles (±50 degrees) required of the feed array for a 3-D dome antenna. Further computations will be performed in an attempt to find a useful 3-D bootlace lens configuration.

A-1.1 THREE-DIMENSIONAL BOOTLACE LENSES

The 3-D bootlace lens is one of a class of constrained microwave lenses. Such lenses act to focus and/or refract incoming waves, and provide the gain of a large-aperture antenna without the need for a large active array. Many types of microwave lenses exist, including the 2-D Rotman lenses[2,3], the Ruze waveguide lens[5], and the 3-D bootlace lens[6].

Two-dimensional lenses have found many applications in wide-band, wide-scan, multiple-beam antenna systems. It is desirable to achieve similar capability with the 3-D bootlace lens fed array.

A sketch of a 3-D bootlace lens array appears in figure A-1. The components of this lens array are:

- radiating array,
- phase-matched cables,
- array port surface, and
- beamport surface.

Although dielectric loading of the space between array port surface and beamport surface could be done (to shrink the lens size), normally that region is just air. The term "space-fed lens" is often used to describe this type of lens.

Functionally, the operation of the 3-D bootlace lens array is as follows. An incoming plane wave from an oblique space angle strikes the radiating array. The received energy then passes through the transmission cables and is rereadiated by the array ports (toward the beamports). The design of the lens is such as to focus the energy from each space angle to a single beamport. That is, total electrical path length from plane wavefront to corresponding beamport is the same (or nearly so).

The performance (gain, side-lobe levels) of the 3-D bootlace lens will depend on how nearly perfect focus is achieved for each beamport and corresponding wavefront. With the limited number of constraints available, perfect focus for all beamports and all array elements cannot be achieved. The goal is to achieve the best performance within the limitations.

---

5. J. Ruze "Wide Angle Metal-Plate Optics" Proc IRE, Vol. 38, pp. 53-59, Jan. 1950

6. H. Gent "The Bootlace Aerial" Royal Radar Establishment Journal, pp. 47-57, Oct. 1957

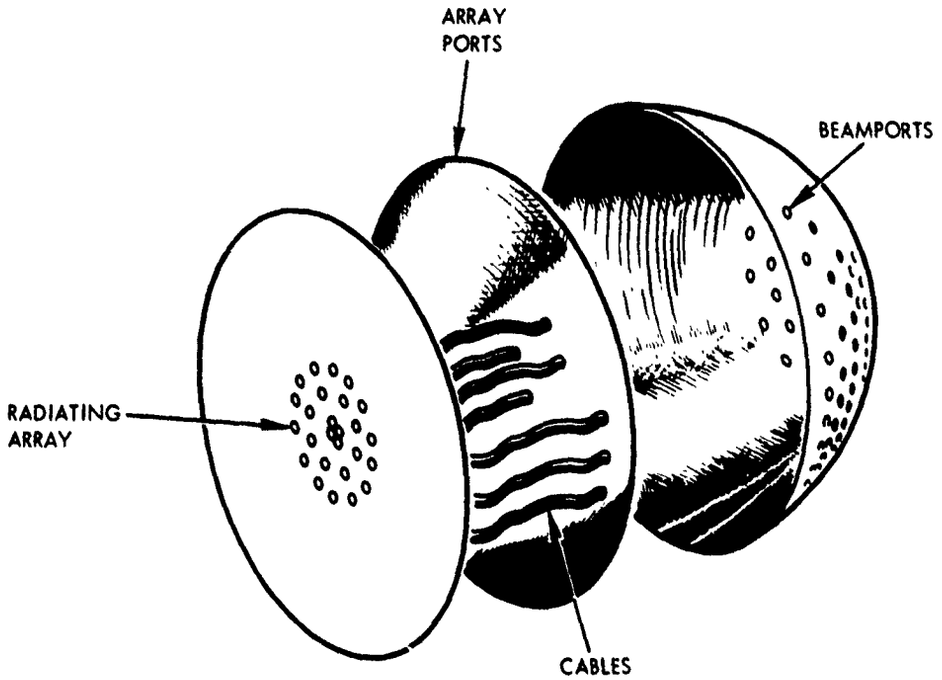

Figure A-1. 3-D Constrained Bootlace Lens Array

For a beamport located at $(R, \theta, \phi = F, \alpha, \phi_o)$ and a desired beam direction $(\theta, \phi = \beta, \phi_o)$, the path length error of any array elements, normalized to the zero element location, is ($Z_2 = 0$ for flat array).

$$P(U_2, \phi_2) = \sqrt{U_1^2+(F\sin\alpha)^2-2F\,U_1\sin\alpha\cos(\phi_1-\phi_o)+(Z_1-F\cos\alpha)^2}$$

$$-F+W-U_2\sin\beta\cos(\phi_2-\phi_o) \qquad \text{(A-1)}$$

This path length error is given in cylindrical coordinates, where $X_1 = U_1\cos\phi_1$, $Y_1 = U_1\sin\phi_1$, etc. (See figure A-2.)

The path length error and other properties of two classes of 3-D bootlace lenses (the axially symmetric lens and a novel, four-focus lens) are examined below. A few preliminary performance results are included.

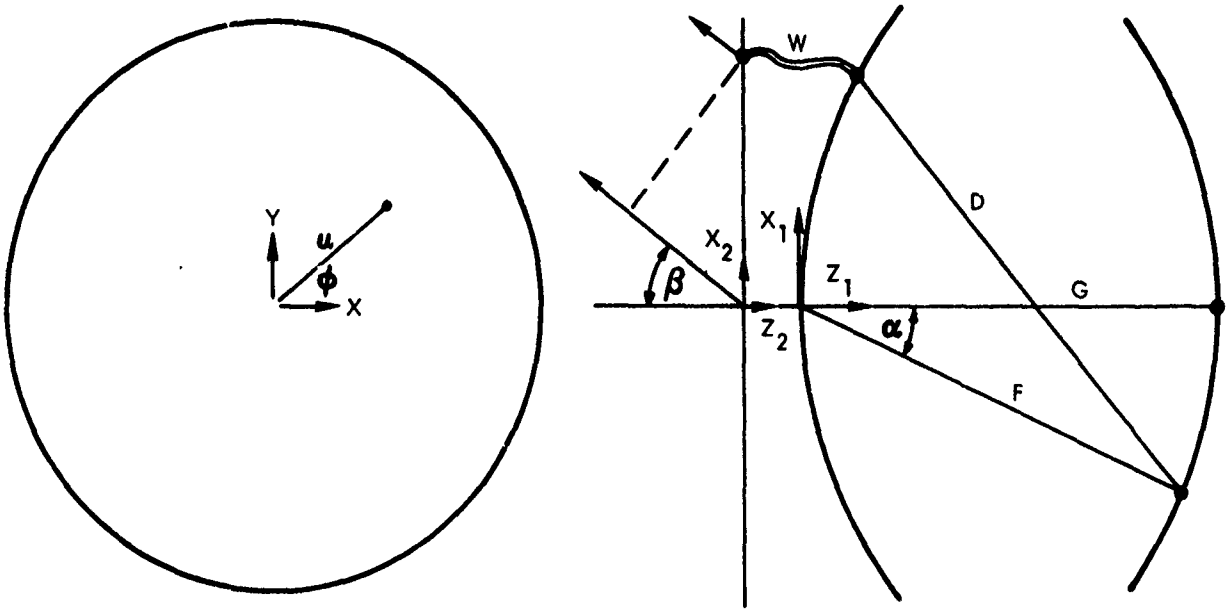

(A) TOP VIEW (B) SIDE VIEW

Figure A-2. Geometry of 3-D Bootlace Lens (Axially Symmetric)

A-1.2 AXIALLY SYMMETRIC 3-D BOOTLACE LENSES

Axially symmetric lenses are advantageous because of their ease of construction. However, scanning off-axis will introduce asymmetry into the path length error function, but (due to axial symmetry) only one direction of scan need be studied.

For axial symmetry (with Z-axes the axes of symmetry), $\phi_1 = \phi_2 = \phi$ and $\phi_0 = 0$ can be chosen. The lens array surface will not depend on ϕ. For this case, the path length error becomes:

$$P(U_2,\phi) = \sqrt{U_1^2+(F\sin\alpha)^2 - 2FU_1\sin\alpha\cos\phi + (Z_1 - F\cos\alpha)^2}$$

$$-F+W-U_2\sin\beta\cos\phi \qquad \text{(A-2)}$$

In addition to axial symmetry, other conditions must be imposed to have a well-defined lens design. The selection of these conditions naturally affects the performance.

The number of conditions which can be imposed is three, since in equation (A-2) the quantities W, U_1, Z_1 are unspecified.

Potential conditions which might be imposed are:

1) A <u>perfect focus point</u> at $Z_1 = G$, ($\alpha = 0$)

$$\text{i.e., } P = \sqrt{U_1^2+(Z_1-G)^2} - G+W = 0. \tag{A-3}$$

Perfect focus is possible only for beamports on the Z-axis of symmetry.

2) <u>Aplanatic lens condition</u>. By making dP/dS=S=0 at $\alpha = 0$ (where $S = G \tan\alpha$), the linear phase error term for scanned beamports is eliminated, and good performance is ensured for small scan angles. This condition is:

$$\left.\frac{dP}{dS}\right|_{\alpha = 0} = \frac{U_1 \cos\phi}{\sqrt{U_1^2+(Z_1-G)^2}} - \frac{U_2 \cos\phi}{R_o} \tag{A-4}$$

where R_o is the radius of the Abbé sine circle. Conditions (1) and (2) are referred to as the Abbé sine conditions. The Abbé radius, R_o, is equivalent to the expansion factor in Rotman lenses, and relates lens size to array size.

Even with both Abbé sine conditions imposed, there is still one degree of freedom to impose. This can be imposed by selecting the shape of the lens array surface, or by making all cable lengths equal (W = 0), or other conditions. However, since wide scan is the goal, primary consideration must be given to minimizing the error.

<u>Case 1</u>. Equal Cable Lengths (W = 0). Solution of equations (A-3) and (A-4) with W = 0 gives:

$$U_1 = U_2 \left(\frac{G}{R_o}\right) \tag{A-5}$$

$$Z_1 = G - \sqrt{G^2-(U_2 \cdot G/R_o)^2} \tag{A-6}$$

These equations will design an aplanatic lens for any given values of G and R_o. Since least error is our criterion, the best error performance (optimum R_o) is shown in table A-1 with maximum scan angle, β, and size, G/R, as variables, where R is the array radius.

Table A-1. Path-Length Error (Peak-To-Peak)

	G/R = 2	G/R = 4	G/R = 20
β = 30 deg	0.056 R	0.028 R	0.0038 R
β = 45 deg	0.091 R	0.045 R	0.0090 R
Scan (beamwidths)	5	10	70

In translating the errors into beamwidths of scan, a maximum edge error of 45 degrees was used as the criterion, and 58 λ/D was used as the beamwidth.

The error levels of axially symmetric 3-D bootlace lenses are much higher than those of comparable size 2-D lenses. This is due to the inherent asymmetry of scan feed positions, which cannot be compensated for in the symmetrical lens design.

For a lens size (diameter) equal to twice the array size (G/D = 2), roughly ten beamwidths of scan are possible before the phase errors degrade the performance. If a ±50 degree scan is needed, the minimum possible beamwidth is about 10 degrees, a low gain array. Larger arrays are not possible for this case.

To use larger arrays, lens size must increase proportionately. For a 1.4-degree beamwidth, lens size must be about ten times array size to maintain acceptable errors (G/D = 10). Such a large size lens is, of course, prohibitive, especially for a large array.

Thus the alternatives are (1) excessively large bootlace lens or (2) severely limited array size.

Case 2. "Spun" Rotman. In two-dimensional lenses, the Rotman lens offers excellent performance. One option for an axially symmetric lens is to "spin" or rotate a Rotman lens design about its center axis. This will retain a perfect focus on-axis (equation (A-3)), and have zero error for one column in the array at the extreme scan angle. The aplanatic lens condition (equation (A-4)) will not be satisfied.

The equations for Case 2 are equation (A-3):

$$\sqrt{U_1^2 + (Z_1 - G)^2} - G + W = 0$$

and the two wide-scan conditions:

$$\sqrt{U_1^2 + (F \sin\alpha)^2 - 2W F \sin\alpha + (Z_1 - F\cos\alpha)^2} - F + W - U_2 \sin\beta = 0 \qquad \text{(A-7)}$$

and

$$\sqrt{U_1^2 + (F \sin\alpha)^2 - 2U_1 F \sin\alpha + (Z_1 - F\cos\alpha)^2} - F + W + U_2 \sin\beta = 0 \qquad \text{(A-8)}$$

Simultaneous solution of equations (A-3), (A-7), and (A-8) follows the usual methods of Rotman lens solution. The results are:

$$U_1 = U_2 \frac{\sin\beta}{\sin\alpha}\left(\frac{F-W}{F}\right) \qquad \text{(A-9)}$$

and, unless F cos =G,

$$Z_1 = W\left(\frac{G - F}{G - F\cos\alpha}\right) + \frac{U_2^2 \sin^2\beta}{2(G - F\cos\alpha)} \qquad \text{(A-10)}$$

Substitution of equations (A-9) and (A-10) into equation (A-3) permits solving for W and completing the solution:

$$W = B - \sqrt{B^2 - AC} \; / A \qquad \text{(A-11)}$$

where:

$$A = 1 - \left(\frac{U_2 \sin\beta}{F \sin\alpha}\right)^2 - \left(\frac{G - F}{G - F\cos\alpha}\right)^2$$

$$B = G - \frac{G(G-F)}{G - F\cos\alpha} + \frac{G-F}{2}\left(\frac{U_2 \sin\beta}{G - F\cos\alpha}\right)^2 - F\left(\frac{U_2 \sin\beta}{F \sin\alpha}\right)^2$$

$$C = \frac{G}{2}\,\frac{(U_2 \sin\beta)^2}{G - F\cos\alpha} - \left(\frac{U_2 \sin\beta}{2(G - F\cos\alpha)}\right)^2 - \left(\frac{U_2 \sin\beta}{\sin\alpha}\right)^2$$

If $G = F\cos\alpha$, a different set of equations results, where:

$$W = -\frac{U_2^2 \sin^2\beta}{2(G-F)} \qquad \text{(A-12)}$$

and

$$Z_1 = -G + \sqrt{\left[G + \frac{(U_2 \sin\beta)^2}{2(G-F)}\right] - \left(\frac{U_2 \sin\beta}{F \sin\alpha}\right)^2 \left[F + \frac{U_2 \sin^2\beta}{2(G-F)}\right]^2} \qquad \text{(A-13)}$$

Unfortunately, this approach to axially symmetric 3-D bootlace lenses does not improve the path-length errors, which are still about the levels of table A-1. It is felt that no approach to axially symmetric 3-D bootlace lenses will offer any substantial improvement in errors.

However, the shape or character of errors are quite different for the two cases. For $G/R = 2$, and $\alpha = 30$ degrees, figures A-3 and A-4 show error contours for the two cases. In Case No. 1 ($W = 0$), maximum errors are along the scan axis, with very low errors in the center strip orthogonal to the scan axis. In Case No. 2 (spun Rotman), very low errors exist along the scan axis, and maximum errors occur along the orthogonal axis. In Raytheon's opinion, the preferable situation is Case No. 1, which would have lowest side-lobes orthogonal to the scan axis (coincident with terrestrial plane).

A-1.5 A FOUR-FOCI, THREE-DIMENSIONAL BOOTLACE LENS

This section presents a novel four-foci, three-dimensional bootlace lens array feed. This lens concept, which is a 3-D equivalent of the 2-D Rotman lens[2,3] has four perfect points on a curved beamport surface, and could provide substantial performance improvements over the axial symmetry lenses just described

Not all designs for a four-focus, 3-D bootlace lens will work. Prior investigations seeking the 3-D equivalent of the 2-D Rotman lens have proved fruitless. Early attempts by the author to find a feasible configuration of four-foci focus for a 3-D bootlace lens also failed when the lens equations could not be solved. However, a useful configuration of four foci has been found which leads to a feasible 3-D lens configuration.

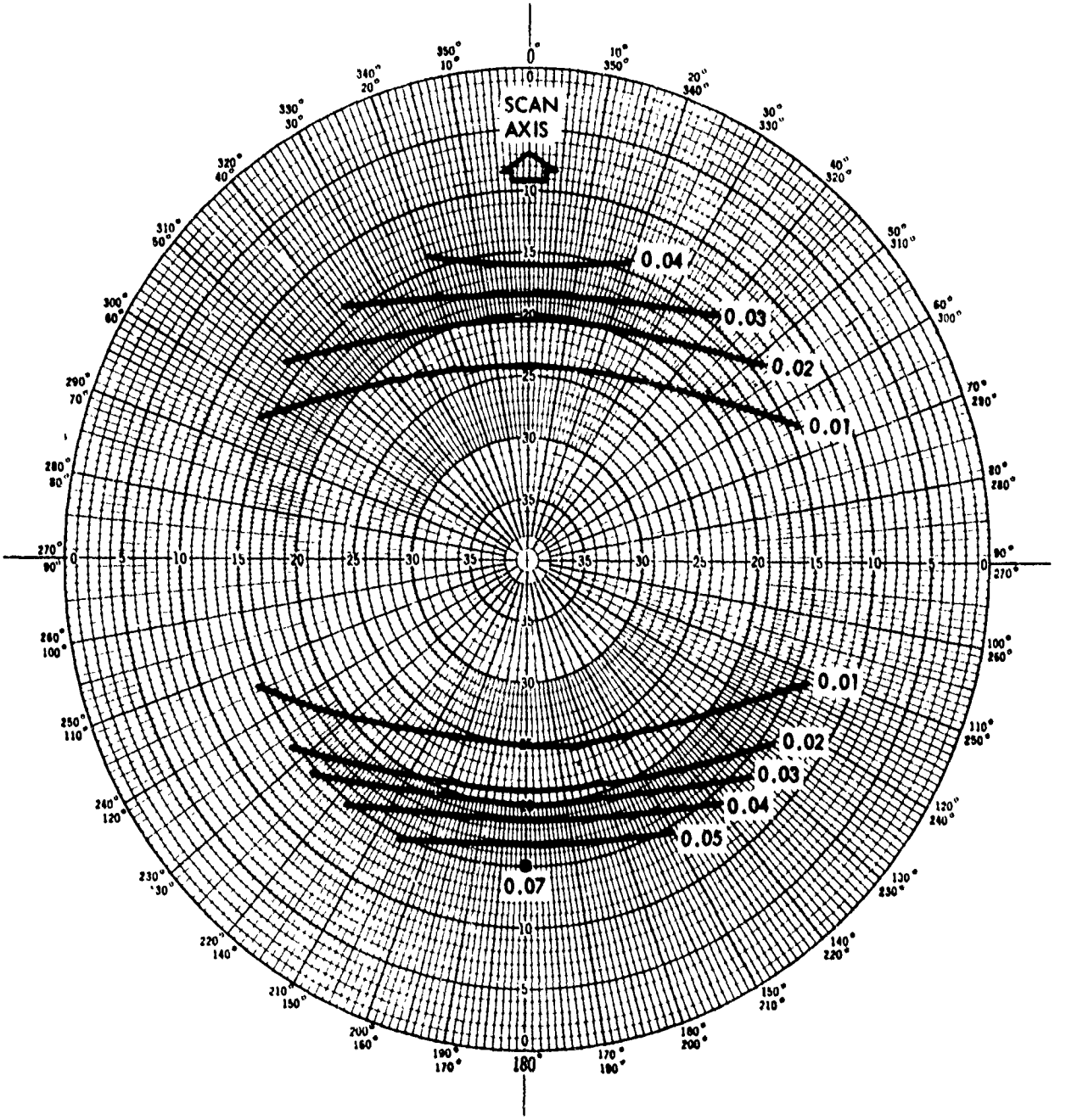

Figure A-3. Errors of Aplanatic Lens (W = 0, α = 30 degrees)

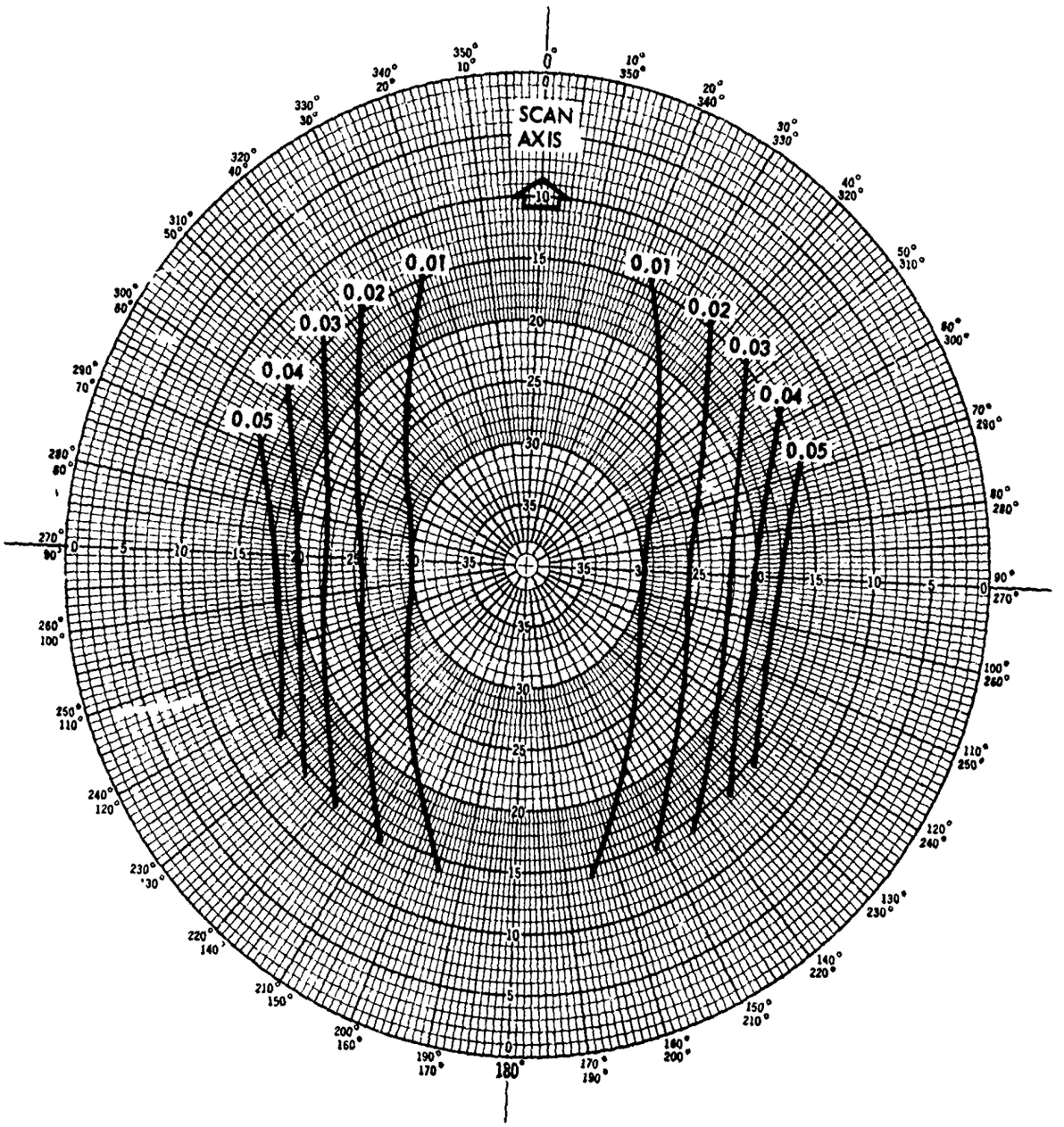

Figure A-4. Errors of Spun Rotman Lens (α = 30 degrees)

A-1.3.1 Analysis

The configuration of four-foci for a 3-D bootlace lens is shown in figure A-5. Three of the four foci are located on a circle of radius, F, and angle, , from the center of the array port surface. The fourth focus is on the Z-axis of the lens at distance, G.

Top and side views of the lens geometry appear in figure A-6. In these views, it is evident that the geometry of the four foci selected is symmetrical with respect to the Y-axis. This greatly simplifies solution, and should be the best choice for lenses which require equal coverage in all directions (360 degrees). Non-symmetrical foci configurations should be possible, but will present difficulties in solution and are not likely to be optimum.

In XYZ coordinates, the four foci of figure A-6 are located at:

Focus 1.	$X_1 = F \sin\alpha \cos\phi_o$	$Y_1 = F \sin\alpha \sin\phi_o$	$Z_1 = F \cos\alpha$
Focus 2.	$X_2 = F \sin\alpha \cos\phi_o$	$Y_2 = F \sin\alpha \sin\phi_o$	$Z_2 = F \cos\alpha$
Focus 3.	$X_3 = 0$	$Y_3 = F \sin\alpha$	$Z_3 = F \cos\alpha$
Focus 4.	$X_4 = 0$	$Y_4 = 0$	$Z_4 = G$

The lens design parameters which can be selected are F, G, α, ϕ_o, and β (the array scan angle corresponding to α). Intermediate beamport angles, as in the Rotman lens, will initially be assumed to be on a spherical surface passing through the four foci. Refocusing, that is, adjusting the intermediate foci locations for best performance, will be investigated at a later date.

Points on the array port surface are denoted XYZ, and points on the radiating array $X_oY_oZ_o$.

If the lens is to "focus" at each of the four foci, the path lengths from the corresponding plane wave front to the focal point must be equal. This gives four equations for each array point $X_oY_oZ_o$.

It is assumed that the incident plane wave is at angles (β_i, ϕ_i) corresponding to the focal point angles (α_i, ϕ_i).

Substituting the locations of the four foci given earlier, we have:

$$\sqrt{(X-F\sin\alpha\cos\phi_o)^2 + (Y-F\sin\alpha\sin\phi_o)^2 + (Z-F\cos\alpha)^2} \qquad \text{(A-14)}$$

$$+W+X_o\sin\beta\cos\phi_o + Y_o\sin\beta\sin\phi_o + Z_o\cos\beta = F$$

$$\sqrt{(X+F\sin\alpha\cos\phi_o)^2 + (Y-F\sin\alpha\sin\phi_o)^2 + (Z-F\cos\alpha)^2} \qquad \text{(A-15)}$$

$$+W-X_o\sin\beta\cos\phi_o + Y_o\sin\beta\sin\phi_o + Z_o\cos\beta = F$$

$$\sqrt{X^2 + (Y+F\sin\alpha)^2 + (Z-F\cos\alpha)^2} + W - Y_o\sin\alpha + Z_o\cos\alpha = F \qquad \text{(A-16)}$$

$$\sqrt{X^2 + Y^2 + (Z-G)^2} + W + Z_o = G \qquad \text{(A-17)}$$

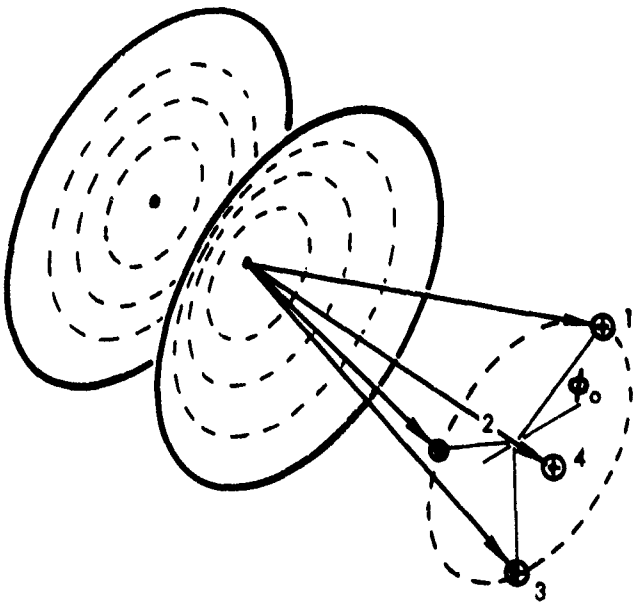

Figure A-5. Three-Dimensional Bootlace Lens with Four Foci

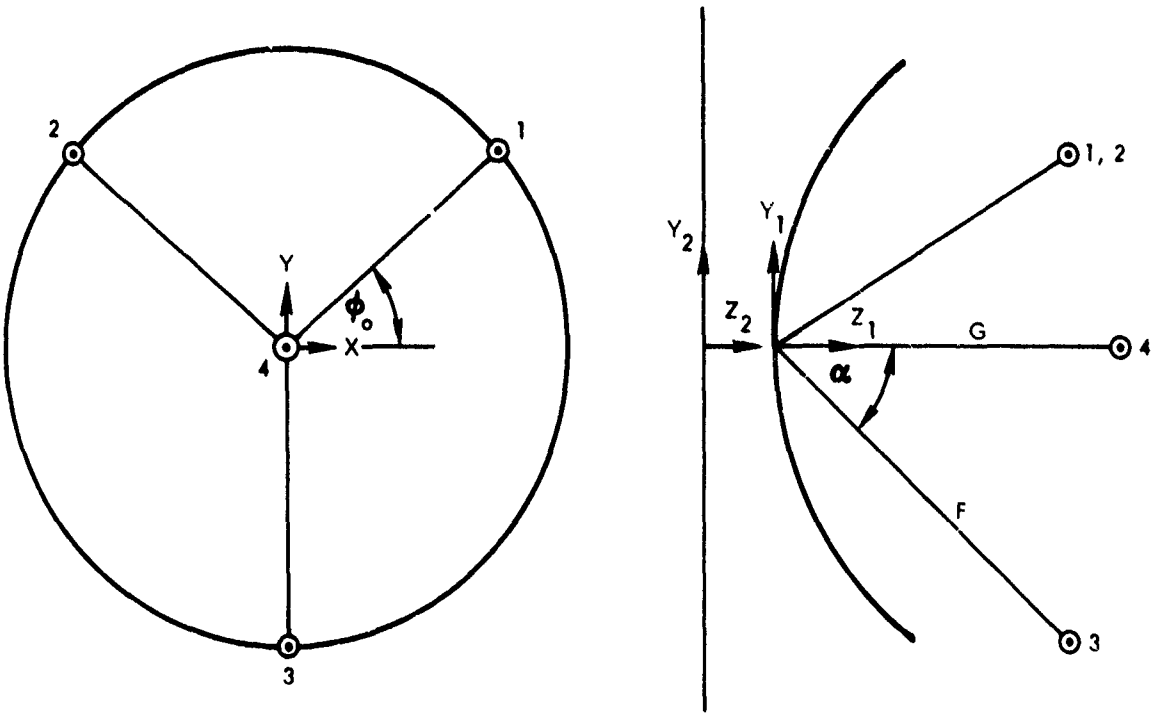

Figure A-6. Top and Side Views of Four-Foci Bootlace

These four equations are now solved for W, X, Y, Z to complete the lens design. As given, no assumption has been made about the nature of the array surface. This surface will normally be specified to be either flat ($Z_o = 0$) or a spherical cap $X_o^2 + Y_o^2 + (Z_o-R)^2 = R^2$.

To solve equations (A-14) through (A-17), from $(A\text{-}15)^2 - (A\text{-}1)^2$,

$$X = \frac{X_o}{F}\left[F - Y_o \sin\beta \sin\phi_o - Z_o \cos\alpha - W\right] = A_o + WA_1 \qquad (A\text{-}18)$$

From $(A\text{-}16)^2 - \frac{1}{2}\ (A\text{-}14)^2 + (A\text{-}15)^2$

$$Y = \frac{Y_o}{F}\left[F - Z_o \cos\beta - W\right] + \frac{(Y_o^2 - X_o^2)\sin\alpha\cos^2\phi_o}{2F(1+\sin\phi_o)} = B_o + WB_1 \qquad (A\text{-}19)$$

Finally, from $(A\text{-}16)^2 - (A\text{-}17)^2$

$$Z = \frac{-YF\sin\alpha}{G - F\cos\alpha} + \frac{(Y_o\sin\beta - Z_o\cos\beta + F)^2 - Z_c^2 + 2GZ_o}{2(G - F\cos\alpha)}$$

$$+ W\left(\frac{G - F - Y_o\sin\beta - Z_o + Z_o\cos\beta}{G - F\cos\alpha}\right) = C_o + WC_1 \qquad (A\text{-}20)$$

Substituting for X, Y, Z in equation (A-17) squared gives:

$$(A_o + WA_1)^2 + (B_o + WB_1)^2\ (C_o - G + WC_1)^2 = (G - Z_o - W)^2 \qquad (A\text{-}21)$$

or

$$W^2A + WB + C = 0 \qquad (A\text{-}22)$$

where $A = A_1^2 + B_1^2 + C_1^2 - 1$

$B = 2A_oA_1 + 2B_oB_1 + 2C_oC_1 - 2GC_1 + 2G - 2Z_o$

$C = A_o^2 + B_o^2 + (C_o - G)^2 - (G - Z_o)^2$

The solution for W is

$$W = \left[-B + \sqrt{B^2 - 4AC}\right]/2A \qquad (A\text{-}23)$$

Substitution of W from equation (A-23) into equations (A-18) through (A-20) completes the lens design.

A-1.3.2 Preliminary Observations

Equations (A-18) through (A-23) have been programmed for computer. Design analyses of potential 3-D bootlace lenses with four foci are just beginning.

Although it is too early for sufficient results from the computer analyses, some observations and predictions are possible:

1) The nature of path length (phase) errors is totally different in 3-D lenses. In 2-D Rotman lens arrays, maximum errors occur at intermediate beamports between the foci, and the error levels are quite small. In 3-D lenses, beamports in general are not between foci, but at some location away from foci. This leads to greatly increased errors, a fact which may preclude use of the 3-D bootlace lens. In essence, there are simply insufficient controls on the design of 3-D bootlace lenses to ensure good error performance for wide scan angles.

2) Lens shape, although asymmetrical, appears to be acceptable for reasonable size lenses.

3) Although some improvement in errors is expected over axially symmetrical 3-D lenses, the error level is likely to be too high to provide a useful wide scan coverage, as needed for 3-D dome applications.

APPENDIX B
COMPUTER FLOWCHARTS

Included is a list of the main programs, auxiliary programs, and data files used to analyze the design of the 3-D dome, its feed array, and the two-stack lens system beneath it. A brief introduction to the tasks performed by each program is also included.

The programs and files generated are functionally separated into the following groups:

1) Main Programs
   a) WAADOMR
   b) WAADOMT
   c) WAADOMT2
   d) ROLEDES
   e) ROLEDES2
   f) CHECKLE
   g) CHECKLE2
   h) CHECKLE3

2) Auxiliary Programs
   a) WDOMPAR
   b) XXXX
   c) TRANSDAT
   d) COPROD

3) Data Files
   a) DMR*T*
   b) DMR*P*
   c) DMR*N*
   d) RODAT*

The output of WAADOMT2 includes phase delay data for a wave generated at the feed array and passing through the hemispherical dome out to a linear wave front. These data, stored in the DMR* files, are used to design two Rotman lens stacks using ROLEDES (or ROLEDES2). The lens parameter output from ROLEDES (or ROLEDES2) is then stored in the RODAT* files. The program WAADOMR yields phase data similar to the WAADOMT2 output when the dome is considered as a receiver instead of a transmitter.

The phase data generated by the lens stack is compared to that generated by the WAADOMT2 using CHECKLE and CHECKLE2. When examining the phase data at a 45-degree angle between the orientation of lens stacks, WAADOMT2 is used to generate the phase data through the dome These data are checked against lens-generated phase data using CHECKLE3.

The auxiliary programs are of lesser interest, due either to their restricted scope (e.g., WDOMPAR, which determines dome parameters from given phase data) or to their simplicity. The programs XXX, TRANSDAT, and COPROD all exist to simplify data manipulation.

B-1. PROGRAM WAADOMT, TRANSMIT CASE (Figure B-1)

The program WAADOMT has been written to implement the mathematics of section 3.1.1. The following inputs are requested by the program:

1) NX = number of x values and NY = number of y values. (The x values are centered at 0; the y values begin at 0 and are all non-negative).

2) DELTX = distance between x values; DELTY = distance between y values. (The total number of valid pairs (x, y) which can be stored is 250. Here 'valid' means that there exists z such that (x, y, z) is a point in the feed array, and the ray emanating from (x, y, z) passes through the hemispherical dome.)

3) Z_0, AK, R_2, R_1, R_4, R_0 as in WAADOMR

The inputs for (1) should be integers; all others should be real values. Output options are similar to those of WAADOMR. Answering the question

X-Y REGION TO BE PROJECTED (PLOT/LIST/CONT)?

with L gives two columns headed by X and Y. Only values of x yielding at least one valid pair (x, y) are present in the table; the y value in the table is the maximum value y such that (x, y) is valid. Answering with P gives a plot of the perimeter of the region of valid points in addition to the circumference of the disk of radius R_0, and answering with C allows the program to proceed to the next section.

The question

PROJECTION IN PLANE WAVE (PLOT/LIST/CONT)?,

when answered with L, gives nine columns of data, headed by X, Y, U, V, TOTL L, THETA, PHI, PHDLA, AMPWT. X and Y are coordinates of the point to the projected; U and V are coordinates of the image; TOTL L is total phase path length; THETA and PHI are angular spherical coordinates of point Q; PHDLA and AMPWT are phase delay and amplitude weight. (See paragraph 3.1.1.) By answering with P, one may plot the grid of (u, v) values corresponding to valid (x, y) values. By answering with C, the programmer has the option of redoing his sample with new data or terminating the program, just as in WAADOMR.

In solving system (3) in paragraph 3.1.1 consisting of two nonlinear equations in two unknowns the IMSL subroutine ZSYSTM was used. ZSYSTM implements Brown's method of solving a system of nonlinear equations, as mentioned in paragraph 3.1.1. The system could not be solvely precisely as presented in paragraph 3.1.1, but upon rescaling the equations by multiplying each equation by 100, convergence to the roots occurred within three iterations in all test cases. Without rescaling, error messages result.

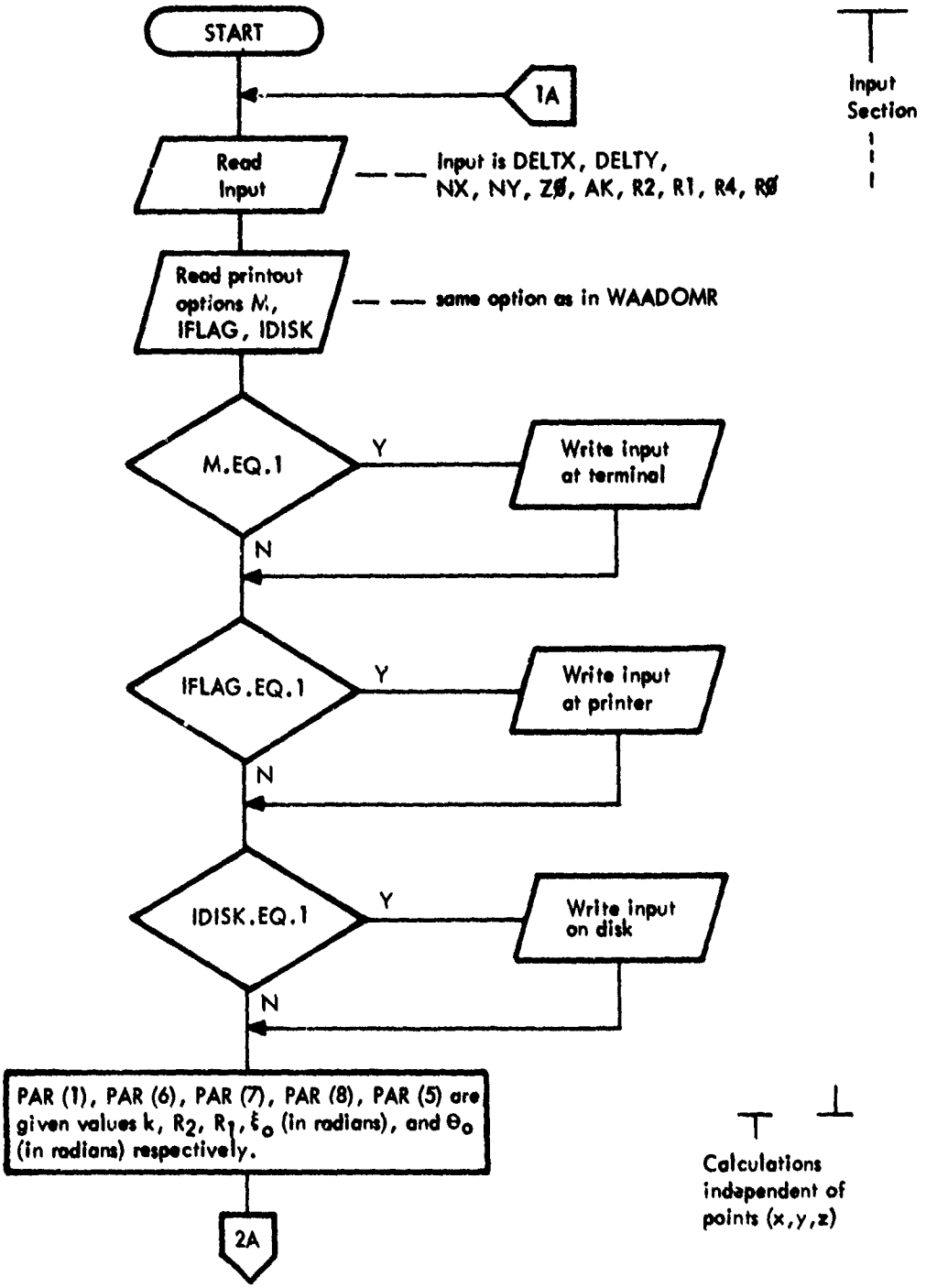

Figure B-1. Program WAADOMT (Transmit) Flow Chart

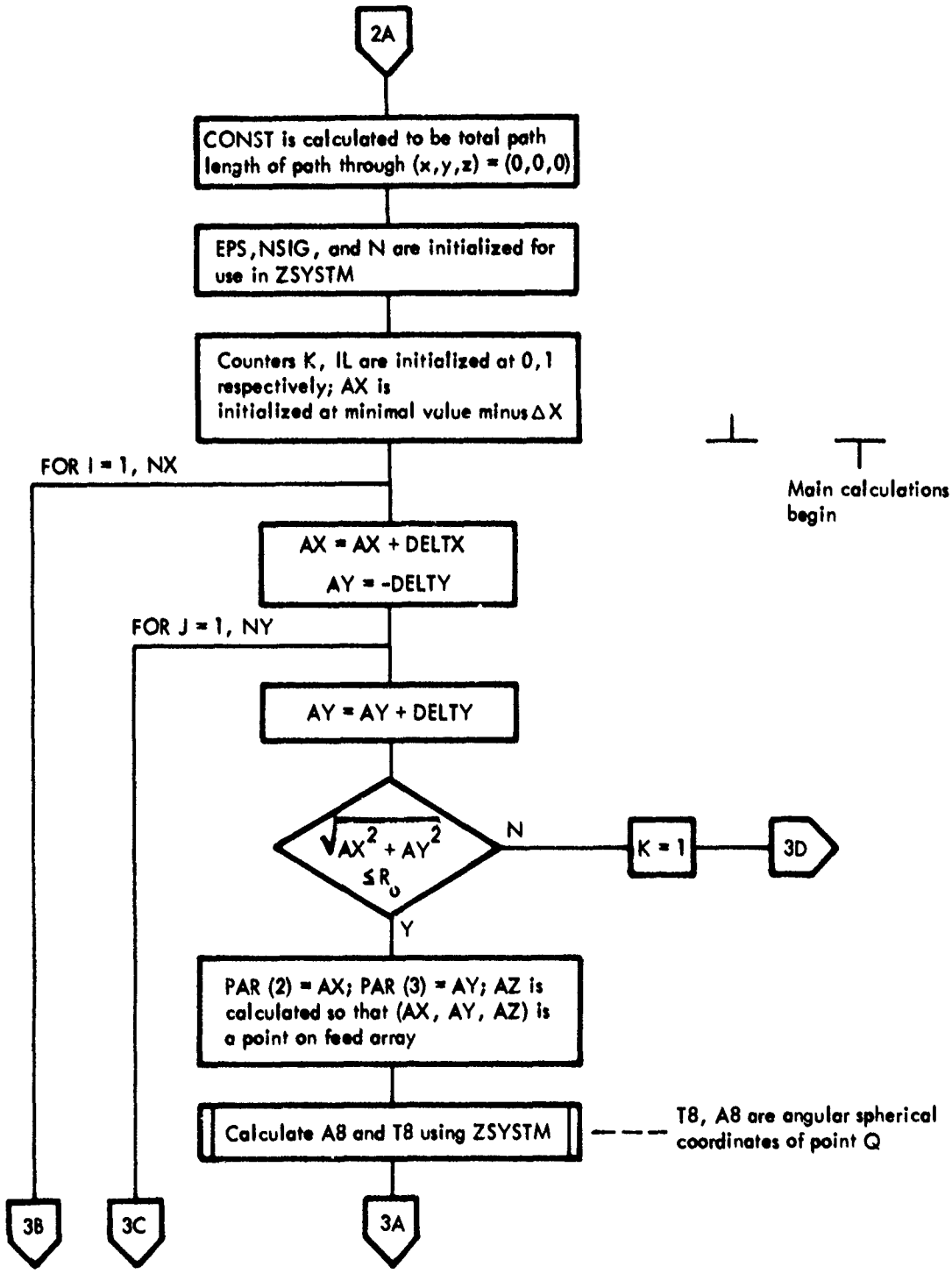

Figure B-1. Program WAADOMT (Transmit) Flow Chart (cont)

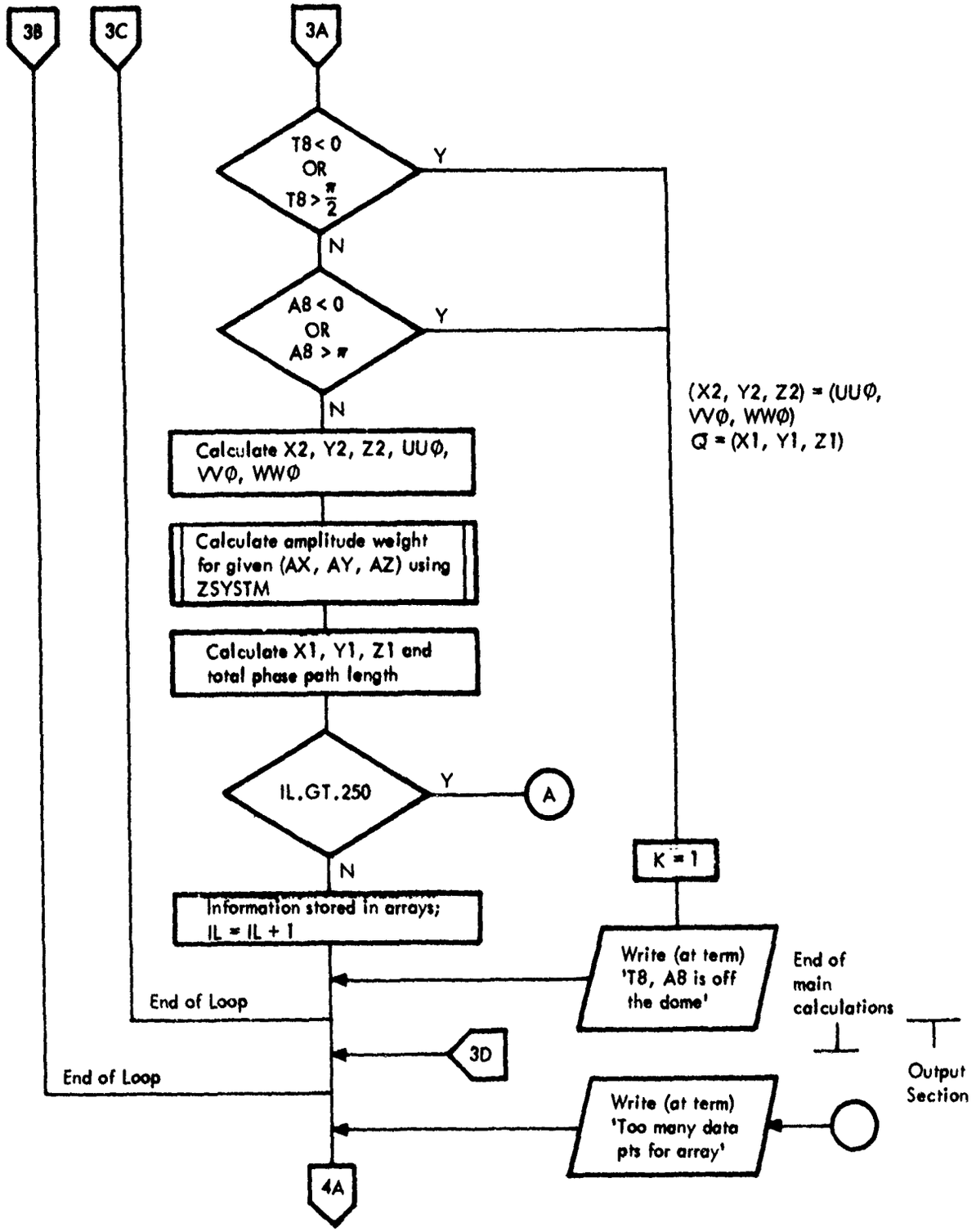

Figure B-1. Program WAADOMT (Transmit) Flow Chart (cont)

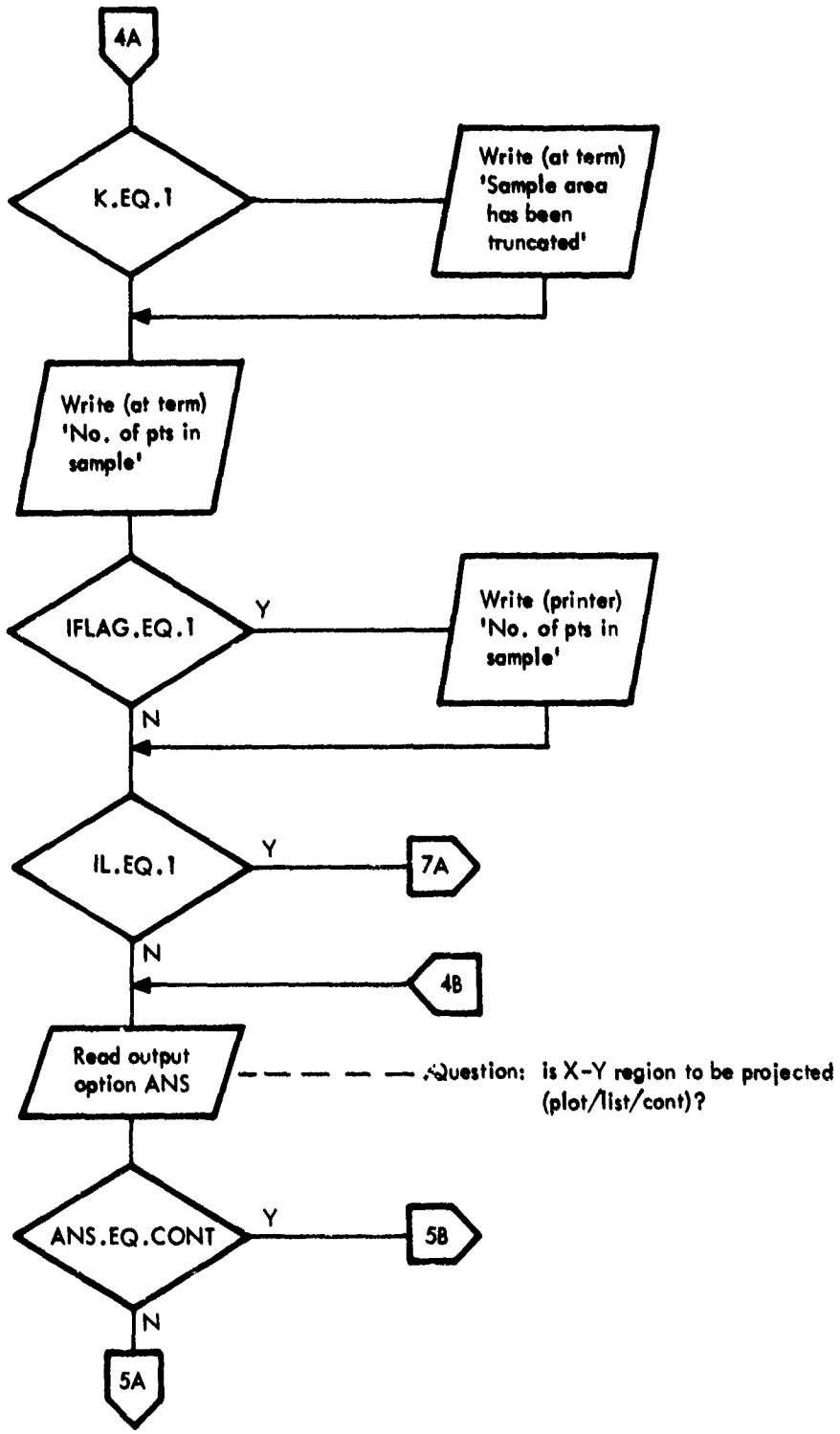

Figure B-1. Program WAADOMT (Transmit) Flow Chart (cont)

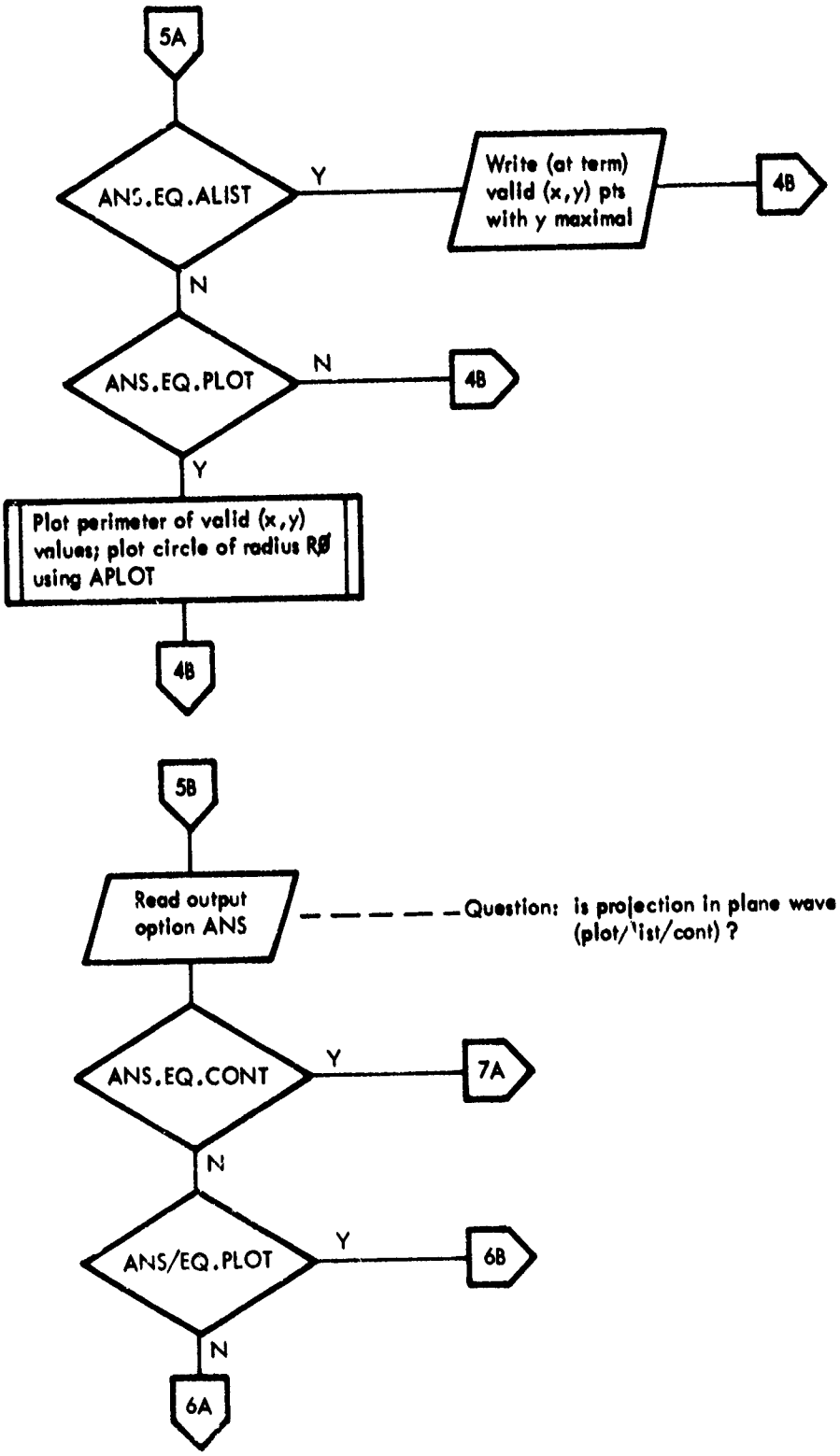

Figure B-1. Program WAADOMT (Transmit) Flow Chart (cont)

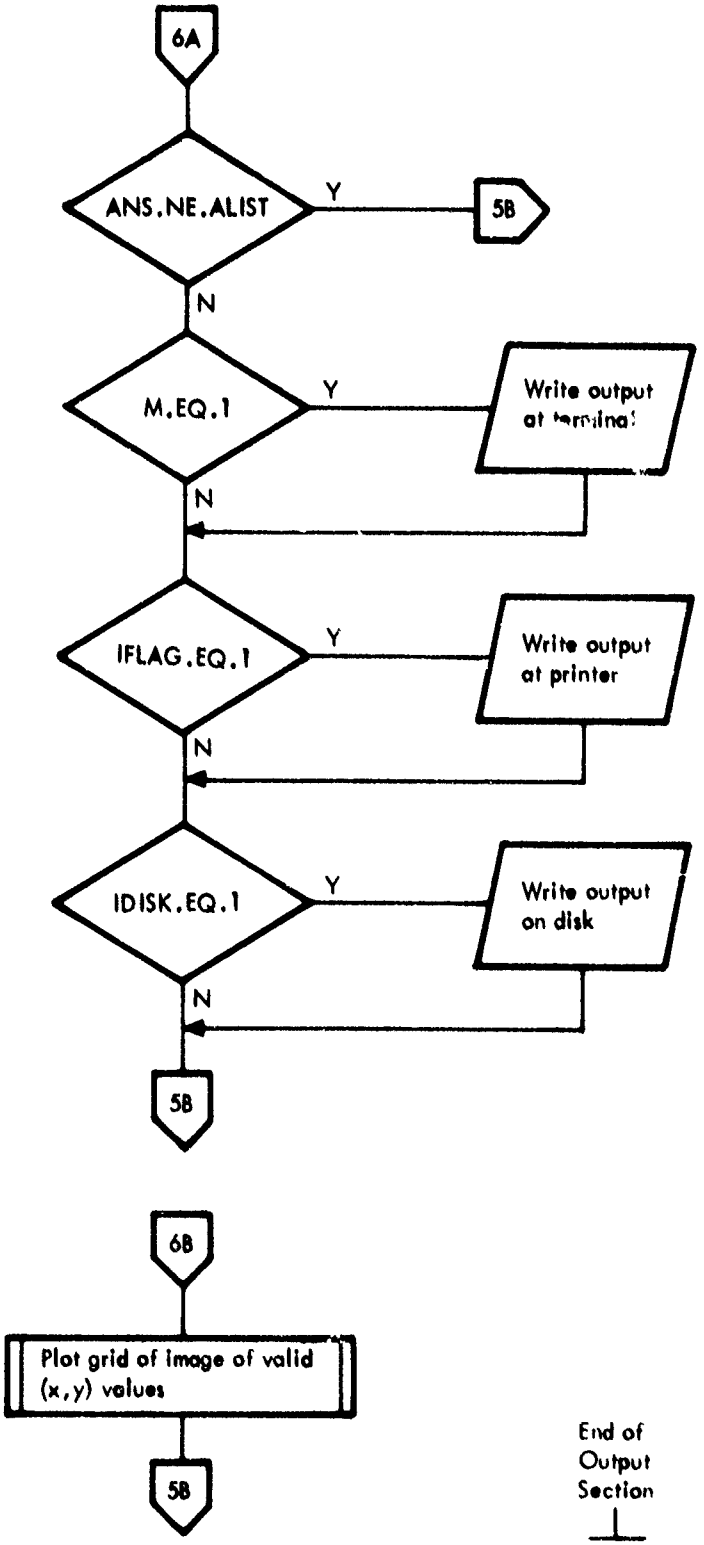

Figure B-1. Program WAAIOMT (Transmit) Flow Chart (cont)

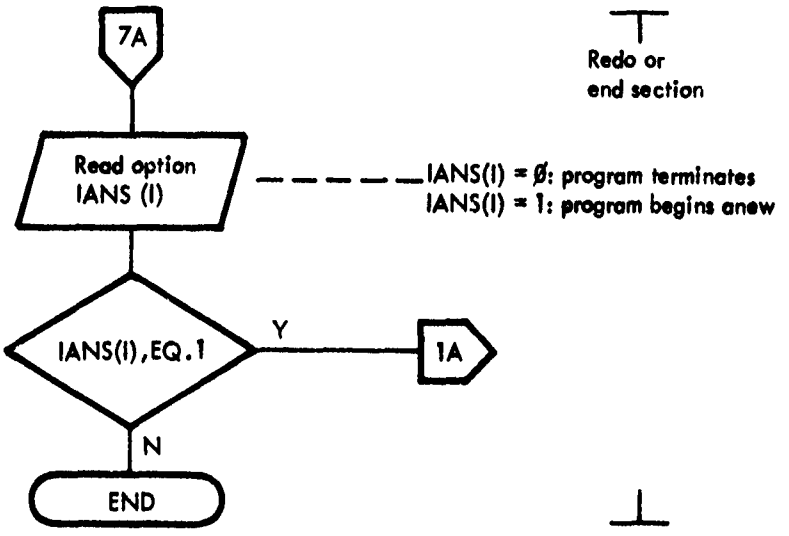

Figure B-1. Program WAADOMT (Transmit) Flow Chart (concl)

```
Z0= 0.300000D+02  K= 0.150000D+01  R2= 0.150000D+01  R1= 0.120000D+01  R4= 0.120000D+01
R0= 0.100000D+01  NX= 5  NY= 3  DELTX= 0.300000D+00  DELTY= 0.300000D+00
 15 POINTS IN SAMPLE

      X=          Y=          U=          V=       TOTL L=      THETA=
        PHI=        PHDLA=      AMPWT=
-0.600000D+00 0.0          -0.231371D+00 0.0          0.184409D+01 0.108589D+02
   0.0             0.794650D-01    0.507502D+00
-0.600000D+00 0.300000D+00-0.235314D+00 0.167413D+00 0.183306D+01 0.123445D+02
   0.314696D+02    0.684359D-01    0.502456D+00
-0.600000D+00 0.600000D+00-0.247481D+00 0.334939D+00 0.179964D+01 0.160754D+02
   0.537455D+02    0.350173D-01    0.484640D+00
-0.300000D+00 0.0          -0.666160D-01 0.0          0.179246D+01 0.174050D+02
   0.0             0.278379D-01    0.536981D+00
-0.300000D+00 0.300000D+00-0.704092D-01 0.170440D+00 0.178157D+01 0.183347D+02
   0.211749D+02    0.169416D-01    0.532944D+00
-0.300000D+00 0.600000D+00-0.821990D-01 0.341565D+00 0.174853D+01 0.209390D+02
   0.395816D+02   -0.160962D-01    0.518701D+00
 0.971445D-16 0.0          0.961743D-01 0.0          0.171736D+01 0.237117D+02
   0.0            -0.472697D-01    0.559659D+00
 0.971445D-16 0.300000D+00 0.925245D-01 0.173875D+00 0.170644D+01 0.243995D+02
   0.162963D+02   -0.581695D-01    0.556000D+00
 0.971445D-16 0.600000D+00 0.811066D-01 0.348849D+00 0.167334D+01 0.264044D+02
   0.315316D+02   -0.912864D-01    0.542932D+00
 0.300000D+00 0.0          0.258678D+00 0.0          0.161851D+01 0.299314D+02
   0.0            -0.146111D+00    0.578120D+00
 0.300000D+00 0.300000D+00 0.255134D+00 0.178152D+00 0.160742D+01 0.304954D+02
   0.135350D+02   -0.157202D+00    0.574273D+00
 0.300000D+00 0.600000D+00 0.243927D+00 0.357765D+00 0.157386D+01 0.321678D+02
   0.266148D+02   -0.190763D+00    0.560134D+00
 0.600000D+00 0.0          0.423265D+00 0.0          0.149459D+01 0.362305D+02
   0.0            -0.270031D+00    0.591798D+00
 0.600000D+00 0.300000D+00 0.419728D+00 0.183762D+00 0.148323D+01 0.367279D+02
   0.118212D+02   -0.281398D+00    0.586700D+00
 0.600000D+00 0.600000D+00 0.408229D+00 0.369230D+00 0.144903D+01 0.382071D+02
   0.234520D+02   -0.315598D+00    0.566953D+00
```

Figure B-2 Sample WAADOMT Output (Transmit)

B-2. PROGRAM WAADOMR, RECEIVE CASE (Figure B-3)

The program WAADOMR has been written to implement the mathematics of paragraph 3.1.1. The following inputs are requested by the program:

1) NU = number of u values and NV = number of v values. (The u values are centered at 0; the v values begin at 0 and are all non-negative.) The u and v values represent a discrete defined grid of points external to the dome, which shares the normal with the dome at U = V = 0.

2) DELTU = distance between u values; DELTV = distance between v values. (The total number of valid pairs (u, v) which can be stored is 200. Here 'valid' means that the ray corresponding to (u, v) passes through the dome and hits the target array.)

3) $Z_0 = \xi_o$ in degrees; K (or AK) = k

4) R_2 and R_1

5) R_4 and R_0

For each of the above inputs, checks are run for inappropriate values. The inputs for (1) should be integers, all others should be real values.

Tabular output can be sent to the terminal or the printer. For such information concerning the u-v plane area to be projected, one should answer the question

U-V PLANE TO BE PROJECTED (PLOT/LIST/CONT)?

with L. As output one receives two columns, headed by U and V. Only values of u yielding at least one valid pair (u, v) are present in the table; the v value in the table is the maximum value v such that (u, v) is valid.

To graph the perimeter of the region of valid points, the above question should be answered with P. This will initiate the subroutine APLOT. To continue in the program without plotting or listing, answer the question with C.

Similar considerations apply to the question

TARGET ARRAY (PLOT/LIST/CONT)?

By answering with L, one receives eight columns of data, headed by U, V, X, Y, Z, TOTL L, THETA and PHI. U and V give the coordinates (u, v) of valid points. X, Y, Z are the coordinates of the image (x, y, z) of (u, v). TOTL L is the total phase path length. THETA and PHI are angular spherical coordinates of point A (figure 22). By answering with P, one may plot the grid of (x, y) values corresponding to valid points (u, v). Also plotted is the circumference of the target disc of radius R_0. The scales for all plotting are identical.

After answering with C, the following question is asked:

REDO SAMPLE - WILL ERASE OLD ONE (N/Y)?

If the answer is Y, the programmer may then input new data and the program will run again. If the answer is N, the program will end.

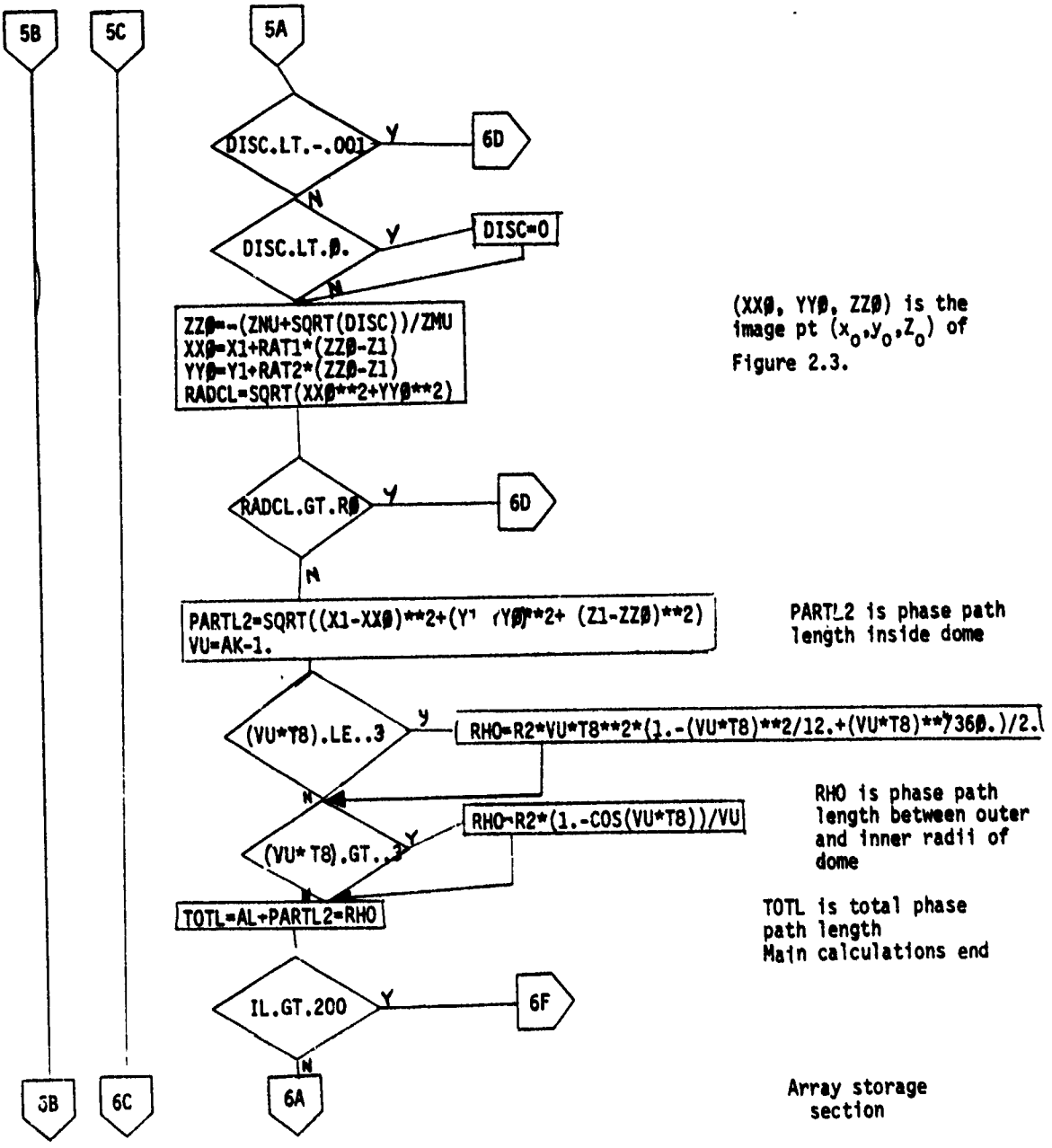

Figure B-3. Program WAADOMR (Receive) Flow Chart (cont)

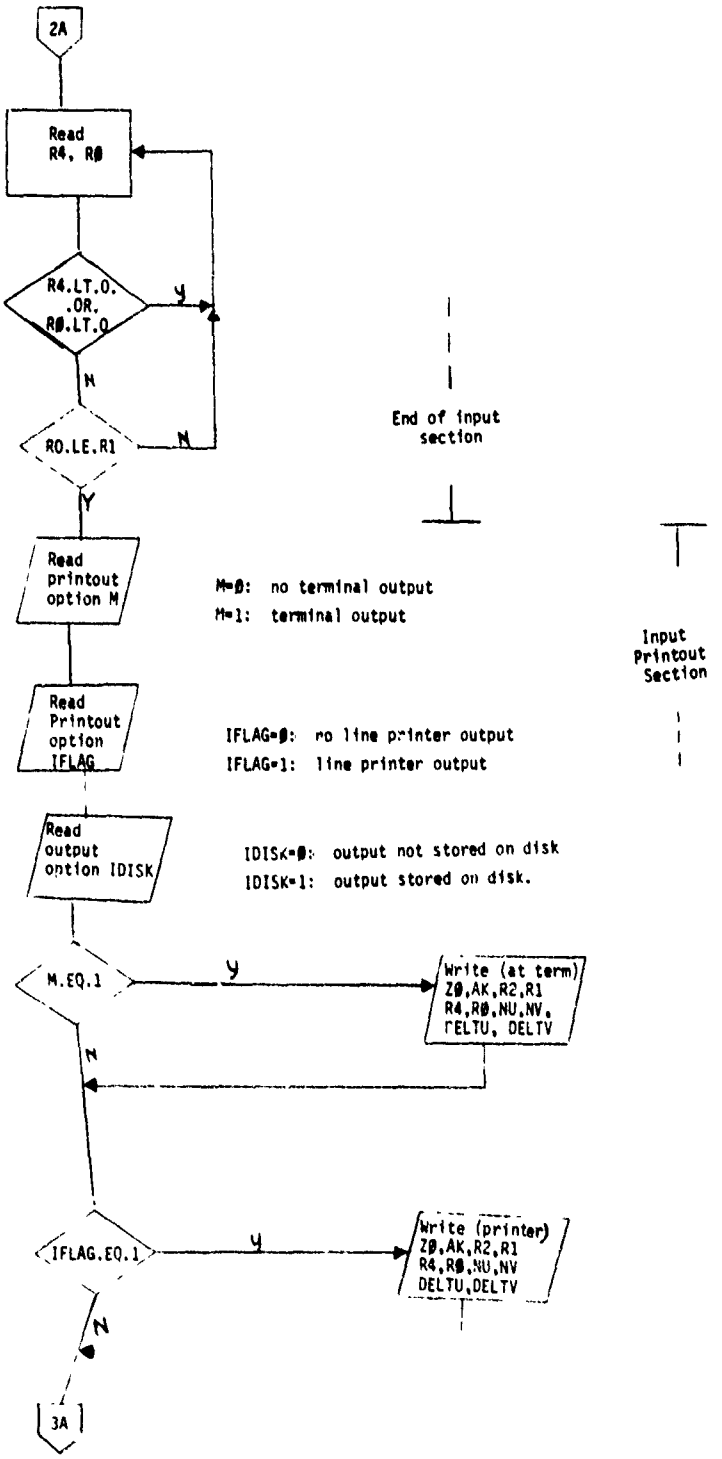

Figure B-3. Program WAADOMR (Receive) Flow Chart (cont)

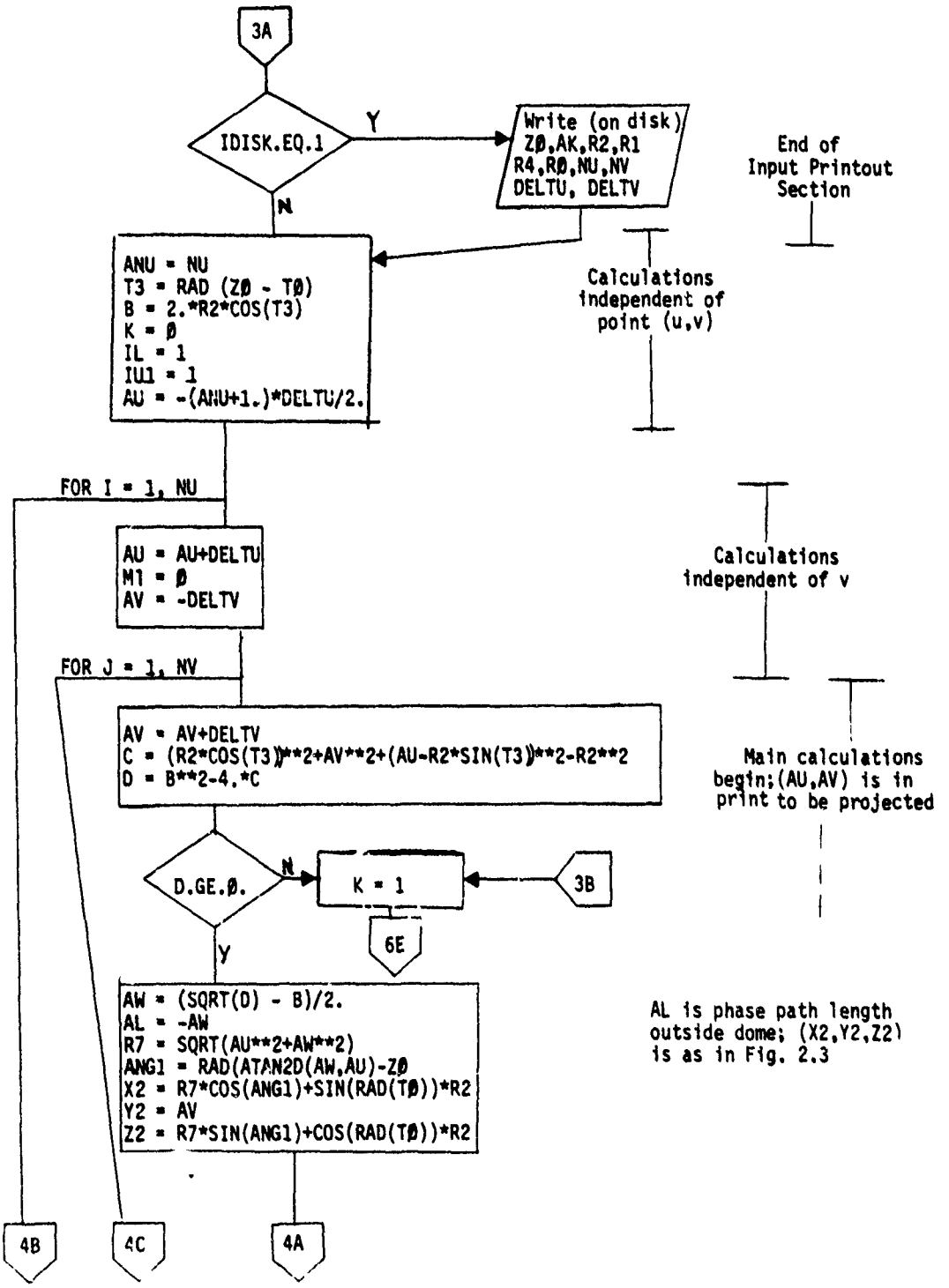

Figure B-3. Program WAADOMR (Receive) Flow Chart (cont)

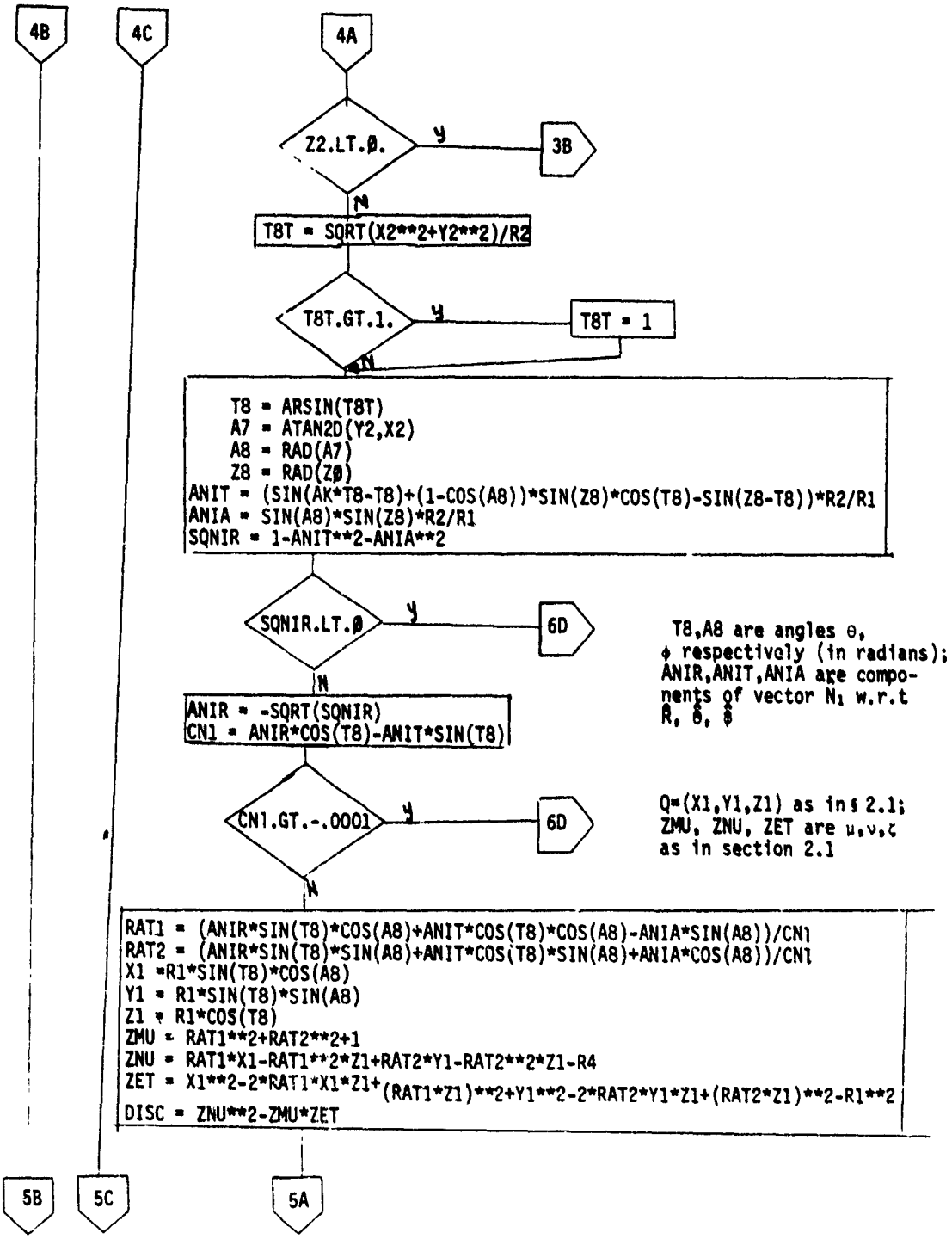

Figure B-3. Program WAADOMR (Receive) Flow Chart (cont)

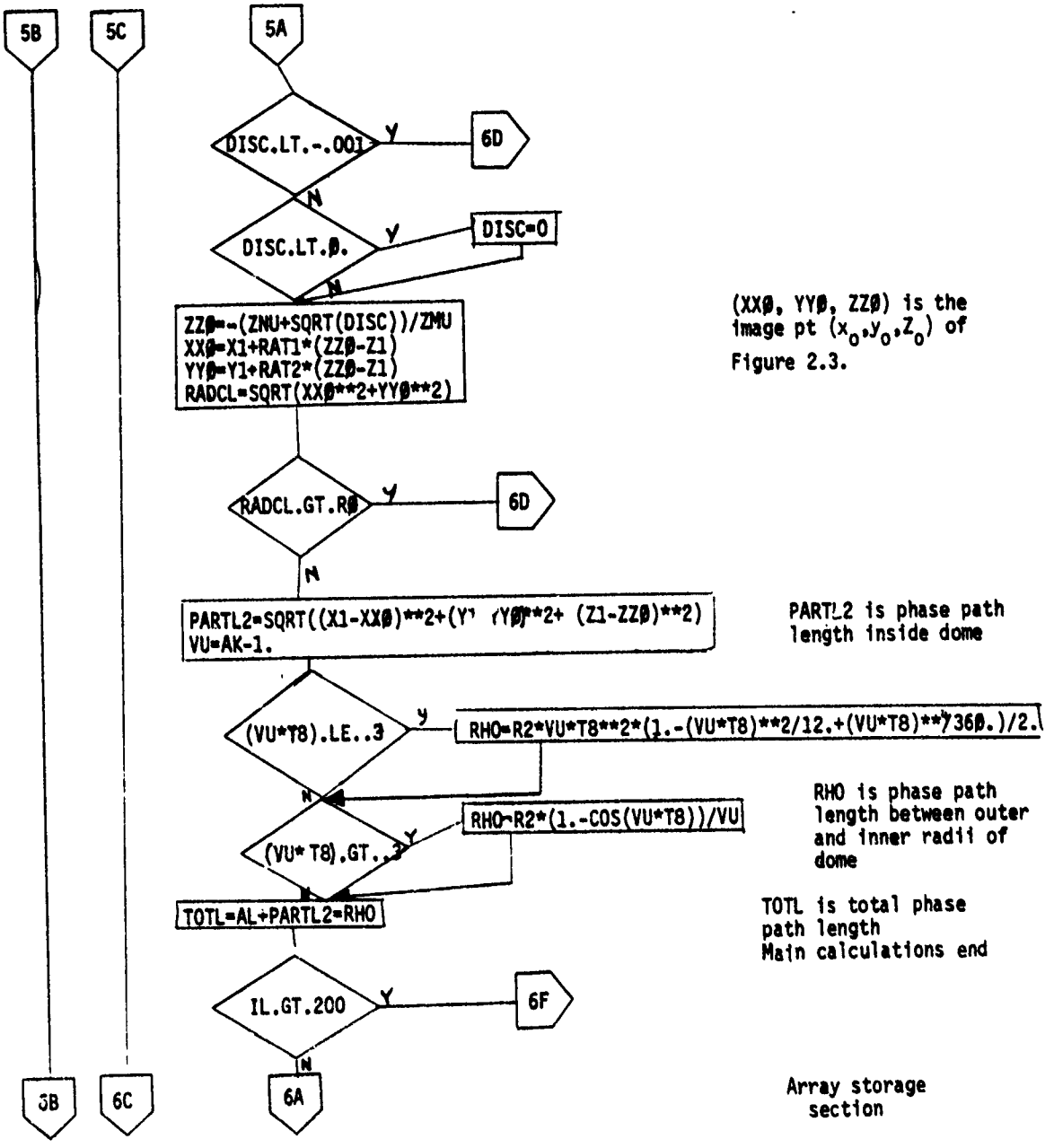

Figure B-3. Program WAADOMR (Receive) Flow Chart (cont)

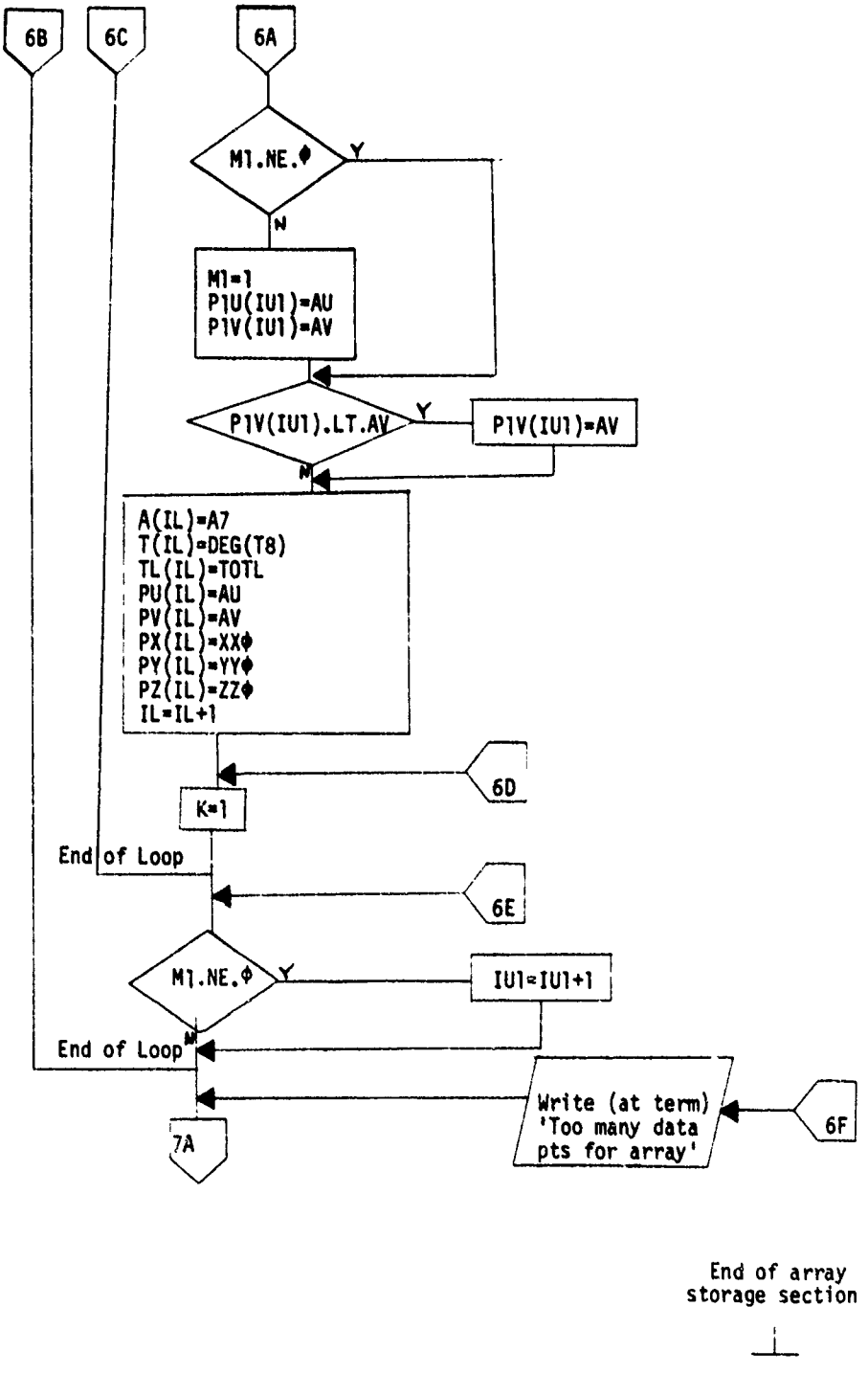

Figure B-3. Program WAADOMR (Receive) Flow Chart (cont)

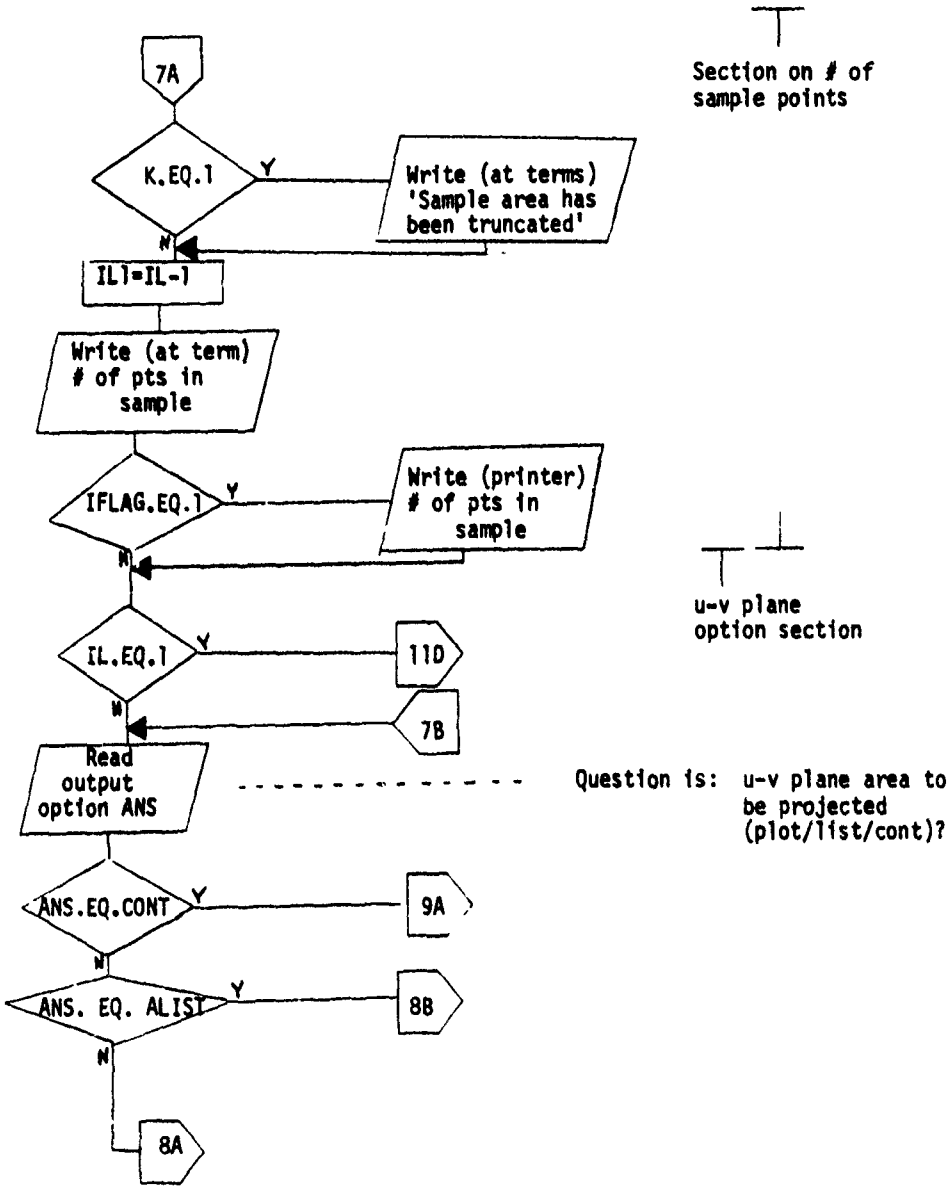

Figure B-3. Program WAADOMR (Receive) Flow Chart (cont)

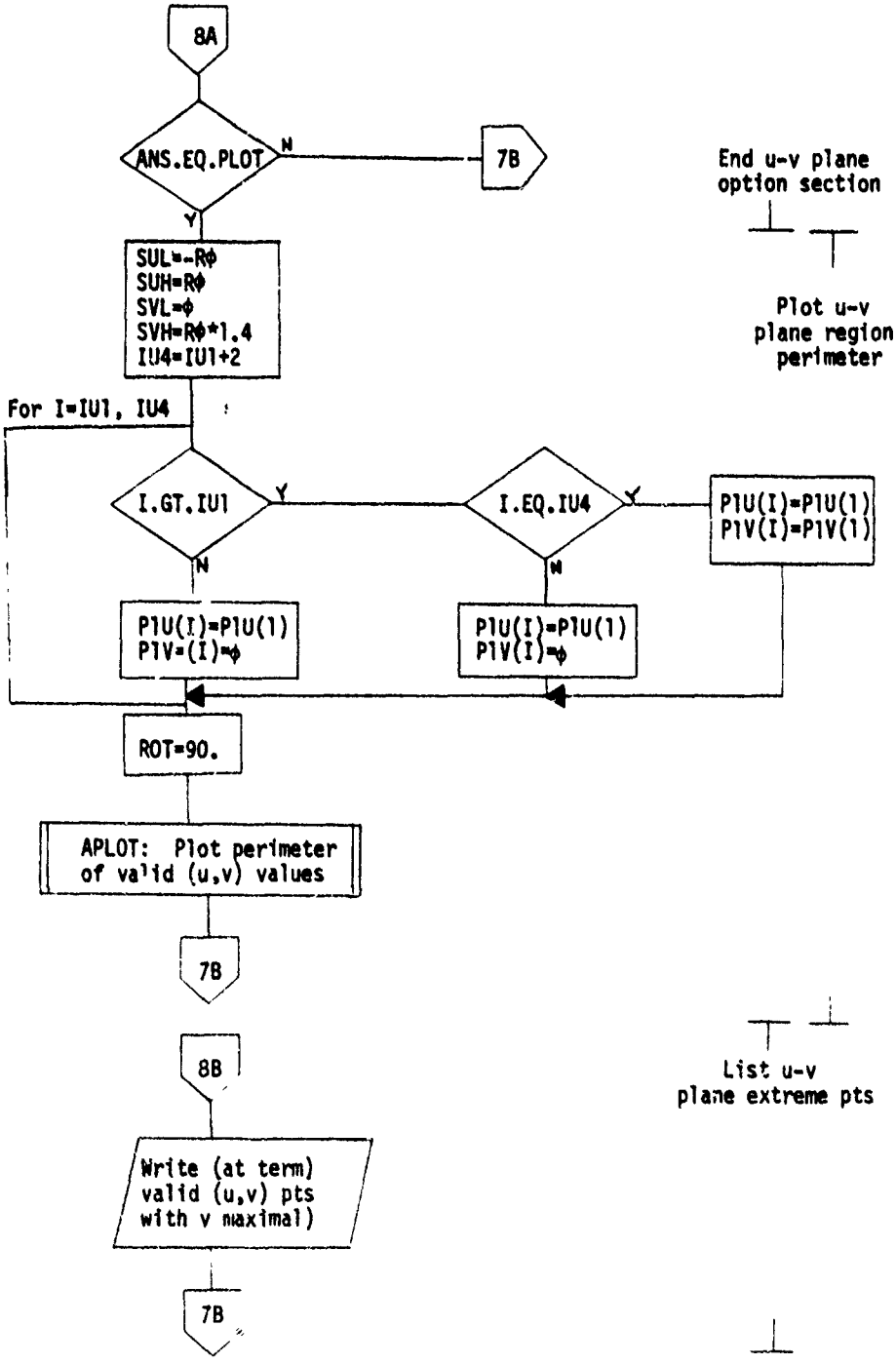

Figure B-3. Program WAADOMR (Receive) Flow Chart (cont)

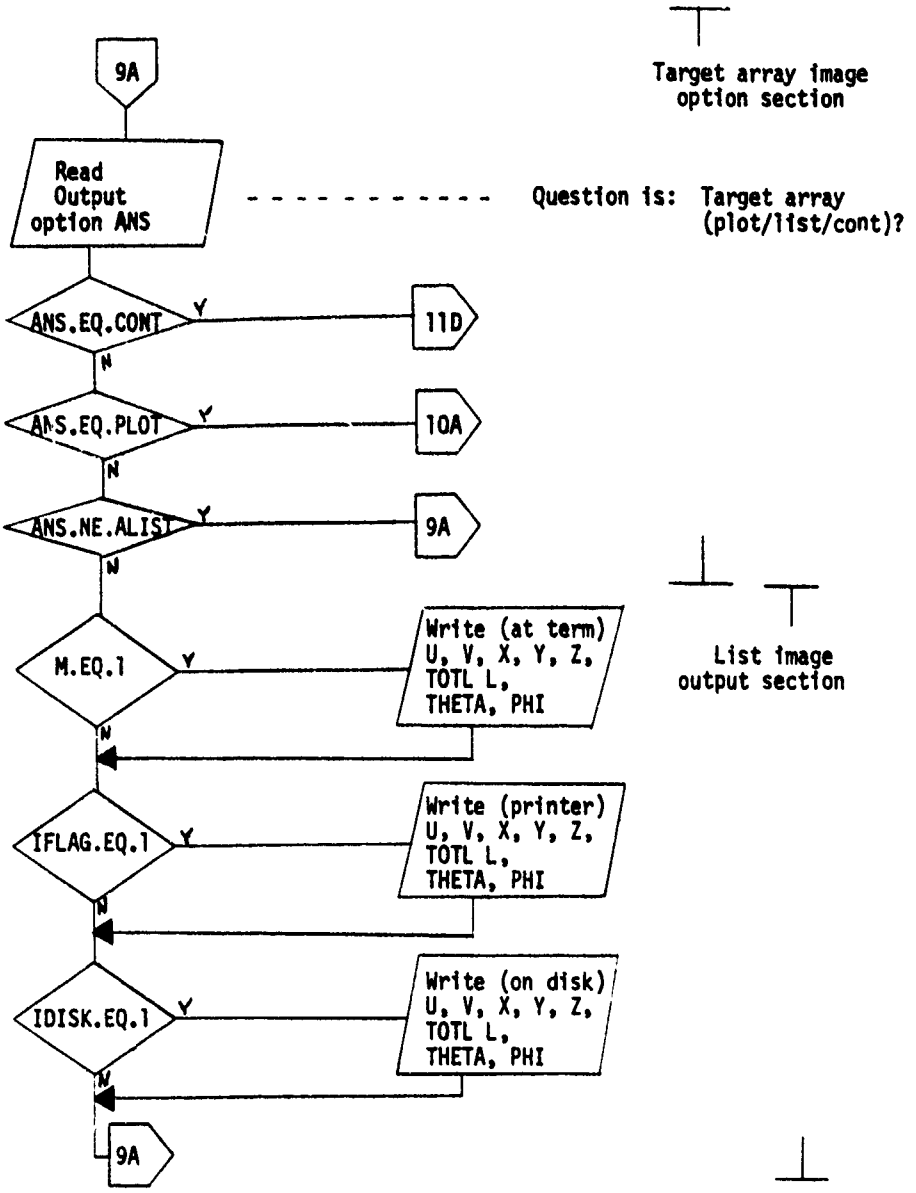

Figure B-3. Program WAADOMR (Receive) Flow Chart (cont)

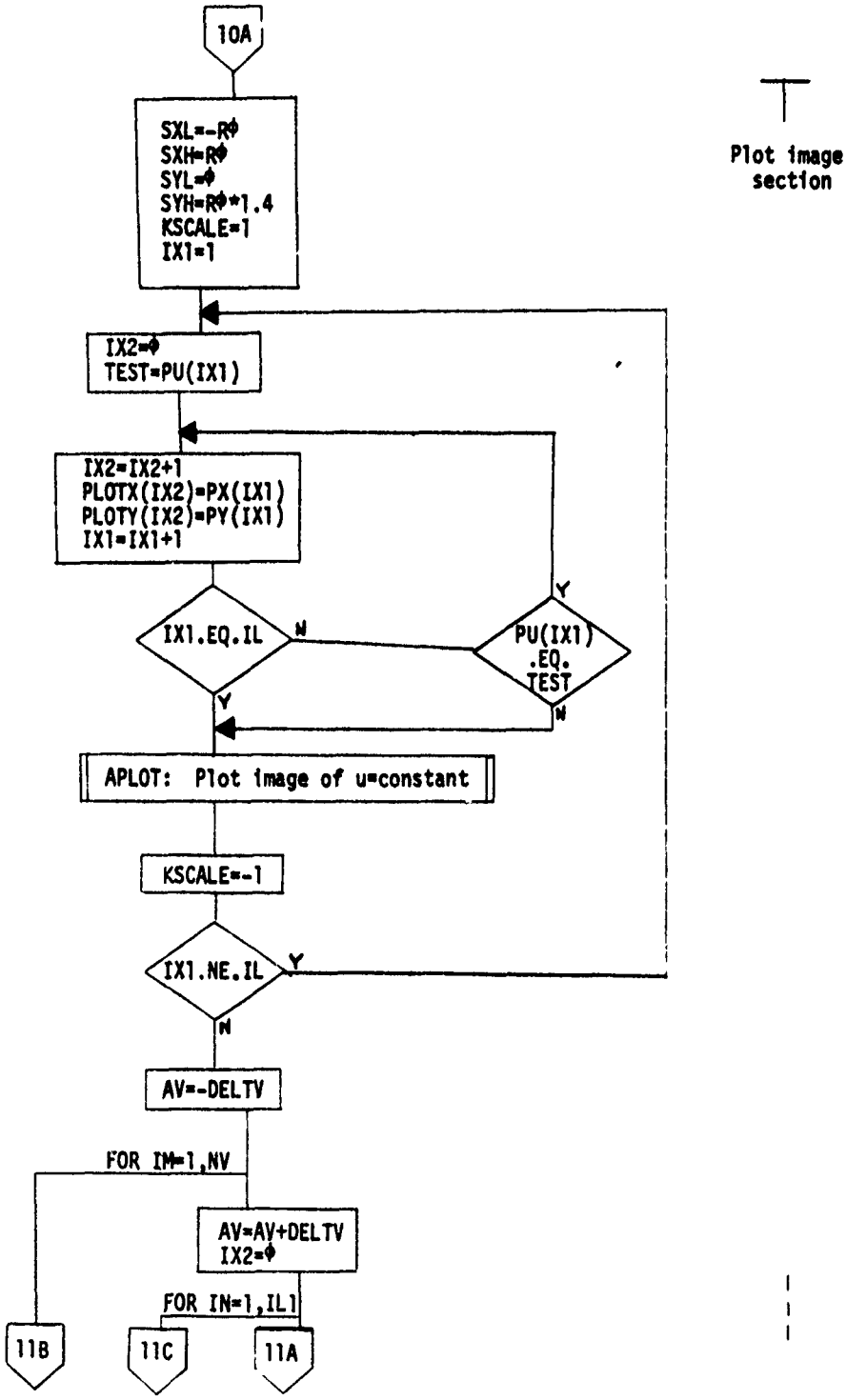

Figure B-3. Program WAADOMR (Receive) Flow Chart (cont)

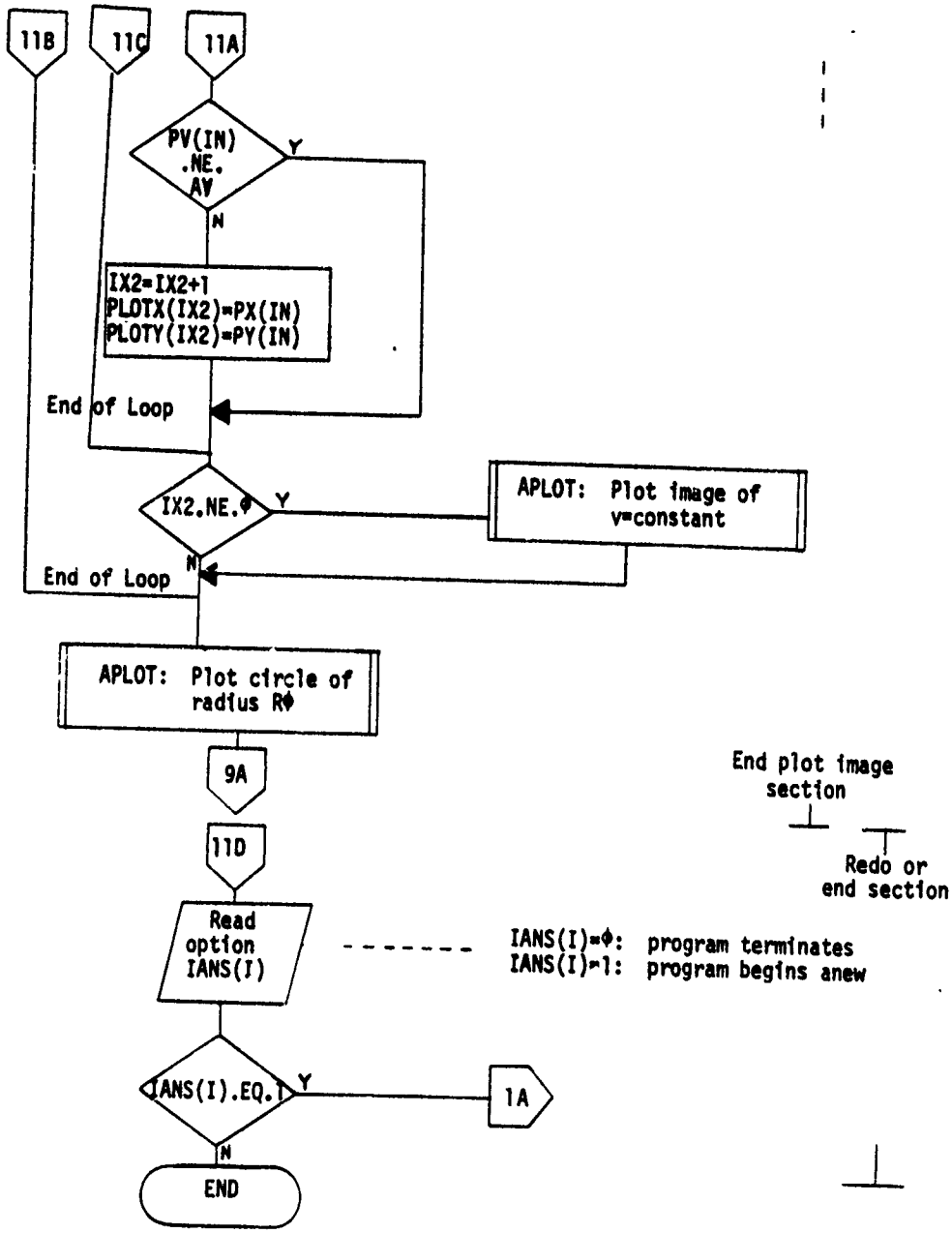

Figure B-3. Program WAADOMR (Receive) Flow Chart (concl)

```
Z0= 30.00  K= 1.500  R2=  1.500  R1=  1.200  R4=  1.200
R0=  1.000  NU=  5  NV=  3  DELTU=  0.100  DELTV=  0.100
 15 POINTS IN SAMPLE


   U=          V=          X=          Y=          Z=          TOTL L=
     THETA=          PHI=
-0.20000     0.0         -0.54325     0.0         -0.40775     1.83615
     12.123          0.0
-0.20000     0.10000     -0.54075     0.17862     -0.39865     1.83189
     12.663          17.705
-0.20000     0.20000     -0.53318     0.35692     -0.37109     1.81908
     14.170          33.001
-0.10000     0.0         -0.36116     0.0         -0.45818     1.80490
     16.095          0.0
-0.10000     0.10000     -0.35874     0.17673     -0.44926     1.80065
     16.500          13.576
-0.10000     0.20000     -0.35144     0.35305     -0.42230     1.78787
     17.667          26.062
 0.0         0.0         -0.17752     0.0         -0.48775     1.76462
     20.000          0.0
 0.0         0.10000     -0.17521     0.17474     -0.47892     1.76037
     20.325          11.065
 0.0         0.20000     -0.16820     0.34898     -0.45225     1.74760
     21.277          21.559
 0.10000     0.0          0.00707     0.0         -0.49704     1.71530
     23.859          0.0
 0.10000     0.10000      0.00929     0.17255     -0.48823     1.71104
     24.132          9.385
 0.10000     0.20000      0.01598     0.34455     -0.46163     1.69827
     24.937          18.435
 0.20000     0.0          0.19186     0.0         -0.48618     1.65694
     27.689          0.0
 0.20000     0.10000      0.19397     0.17011     -0.47733     1.65268
     27.926          8.184
 0.20000     0.20000      0.20034     0.33960     -0.45062     1.63991
     28.629          16.157
```

Figure B-4. Sample WAADOMR Output (Receive)

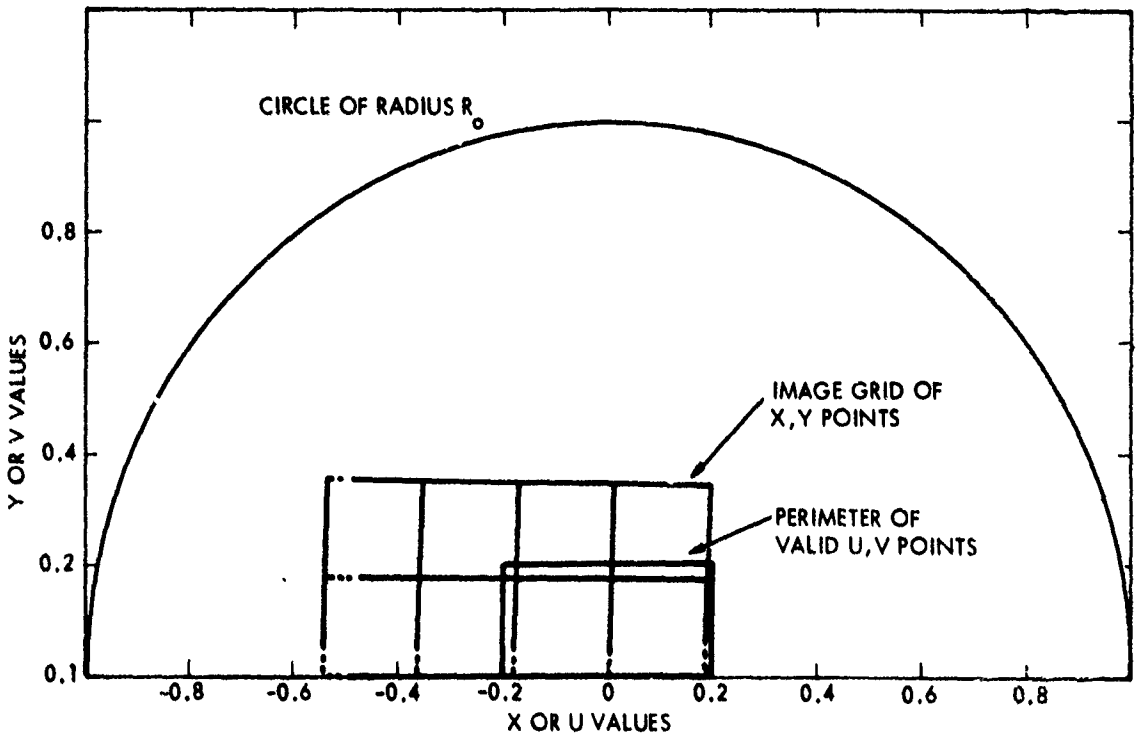

Figure B-5. Comparison of Feed Array and Projected Image (Transmit Case)

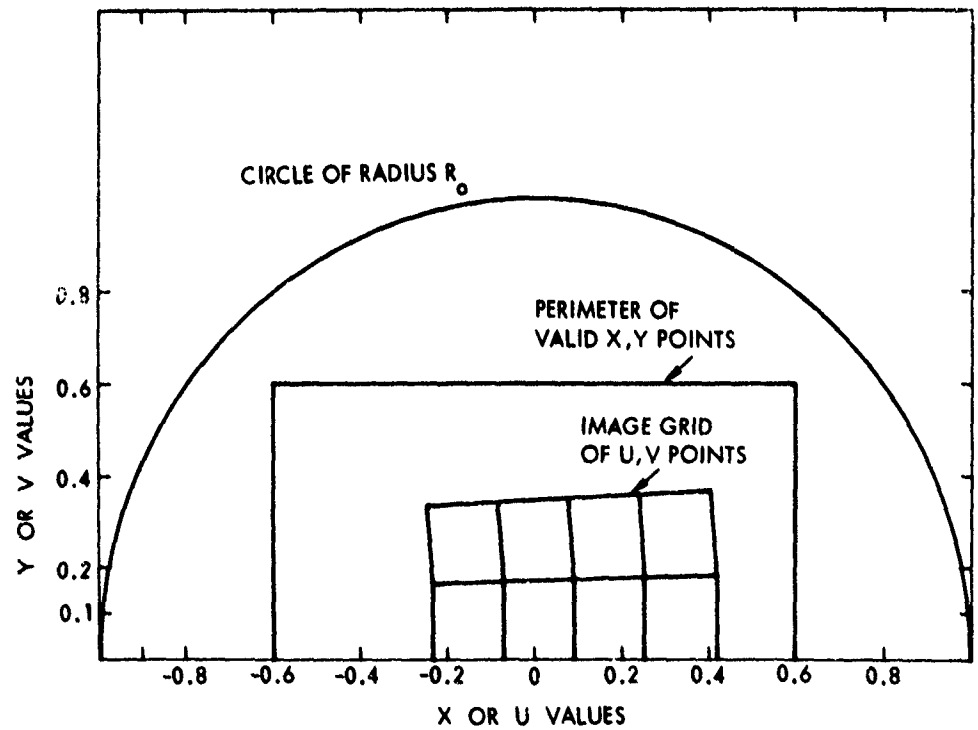

Figure B-6. Comparison of Feed Array and Projected Image (Receive Case)

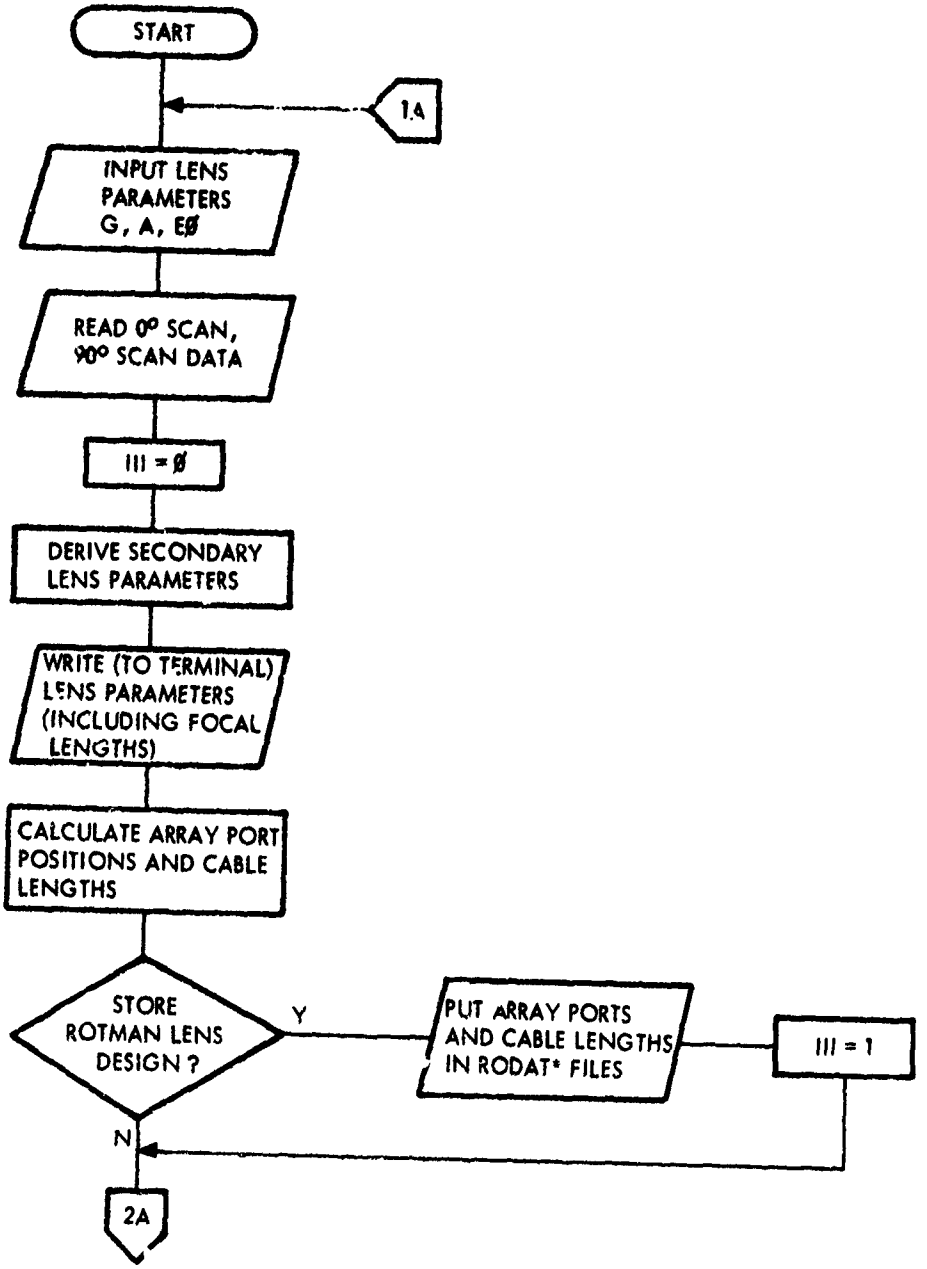

Figure B-7. Program ROLEDES (Rotman Lens Design) Flow Chart (Sheet 1 of 2)

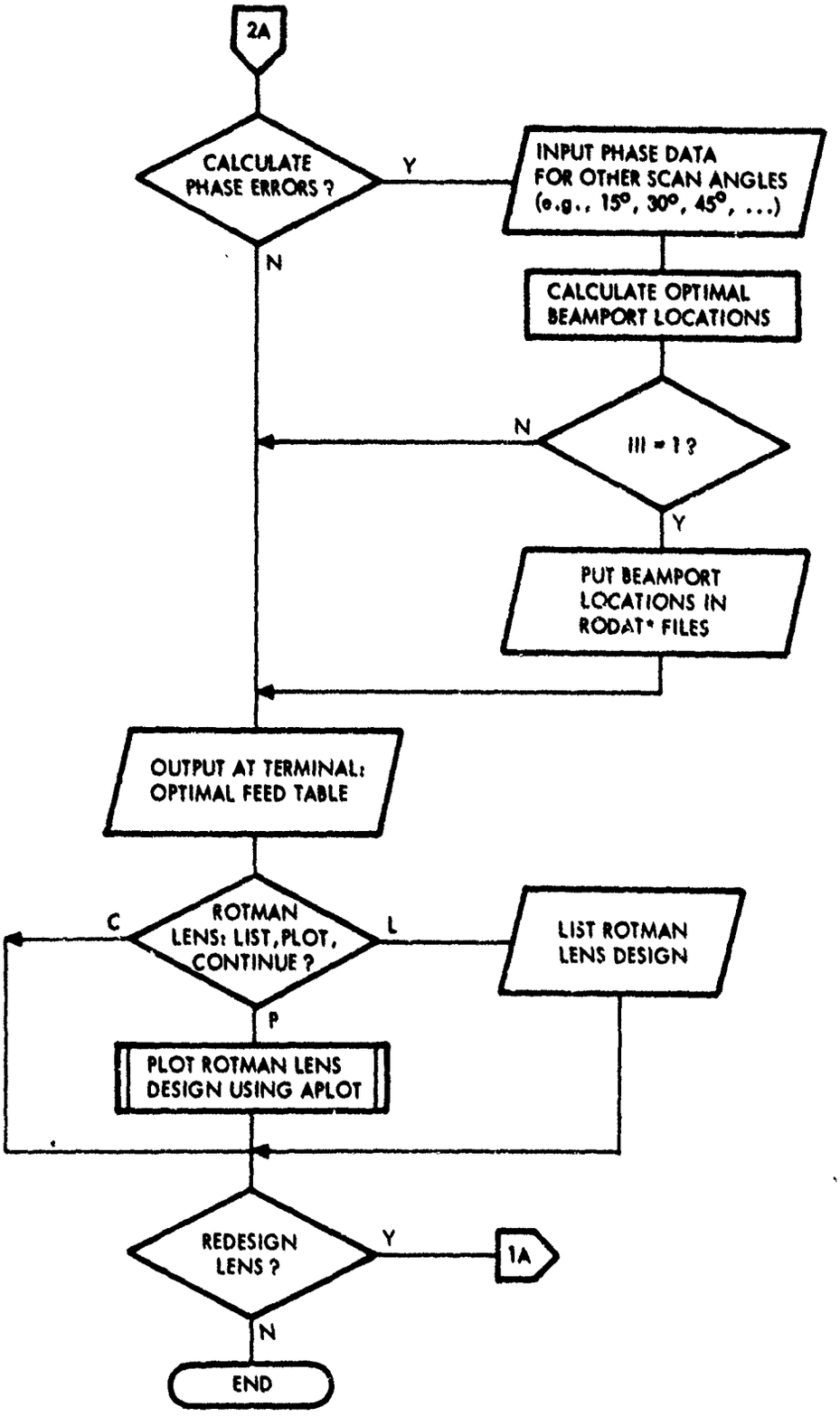

Figure B-7. Program ROLEDES (Rotman Lens Design) Flow Chart (Sheet 2 of 2)

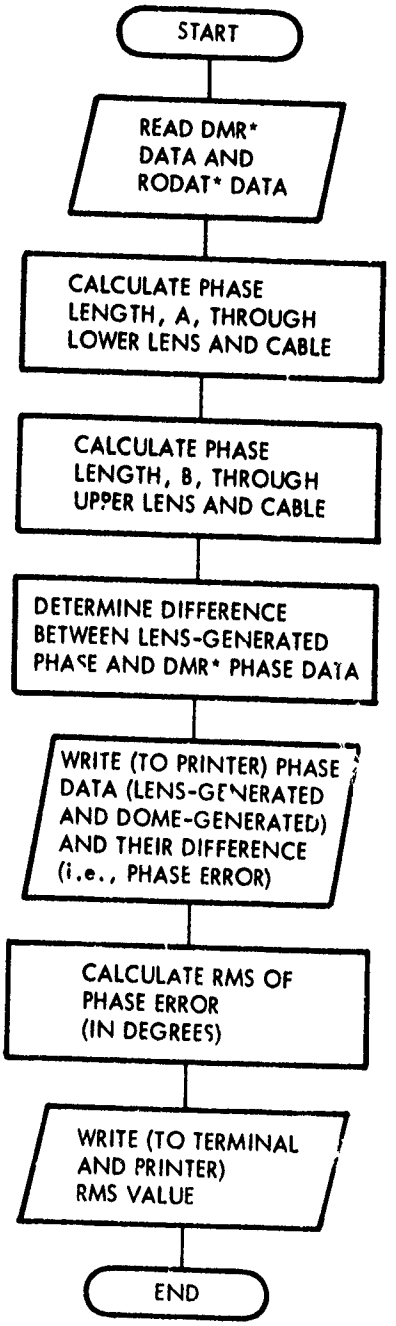

Figure B-8. Program CHECKLE Flow Chart (3-D Lens Design and Performance)

DISTRIBUTION LIST

Defense Documentation Center Cameron Station Alexandria, VA 22314	2*
Office of Naval Research Arlington, VA 22217 Attn: Code 221	5
Director Naval Research Laboratory Washington, DC 20390	
Attn: Code 2627	1
Attn: Code 4700	1
Commandant of the Marine Corps Scientific Advisor (Code RD-1) Washington, DC 20380	1
Commander Naval Air Systems Command Washington, DC 20360 Attn: AIR 360	1
Commander Naval Ocean Systems Center Attn: Code 7303, J. Whittikar San Diego, CA 92152	1
Commander Naval Sea Systems Command Washington, DC 20360	
Attn: SEA 652	1
Attn: PMS 403	1
Attn: PMS 404	1
Office of Naval Research Branch Office 1030 East Green Street Pasadena, CA 91106 Attn: Code 400	1
Commander Defense Contracts Administration Services District 8900 DeSoto Avenue Van Nuys, CA 91304	1

*Forwarded with DDC Form 50